Microdevice for Sedimentation-based Separation of Blood Microsamples at the Point of Collection

THÈSE N^{O} 7782 (2017)

PRÉSENTÉE LE 20 OCTOBRE 2017
À LA FACULTÉ DES SCIENCES ET TECHNIQUES DE L'INGÉNIEUR
LABORATOIRE DE MICROSYSTÈMES 4
PROGRAMME DOCTORAL EN MICROSYSTÈMES ET MICROÉLECTRONIQUE

ÉCOLE POLYTECHNIQUE FÉDÉRALE DE LAUSANNE

POUR L'OBTENTION DU GRADE DE DOCTEUR ÈS SCIENCES

PAR

David FORCHELET

acceptée sur proposition du jury:

Prof. P.-A. Farine, président du jury
Prof. Ph. Renaud, directeur de thèse
Dr E. Sollier, rapporteuse
Prof. A. Thomas, rapporteur
Prof. F. Gallaire, rapporteuse

ÉCOLE POLYTECHNIQUE
FÉDÉRALE DE LAUSANNE
Suisse
2017

To my family

Résumé

Les tests sanguins de laboratoire jouent un rôle central dans les décisions thérapeutiques et les diagnostics actuels. Ainsi, les erreurs ont un impact direct sur la qualité et le coût des soins. La majorité des erreurs se produisent dans la phase pré-analytique ; lorsque les échantillons sont recueillis, stockés et préparés. Pour l'analyse biochimique, l'opération de préparation la plus courante est la séparation du plasma sanguin: la réalisation de cette opération, lors de la prise de sang, a le potentiel de rendre plus simple et plus fiable le cycle de test de laboratoire. Par conséquent, dans ce travail, un microdispositif effectuant la séparation du sang au point de collecte est présenté. Le microdispositif traite des microéchantillons sanguins prélevés au bout du doigt sans avoir recours à un équipement externe. La capillarité génère spontanément le mouvement du liquide dans le système.

Le dispositif repose sur la sédimentation comme force motrice, simple et spontanée, pour la séparation du sang non dilué. Le sang s'écoule dans le dispositif à une vitesse permettant aux cellules de se déposer sur le fond d'un canal et de créer une fraction liquide de viscosité élevée. Le plasma surnageant, de viscosité inférieure, est pompé à une vitesse plus élevée que le sédiment dans le dispositif. Ainsi, à mesure que le dispositif se remplit, une portion de plasma est générée dans la partie aval du canal. Dans ce travail, un modèle unidimensionnel combinant les théories de sédimentation de Kynch et de flux de Poiseuille est établi pour décrire ce nouveau phénomène de séparation. L'impact sur la séparation de paramètres géométriques et sanguins est étudié.

Le dispositif est utilisable pour séparer les échantillons frais ou anti-coagulés obtenus par ponction cutanée. Pour les deux natures d'échantillon, le liquide, exempt de cellules, apparaît après un délai de séparation de 400 s. Ce délai est nécessaire pour l'établissement d'un contraste de viscosité suffisant par sédimentation. Par la suite, pour des échantillons anti-coagulés, le liquide exempt de cellules est extrait avec un rendement de 17%. Pour les échantillons frais, la coagulation conduit à une augmentation du rendement à 67%. La combinaison de sédimentation et de filtration à travers un caillot est la raison de cette augmentation. Les échantillons séparés sont extraits du dispositif par l'utilisation d'un mécanisme d'éjection intégré. Le dispositif est conçu pour éjecter un volume de 2 µL de liquide séparé à partir de 25 µL de sang complet.

La qualité des échantillons séparés est établie en mesurant la concentration des particules contaminantes et le profil protéique. La concentration de contaminants, dans le liquide provenant du microsystème, est plus faible et plus répétable que dans les échantillons de plasma ou de sérum centrifugés. Dans le profil protéique, seul 4,5% des protéines quantifiées présentent des niveaux significativement différents entre les échantillons de sérum et ceux séparés par le microdispositif. Ceci montre que les échantillons séparés et le sérum peuvent être utilisés de façon interchangeable.

Le microdispositif a été combiné avec des analyseurs cliniques standards pour effectuer des analyses sanguines sur 12 patients obèses. Sur les 8 marqueurs sanguins analysés, 7 marqueurs ont montré une corrélation significative entre les échantillons séparés sur le micro dispositif et le standard. Cela montre que le microdispositif peut être utilisé en combinaison avec des outils analytiques standards.

Le nouveau microdispositif présenté dans ce travail ouvre la voie à une famille de microsystèmes qui effectuent des opérations purement pré-analytiques. La performance du dispositif, la qualité des échantillons prélevés et les possibilités de combinaison avec les techniques d'analyse standard indiquent que le microdispositif peut avoir un impact sur les cycles de test actuels: le dispositif pourrait réduire les sources d'erreurs pré-analytiques en effectuant la séparation de microéchantillons sanguins au point de collecte.

Mots-clés : sédimentation; préparation d'échantillons ; séparation du sang; pompage capillaire ; microfluidique

Abstract

Laboratory blood testing plays a central role in current diagnostics and therapeutical decisions. Thus, errors have a direct impact on care quality and cost. The majority of errors occur in the pre-analytical phase, when samples are collected, stored and prepared. For biochemical analysis, the most common preparation operation is the separation of blood plasma: performing this operation upon sampling has the potential to simplify and render the testing cycle more reliable. Hence, in this work, a microdevice that performs blood separation at the point of collection is presented. The capillary-driven microdevice processes finger-prick blood microsamples without the need for external equipment.

The device relies on sedimentation as a simple and spontaneous driving force for the separation of undiluted whole blood. Blood flows in the device at a velocity allowing cells to settle on the bottom of a constant height channel and create a higher viscosity liquid fraction. The supernatant plasma of lower viscosity is pumped at a higher speed than the sediment in the device. Thus, as the device fills, a plasma plug is generated in the downstream section of the channel. In this work, a unidimensional model of combining Kynch sedimentation and Poiseuille flow theories is established to describe this novel separation phenomenon. The impact of design and blood parameters on the separation is studied.

The device can be used to separate fresh or anti-coagulated samples obtained through skin puncture. For both sample natures, the cell-free plug appears after a separation delay of 400 s. This delay is necessary to establish a sufficient viscosity contrast through sedimentation. Subsequently, for anti-coagulated samples, cell-free liquid is extracted with a 17 % yield. For fresh samples, coagulation leads to an increase of yield to 67 %. The combination of sedimentation and filtration through the clot are the reasons for this increase. Separated samples are retrieved from the chip through the use of an integrated ejection mechanism. The device is designed to eject a volume of 2µL of cell-free liquid out of 25µL of whole blood.

The quality of separated samples was established by measuring particle contaminant concentration and proteomic profile. The contaminant concentration is lower and more repeatable than in centrifuged plasma or serum samples. In the protein profile, only 4.5% of quantified proteins show significantly different levels between serum and chip-separated samples - thus, showing that the separated samples and serum could be used interchangeably.

The microdevice was combined with standard clinical automated analyzers to perform blood panels on 12 obese patients. Of the 8 blood markers analyzed, 7 markers showed significant correlation between the chip-separated and standard plasma samples. This shows that the microdevice can be used in combination with standard bench top analytical tools.

The novel microdevice presented in this work paves the way to a family of microsystems that perform purely pre-analytical operations. The performance of the device, quality of retrieved samples and combinability with bench-top techniques indicate that the microdevice could impact on current testing cycles: the device could reduce the pre-analytical sources of errors by performing blood microsample separation at the point of collection.

Keywords: sedimentation; sample preparation ; blood separation; capillary-driven ; microfluidic

Acknowledgments

This thesis has been a fascinating experience, both scientifically and personally. It was shaped through numerous interactions with inspiring and interesting people.

I would like to thank Prof. Philippe Renaud for the opportunities he has given me. His unconditional support and the freedom he grants his students are instrumental foundations in the lab successes. His versatile knowledge and comprehensive vision inspire me.

I would like to thank the jury members: Prof. Francois Gallaire, Prof. Aurélien Thomas and Dr. Elodie Sollier for acting as my jury, and Prof. Pierre-André Farine for presiding the jury.

I would like to thank the group of people I met through their contact or belonging to DBS Systems SA. I enjoyed collaborating with these supportive people during this work. Steve Béguin initiated this work and performed the flow cytometry experiments. We shared many interesting discussions and he was instrumental in establishing a significant part of the arguments in this work. Julien Déglon and Aurélien Thomas have performed the automated analyzer experiments and assisted in generated the samples for a number of analysis. Their vision of blood sample analysis drove this project and the company they founded. Tatjana Sajic has performed the mass spectrometry characterization reported in this work. Her help and involvement were greatly appreciated.

I would like to thank Duccio Malinverni for his help with the modeling aspects.

I would like to thank Guillaume Petit-Pierre, George Muller and David Bonzon. We shared many doubts and joys during our time in LMIS4. Starting the thesis simultaneously with David was a stroke of luck.

I would like to thank my colleagues in LMIS4: Amélie, Margaux, Patrick, Benoit, Ludovic, Stefano, Haine, Harald, Elodie, Sébastien and Marc. Thanks to Jonathan for all the brainstorming. I thank Arnaud for the critical inputs and proofreading. I would like to thank past colleagues: Sylvie, Sophie, Oscar, Pierre, Willyan, Fabien. I would like to thank my office mates with whom I have shared many thoughts and laughs: Rob, Mojtaba, Faye, Fatemeh, Clarisse. I have enjoyed being helped and helping the students I supervised: Niklas, Camille, Florence and Christian.

I would like to thank the many friends I have made in sport societies over the years. My close friends from Red Fish Neuchâtel with whom I have shared a passion and many unforgettable times: Bryan, Jeff, Florian, Jeremy, Emilie. Upon moving to the Lausanne area, I have enjoyed many sportive challenges and some laid back Sunday rides with the Rushteam Ecublens. I would like to thank its members for their friendship: in particular Matthieu, Daniel and Jean-Claude for making easy training days so rare and for proofreading part of this work. I would like to thank the lunch break runners from the BM building for the numerous jogs around the apple trees: Matteo, Yvan, Eric, Giancarlo, Tonio, Karim.

I would like to thank Estelle. She has been by my side during this journey. Her kindness and caring attitude, as well as her fascination with simple thinks, make sharing life with her a wonderful experience.

I would like to thank my family: my parents, Carmen and Daniel, for their support and unwavering belief in me; my sister, Sandra, for the complicity ; my grand-parents, Memela and Manolo, for their support and generosity which left a profound imprint in me.

Table of Content

List of Figures

List of Tables

Abbreviations

ACd	Acid Citrate Dextrose
CCL	Central Clinical Laboratory
CRP	C-Reactive Protein
CV	Coefficient of Variation
DBS	Dried Blood Spot
DLD	Deterministic Lateral Displacement
EDTA	Ethylenediaminetetraacetic acid
ESR	Erythrocyte Sedimentation Rate
FDR	False Discovery Rate
FSR	Forward Scatter
gGT	γ-Glutamyl Transferase
Hct	Hematocrit
HDL	High Density Lipoprotein
IFCC	International Federation of Clinical Chemistry
LOC	Lab On Chip
MBS	Modes of Batch Sedimentation
PBS	Phosphate-buffered saline
PDMS	Polydimethylsiloxane
POC	Point Of Care
RBC	Red Blood Cell
RCF	Relative Centrifugal Force
Re	Reynolds number
SSC	Side Scatter
SWATH-MS	Sequential Windowed Acquisition of All Theoretical Fragment Ion Mass Spectra
µTAS	Micro Total Analysis System

Chapter 1 Introduction to blood testing and associated separation methods

This chapter presents an overview of current blood testing practices. It discusses the impact of sample preparation on the reliability and efficiency of the whole process. Lastly, an alternative test cycle is proposed and the technological requirements for the associated sample separation method are established.

1.1 Blood : role and clinical pertinence

Blood makes up 7-8% of a human's mass: corresponding approximately to 5 liters for an adult (Hall 2010). It is the vital liquid flowing continuously through their veins and heart. Its role is to transport gases, nutrients, actors of the immune systems, and hormones amongst other. Blood movement is generated through the action of the heart. Gaseous exchanges occur upon its passage in the lungs (pulmonary circulation) and through the tissues (systemic circulation). Arterial blood is the oxygenated blood that flows through the arteries. In the capillaries, oxygen is partly transferred to the tissue and blood pH is lowered. The blood returning through the veins to the heart is the venous blood.

Blood volume is composed of approximately 55% of a liquid called plasma as illustrated in Figure 1:1a. This liquid fraction contains mainly water with salts and proteins. The 45% remaining volume is composed of cells: mainly red blood cells (RBC), or erythrocytes, that transport oxygen, leucocytes, that are immune cells, and platelets, that are cell debris and have a major role in blood coagulation. Figure 1:1b shows the repartition in concentration of the cellular components. Hematocrit (Hct) is the volume fraction of RBC in blood. The destruction of RBC and the release of their intracellular content in the plasma is called hemolysis (Hall 2010).

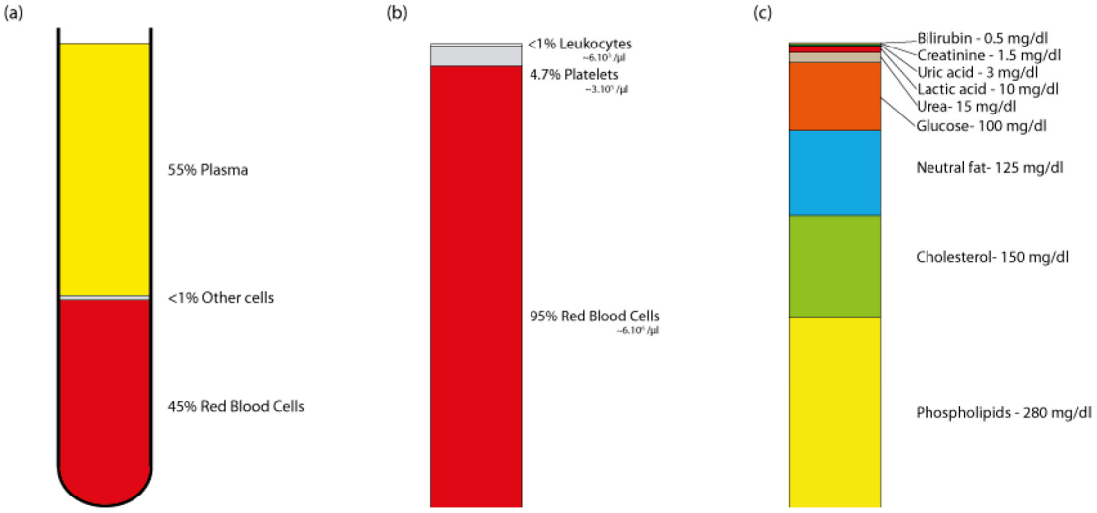

Figure 1:1: Blood content (a) Blood volume composition (b) Cellular content of blood (c) Non-electrolyte plasma molecules

Blood has a major impact in a large portion of laboratory test and in clinical chemistry in general (Burtis, A et al. 2008). Clinical chemistry is the study and analysis of the molecular content of bodily fluids (i.e. urine, blood, cerebrospinal fluid). The main matrices derived from blood in clinical chemistry are plasma and serum; plasma being the liquid fraction of whole blood and serum the liquid recovered from coagulated blood clots. Serum is similar in composition to plasma but differs in that it doesn't contain fibrinogen (the fibrin precursor essential in coagulation) and related compounds active in the coagulation process. Both fluids can be used interchangeably for most biomarkers: the main composition differences are the increase of potassium and absence of fibrinogen in serum, both due to coagulation (Lum & Gambino 1974).

Plasma is rich in markers used, for example, in toxicology, oncology, and endocrinology. The main analytical targets in plasma are electrolytes (such as calcium, potassium, etc.), lipids (such as phospholipids, cholesterol, etc.) glucose, gases, proteins, genetic or genomic material. Figure 1:1c shows a summary of plasmatic molecular content excluding electrolytes. As an example, in oncology, liquid biopsies often target blood and are used to replace the complex and risky traditional tissue biopsies (Crowley et al. 2013). Circulating tumor DNA is the usual analytical target and is present in plasma or serum.

Many analytical techniques can be used to quantify the plasmatic molecules of interest. Their detection might rely on optical techniques (photometry, spectrophotometry,...), electrochemical techniques (potentiometry, voltammetry, amperometry, coulometry,..), electrophoresis (2D, isoelectric focusing, capillary electrophoresis), mass spectrometry (often coupled with a chromatographic separation), or immunochemical techniques (ELISA, radioimmunoassays,...).

Clinical chemistry techniques have seen an important integration and automatization effort (Armbruster et al. 2014). Starting in 1956 with the AutoAnalyzer, for measuring urea, glucose and calcium, instruments have integrated and automatically performed several tasks (Kane & Sullivan 1970). They usually rely on mechanizing manual operations performed in a number of vials placed in the instrument. The automation aims at reducing the number of errors and increasing the reliability of the analysis by reducing the number of sample labeling, identification, and manipulation steps necessary. The reduction in operation complexity and the parallelism in such machines increase throughput

and repeatability. This contributes to the low number of errors shown in paragraph 1.2 below. On such devices, the measurement typically is based on photometry, fluorometry, turbidimetry, chemiluminescence or electrochemical technique. Pre-analytical steps might be integrated in the machine and consist typically of mixing, centrifugation and aliquot sampling steps (Burtis, A et al. 2008). Such pre-analytical automated operations are supposed to increase throughput and reduce errors but the quality of the raw sample received strongly depends on the collection, transportation and storage. These factors impact greatly the reliability of the final measurement: e.g. hemolysis depending on delivery time by courier service. Reliability and repeatability are increased when pre-analytical steps are performed as soon as possible after collection.

A common cause of sample deterioration is hemolysis: the process of membrane disruption that causes the release of the RBC intracellular content in the plasma, amongst which is hemoglobin. This process is visible through the pink coloration of the plasma noticeable by eye when the hemoglobin reaches 200 mg/L. If most tests tolerate slight hemolysis, severe hemolysis can have consequences on the results quality. For analytes that are at low concentrations in RBC, dilution of plasmatic concentrations occurs. For analytes at high concentrations in RBC, a more drastic change occurs as they are released in the plasma. This might create poor readings for analytes such as lactate dehydrogenase, potassium, magnesium and phosphate (Burtis, A et al. 2008).

1.2 Traditional macrosample testing and its separation

1.2.1 Typical model of blood testing

An extremely common and central operation - onto which most therapeutical decisions are at least partly based - is the laboratory test. The tests could be used for one of four reasons: diagnostic, monitoring, screening or research purposes. In the context of this work, the analytical matrix is supposed to be blood, even though the lab test cycle is similar for other biological matrices. A laboratory test requires the intervention of several actors: the clinician, the collection center, the analytical lab and the patient. Several of these actors might be geographically unified; e.g. a collection point with a nurse in an analytical lab. The laboratory test follows a laboratory testing cycle illustrated in Figure 1:2. This cycle consists of three phases: a pre-analytical phase, an analytical phase and a post-analytical

phase (Wians 2009). The pre-analytical phase starts when the clinician decides to perform the test and orders it. The sample of blood, in this particular case, is typically collected from the patient in a collection center through venipuncture performed by a trained nurse. The sample is then transferred to the lab where storage and sample preparation occur. The analytical phase consists solely of running the analysis, e.g. a Coulter counter, Mass Spectrometry or clinical chemistry automaton. The post-analytical phase starts in the analytical lab when results are computed and aggregated in a report. The report is then transferred to the clinician who interprets the data. Using this data and other information collected (such as imagery, symptoms and anamnesis), the clinician makes an assessment of the patient medical state and gives feedback to the patient and potentially starts or adapts his treatment.

The many operations and interactions needed to complete this laboratory test cycle make for a cumbersome process and increase the possible sources of errors. The patient in this typical model attends three appointments: 1. when the clinician establishes the need for the test (step1 in Figure 1:2), 2. for the sample collection (step3 in Figure 1:2) in the collection center, 3. for the feedback with the clinician (step10 in Figure 1:2). The patient is usually present physically at those meetings having the burden of commuting and freeing up time in his schedule. All other actors do not physically move as transfers are done either through transport services or in electronic format. Reducing the complexity, the burden and the turnaround time of this cycle would potentially allow for running more tests and increase the market for such analysis.

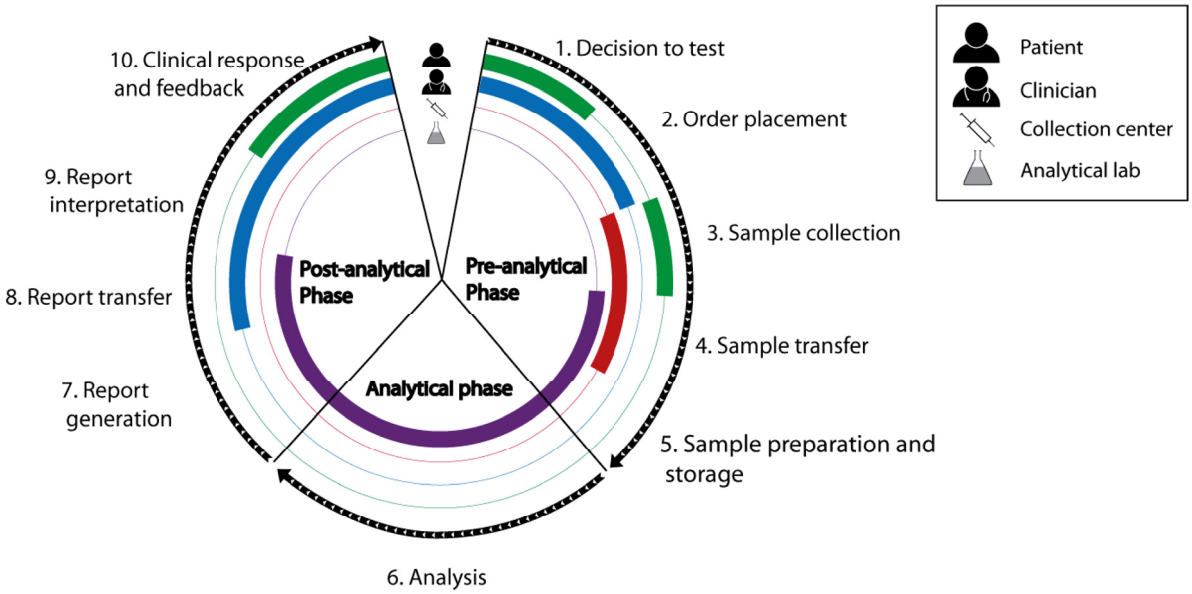

Figure 1:2 The Laboratory Testing Cycle. Each color circle corresponds to the intervention of an actor in the cycle step. Adapted from (Wians 2009)

First reports of errors during laboratory test date back to the 1950s (Henry 1953). At the time, the main worries were with analytical accuracy and reliability of laboratory methods. Since then, studies have shown that analytical methods have grown more and more reliable thanks to the efforts to improve, optimize and standardize operations, reagents and instruments (Ceriotti et al. 2012). However pre-analytical operations have not been subject to such efforts and nowadays fall short in terms of reliability. Studies performed in 1996 and 2006 (Carraro & Plebani 2007) in a hospital setting show that the total error rate is of 3092ppm in 2006 and a clear reduction from 1996 (4700ppm). The Padova hospital involved in these studies had 1750 beds in 2006 and performed approximately 8 millions tests a year. The number of errors amounts to 24700 errors a year. If a minority of errors occur in the analytical (15%) and the post-analytical (23%) phases, the vast majority of errors occur in the pre-analytical phase (62%) as illustrated in Figure 1:3a. This remains true eventhough the hospital made some effort to render the pre-analytical phase workflow more reliable after the first 1996 study. The main pre-analytical errors were: tube filling errors (13.1 % of total), patient identification error (8.8%) and inappropriate container (8.1%). These errors resulted, as an example, in poor quality samples, non-suitable sample volumes or untraceable samples. The errors had consequences in terms of cost for the hospital

and even in 25% of cases in terms of care for the patient. For such a medium size hospital, errors impacted 6200 patient coverage. The majority of cases of rejection before analysis were identified to be due to problems of quantity or quality of the sample collected (Lippi et al. 2013) : the major ones being insufficient volume and hemolysis or clotting. In San Raffaele Hospital in 2000 (Bonini et al. 2002), error rate was reported to be 6000ppm for inpatients solely for pre-analytical errors with the main issues, illustrated in Figure 1:3b, being hemolyzed (55% of pre-analytical errors), insufficient (21%), incorrect (12%) and clotted (5%) samples.

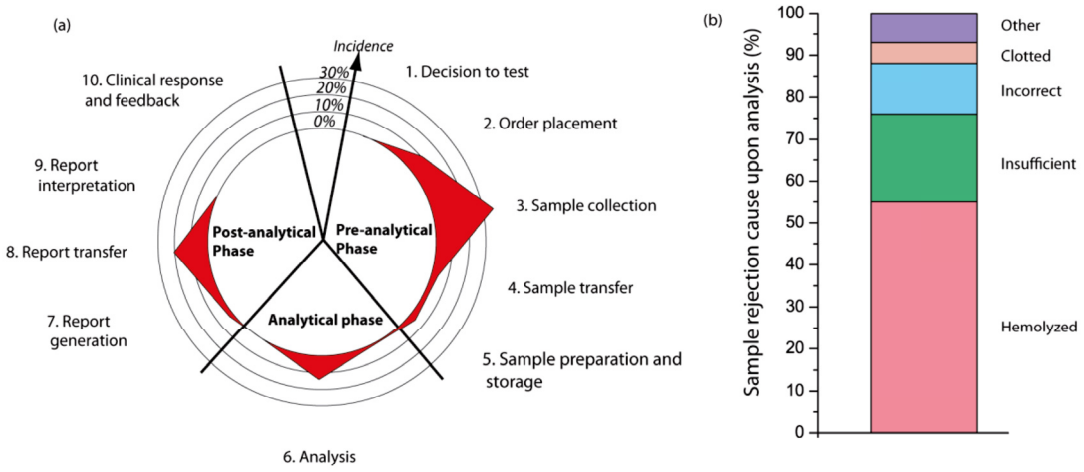

Figure 1:3 Errors in laboratory testing (a) Error burden repartition during the lab test cycle in Padova hospital in 2006 (Carraro & Plebani 2007) (b) Causes for sample rejection at the moment of analysis in San Raffaelle hospital in 2000 (Bonini et al. 2002)

Standardization organizations have only recently started working on a coherent way to analyze and prevent errors in laboratory test schemes (International Organization for Standardization. 2008). Quality indicators have been devised to assess the quality of laboratory services and more specifically the pre-analytical phase (Plebani et al. 2014). If workflow and administrative modifications are needed, some technological answers could greatly help make the process more reliable. The integration of most steps on a single platform could reduce some error sources: this model is discussed in section 1.3. Obtaining suitable samples for analysis could alternatively come from changing the test cycle structure to transferring only prepared samples to an analytical platform: such an alternative protocol is proposed in section 1.4.

1.2.2 Blood macrosampling and its separation techniques

The most common blood collection technique is venipuncture or phlebotomy. This technique consists of drawing venous blood from the vein of a patient (Burtis, A et al. 2008). This procedure requires a skilled nurse and is uncomfortable for the patient in terms of pain. Traditionally, a seated patient is pricked in the median cubital vein in the elbow crook. First, the skin is disinfected (if there is still alcohol on the skin it is known to cause hemolysis) before a tourniquet is applied to his arm. The tourniquet retains blood and dilates the veins. This tourniquet might cause venostasis which alters the components of the sampled blood compared to circulating blood. After the vein is pricked with typically a 0.8mm diameter needle, the tourniquet is released and an evacuated tube is connected. An evacuated tube is a plastic (more common) or glass tube that is under vacuum. This tube might contain an additive that is to be mixed with the whole blood. The evacuated tubes are filled until all vaccum is relaxed and a fixed volume of blood is metered so that additive to blood mixing ratios are correct. If a cannula is already installed in the patient's vein, the infusion root is to be stopped and a quantity of blood is to be drawn through the canula and discarded before the blood sampling can be performed. The contamination by the infusion root is a common cause of error in the pre-analytical phase. Arterial blood might also be drawn through arterial puncture most often for blood gas analysis. This operation requires considerable skills and is usually performed on radial artery of the wrist, brachial artery in the elbow or femoral artery of the groin.

The additives present in the evacuated tubes are usually anticoagulants or preservatives (Burtis, A et al. 2008). Anticoagulants are added to prevent the blot from clotting. Available coagulants include heparin, ethylenediaminetetraacetic acid (EDTA) and Acid Citrate Dextrose (ACd) amongst others. Preservatives are used to prevent alteration of certain parameters before analysis: such as sodium fluoride for light anticoagulation and glucose preservation. Heparin is the most common anticoagulation agent with EDTA and ACd being used when preservation of cellular components and molecular diagnostics are to be performed.

1.2.2.1 Separation through centrifugation

The process for separating the surrounding liquid from the suspended cells is most commonly centrifugation. Centrifugation is the process of separating multiphase liquids or suspensions of different densities through the application of a centrifugal

force. The centrifugation is performed in a swinging bucket or fixed-angle centrifuge. Centrifugal force at which the process is performed is called the relative centrifugal force (RCF) (Burtis, A et al. 2008; Gufer et al. 1998). This value is expressed as a multiplication of gravity ($x\ g$) and is computed as follows:

$$RCF = 1.118 * 10^{-5} * r * rpm^2$$

Equation 1:1 – Relative centrifugal force computation

where r is the radius of the centrifuge from center to bottom of centrifuged tube and rpm is the rotation frequency.

Plasma and serum separation are both performed through centrifugation; plasma separation being the most common one. For plasma separation, anti-coagulated whole blood tubes are processed in a refrigerated centrifuge for 10minutes at 1000-2000 x g (ThermoFischer n.d.). If platelets are to be depleted, 2000 x g are applied during 15minutes. For serum separation, before centrifugation, the blood sample is allowed to clot for 30-45min in a vertical position in a non-anticoagulant or clot activator coated tube. Then, similarly to the plasma sample, centrifugation is performed at 1000-2000g for 10minutes in a refrigerated centrifuge. Following serum or plasma separation, supernatant aliquots are taken and stored at 2-8°C. If a significant amount of time separates the separation from the analysis, samples are to be stored at -20°C or lower. Centrifugation is a very effective method for separating large amounts of blood in a relatively short time. However, the process requires several steps of pipetting by an operator. Thus, a trained operator is required and operator-dependent variability may be introduced. The bench-top equipment required is complex, expensive and cumbersome. The operation of the centrifuge also usually requires training.

1.2.2.2 Separation through filtration

Centrifugation is the ubiquitous method for blood separation for testing purposes. However, blood separation is also performed in a therapy called plasmapheresis (Nosé & Malchesky 2000). In plasmapheresis, the plasma of the patient is extracted continuously and replaced either by the same plasma altered or substitution plasma. This therapy requires the continuous extraction of blood from the patient and the continuous separation of the patient plasma. This operation can be performed either by continuous centrifugation or filtration. Filtration is usually performed in a crossflow configuration (perpendicular to the main flow

direction) through a porous membrane with submicron pore sizes. This method is cumbersome for any non-continuous separation to be envisioned and, as mentioned in latter sections for microfiltration, is subject to hemolysis and membrane affinity issues.

1.3 µTAS microsample testing and its separation

1.3.1 µTAS testing model

Microfluidic is "the science and technology of systems that process and manipulate small amounts of fluids using channels with dimensions of tens to hundreds of micrometers" (Whitesides 2006). If this field existed priory, the 1990s have seen a strong increase in interest for microfluidics. Amongst other factors, the explosion of microanalytical methods and genomics in the 1980s and the technical advances in microelectromechanical systems in silicon were influential factors leading to the creation of the field (Whitesides 2006). In 1990, the creation of the micro total analysis system (µTAS) concept is the emblematic beginning of an era of intense microfluidic research (Manz et al. 1990). Those systems are the unification in a single microfluidic device of the liquid handling (e.g. sample preparation, mixing) and microanalysis (e.g. fluorescence, electrical) steps usually performed on complex bench-top laboratory equipment. Later a more generic term was introduced: Lab-On-a-Chip (LOC). This concept describes any microfluidic alternative one or several bench-top standard methods with integrated microfluidic. These systems could be used to reduce labor intensive operations, minimize reagent use, take advantage of small precious sample, reduce operation time or decrease costs (Volpatti & Yetisen 2014; Sackmann et al. 2014). Their potential for field testing or low resources laboratories is obvious. Since the inception of the field, researchers have made efforts into using more convenient materials such as thermoplastics and silicone, building new functions such as valves, mixers, etc... The phenomena used in those devices usually take advantage of the low influence of inertial forces and the high surface-to-volume ratios at these scales. If those devices have had great success in academic settings, barring for a few exceptions, their commercial impact is still limited when compared with bench-top tools. A strong barrier for the adoption of those systems is the use of the devices that still usually requires manual operations and external equipment (such as pumps or energy sources)(Mohammed et al. 2015; Volpatti & Yetisen 2014). Often sample

pretreatment or metering are necessary and liquid loading needs to be performed. That is why usually a skilled trained operator is still required. Simple operation-free impactful microfluidic devices are required to replace standard bench-top technologies.

Microsample preparation systems are usually meant to be integrated in or are already part of µTAS devices. Those devices are typically used in a two-actor testing configuration where the doctor prescribes the testing and the patient executes the sample collection and the analysis himself. He then reports back to the clinician for the interpretation and feedback. This model usually completely discards the need for an analytical lab. As described in 1.2.1, the analytical phase has grown to be a very efficient and reliable phase. The technologies used in the analytical labs have been refined and made ever more reliable by decades of incremental developments. Thus, the clinicians have trust in current analytical methods. The flexibility and the robustness of the methods are recognized and machines are standardized and certified. The trained and qualified operators are also less prone to misuse the devices. The data compiled in the lab report already has seen some degree of technical interpretation (possibility of false positives, analytical methods shortcomings, specificity, sensitivity, etc.) that can guide the medical interpretation and therapeutic decisions. These factors lead to the difficulty of implantation of a 2-actor µTAS testing cycle.

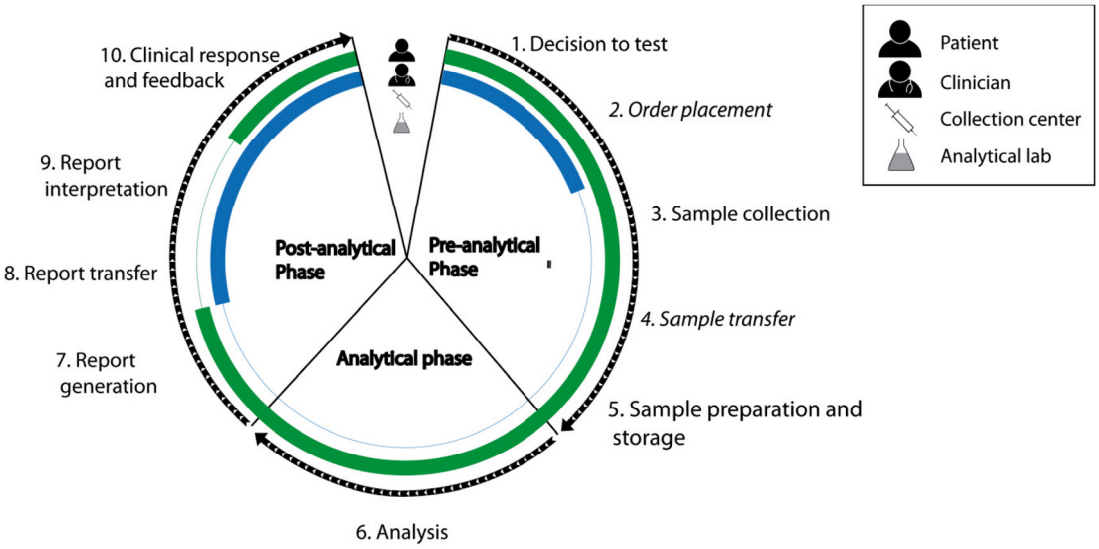

Figure 1:4 : µTAS testing cycle: two actor configuration

With patient-oriented devices, the scheme can even be reduced to a 1-actor µTAS testing cycle: the patient decides unilaterally to run the test, collects the samples, runs the µTAS, receives the data and decides how to act on it (Waltz 2017). This approach, while completely empowering the consumer/patient, contains many risks through the lack of intervention in the cycle of experts in the analytical and medical fields. Even though, the devices sometimes have some automatic data interpretation capabilities replacing the analytical expertise needed. The self-testing schemes might increase the general level of health level consciousness but might also increase fears and angst. A wide number of untargeted tests on normal population would result in an elevated number of false positives possibly hiding the real diseased population. The number of medical visits and additional tests or imagery needed due to abnormal µTAS results might put health systems under heavy load. On the contrary, patients with low health awareness might test themselves insufficiently. The intervention of the clinician in the scheme at the moment of making the decision to test is instrumental: he takes the responsibility (thereby possibly reducing patient stress) and makes an inform decision to test based on a number of factors (medical history, family history, symptoms, observation,...). These factors help target the possibly diseased population and reduce the number and impact of false positives. Also, the clinician's interpretation of an abnormal test result takes into account these factors thereby detecting false positives or negatives. The clinician has a more comprehensive view of the patient health status that is not limited to the sole test result and orients his therapeutic decisions in accordance : clinician don't treat lab results, they treat patients.

1.3.2 Blood microsampling and its separation techniques

Skin puncture is a capillary blood collection method usually used to retrieve small volumes of blood. This blood microsampling method is usually employed to retrieve between 5 µl and 500 µl of whole blood. The convenience of this method makes it an excellent candidate when frequent sampling is needed (even in animal trials)(Parasuraman et al. 2010). However, for very low concentration analytes, such small volumes might not be adequate due to the small quantity of analyte in the microsample. Traditionally, skin puncture is performed when either small blood volume is available (in infants for example), repeated venipuncture damaged the patients veins or burns and bandages cover the venipuncture sites. Alternatively, point-of-care (POC) analytical devices have also used this sampling

method. Three main collection sites have been used to collect capillary blood: fingertips, earlobes or heels for infants (Lenicek Krleza et al. 2015). The procedure starts by cleaning the skin of the patient with an alcohol based solution. When the skin has dried, the skin is punctured by a fast stab with a lancet. Massage is to be avoided as it might contaminate the sample with cellular debris and interstitial fluid. In case of need, warming the area for a few minutes is recommended to increase arterial blood flow to the area. After the first blood drop is discarded, the sample can be retrieved in 2 forms: liquid or dried form. Liquid samples are usually retrieved in capillary blood tubes loaded through capillary forces. These tubes, which might be coated with additives, should be loaded at once to prevent bubble formation. Issues of mixing are common in coated microcapillaries and surface interaction have a predominant role with containers of this size (Bowen et al. 2010). Alternatively, dried samples are handled as dried blood spots (DBS). Again, after the first blood drop is discarded, a large drop of blood is absorbed into a filter paper all at once in order to completely fill a printed circle on the collection card. The liquid is let to dry at the contact of air at ambient temperature for 2-3 hours before packaging in an envelope. This method inactivates enzymes and pathogens in the sample reducing security risks.

For most markers, arterial, venous and capillary blood samples are equally relevant (Lenicek Krleza et al. 2015). As an example, the acid-base panels exhibits excellent correlations between the three types of samples in terms of pH, PCO2,PO2, base excess and HCO3 (Yildizdaş et al. 2004). Capillary blood is however closer to arterial blood than venous blood, especially if the sample was taken after warming of the puncture area. Capillary blood glucose concentration is reported to be higher than venous concentration due to its metabolism in the tissue (Kupke et al. 1981). The contamination with interstitial and intracellular fluid typically dilutes sodium, chloride and protein content and increases potassium concentration. Dilution is still marginal in most cases (<5%) (Kupke et al. 1981) and variations stay below any therapeutically significant difference.

1.3.2.1 Standard separation methods for microsamples

Similarly to macrosamples, the standard method used for separation of blood microsamples is also centrifugation (Bowen et al. 2010). The samples are collected in glass or plastic micro capillary tubes for this operation. The tubes are sealed on one end either with a cap or a plug in the tube. The samples are then placed in a

centrifuge for separation. This method is most common for hematocrit determination with high centrifugal force for strong cell packing (Strumia et al. 1954).

1.3.2.2 On-chip separation methods

Microfluidic systems have been developed for blood processing since the birth of the domain. Analytical systems, bearing a few exceptions, require off-chip sample preparation and lack any integration of this process. Lab on-chip (LOC) approaches for plasma/serum separation have been proposed since the mid-2000s. This section will go through an overview of available on-chip techniques. These techniques are predominately aimed towards microsamples however some high throughput continuous methods could be used for venipuncture or dialysis applications. All methods will be presented here, commenting on their adaptability to microsample volumes. Device performance is usually characterized around two numbers: purity and yield. Purity is the percentage of rejected cells compared to the total number of cells in the raw sample. Yield is the separated volume percentage compared to the total volume of the raw sample.

A main division between methods can be elaborated on whether there is an external field applied by the device or not: they are active vs. passive devices. Passive devices, sometimes referred as "fluidic-only", rely only on spontaneously occurring phenomena in a flowing liquid at microscale. In passive methods, cells are separated through physical properties such as size, deformability, density, etc. Sedimentation, even though gravity is an external force field, is considered to be a passive method as no external force field is applied by the device. Active methods use an electrical, magnetic, acoustic or centrifugal external force to separate cells from their surrounding liquid. These separation methods rely usually on properties such as dielectric, magnetic or mechanical. If the separation method is described here as passive or active, the pumping mechanism could be also described as such, depending on the method for generated pressure. The devices will be separated in pumpless and pump actuated devices. This document will prefer *capillary-driven* to describe devices were surface tension forces generate the driving forces for the liquid propagation. Passive and active will hereafter be used to solely describe the separation methods.

Sedimentation is a phenomenon that is used commonly in hematology as a test where erythrocyte sedimentation rate (ESR) is measured. This spontaneous

separation is used in different implementation in microfluidic systems either alone or combined with filtration for increased performance, as illustrated in Figure 1:5. A common characteristic of a number of microfluidic systems based on sedimentation is to use multilevel structures to take advantage of the vertical separation of the different components of blood. Trenches might be used to take advantage of this stratified phases structures (Dimov et al. 2011; Samborski et al. 2015). Dimov *et al.* have developed a vacuum-driven (self-generated in vacuumed PDMS structures) system generating plasma by filling a trench and having an outlet at the top of the trench (Dimov et al. 2011). Once the trench is filled, the supernatant plasma - generated gradually during the filling of the trench - enters the plasma outlet. The plasma subsequently enters a channel where fluorescent biotin is immobilized and detected. Plasma purity reported is excellent through microscopy observation and yield is not reported using undiluted whole blood. Samborski *et al.* have developed a similar system, however with a milimetric trench that is rapidly filled before pumping is stopped (Samborski et al. 2015). After a 6 to 8min delay time, 6 µl of supernatant plasma is extracted through an output channel. The purity achieved is not characterized and yield is reported to be approximately 20% with undiluted whole blood. The device is integrated with reagent mixing and onchip spectrophotometric detection. Zhang *et al.* devised a system using a backfacing step to separate plasma from 1:5 diluted whole blood (Zhang et al. 2012). This structure uses a 90^{o} steering angle of a glass channel to convert vertically stratified flows to side-by-side flows of plasma and cellular suspension before the backfacing step is used for separation. A combination of sedimentation and crossflow filtration is described by Tomoya *et al* (Tachi et al. 2009). Small channels are placed perpendicular on the top part of a main supply channel and bring supernatant plasma to a parallel channel. However, this device required the dilution of blood sample with 1:9 parts of PBS. Sun *et al.* developed an approach consisting in blood sedimentation in plugs (Sun et al. 2012). Blood plugs are created and segmented by an oil phase in tubing. The combination of sedimentation and droplet movement separates the cellular components to the rear part of the droplet considering droplet movement direction. Those droplets are then fragmented and a colorimetric reaction is then used to characterize the plasmatic cholesterol content. As the separation time and efficiency is highly dependent on viscosity and thus hematocrit, a 1:5 to 1:10 dilution was used on the blood samples. A 30% yield was achieved in each plug with such dilution ratios.

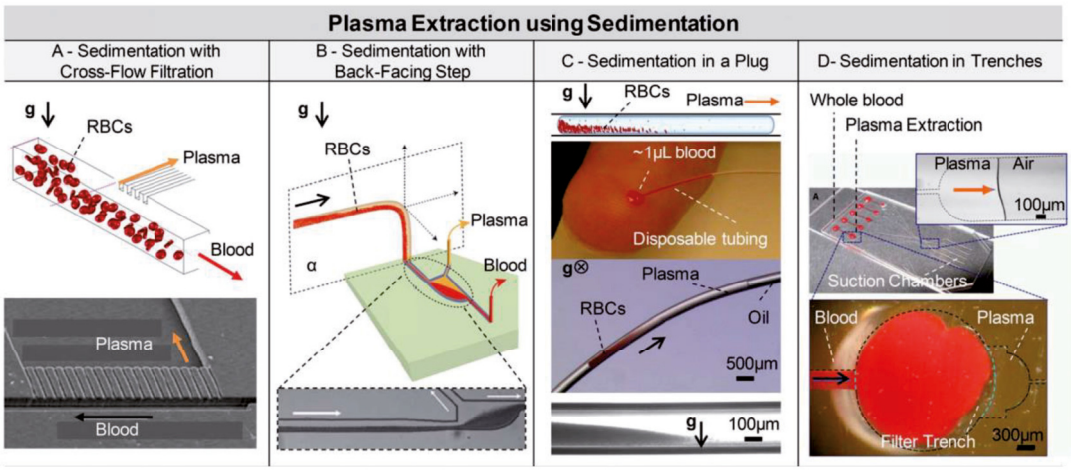

Figure 1:5 : Plasma Extraction using sedimentation. Reprint from (Kersaudy-Kerhoas & Sollier 2013)

Filtration is an obvious method to exclude components of blood. The filter uses pores defined in the structures to geometrically exclude cellular components bigger than the pore size from the flow of liquid. Two configuration have been reported : *dead-end* where the cell-free liquid is extracted in the direction of incoming cell suspension and *cross-flow* where the cell-free liquid is extracted perpendicularly to the incoming cell flow, as illustrated in Figure 1:6. Commercial membranes for filtration of macrosamples have been integrated in microfluidic systems. Thorslund *et al.* placed a portion of such membranes in a PDMS structure (Thorslund et al. 2006). To avoid cell breakage and leakage, hematocrits were adjusted to 20%. This hematocrit allows for a viscosity sufficiently low for the separation to be performed at reasonable pressure, hence reducing mechanical stress on RBC and thus hemolysis and cellular components deforming through pores. A similar approach was reported by Homsy *et al.* in a rigid polycarbonate and UV-glue sandwich (Homsy et al. 2012). Clogging is usually an issue with such devices even when the membrane size is in the millimeter range. Wang *et al.* showed the strong dependence of the pore size on clogging and cellular components passing the membrane (Wang et al. 2012). In their approach, samples are effectively diluted 1:4 before passing the membrane. Microfilters have been reported to be created *in-situ* by packing micro-beads in a microchannel. Shim *et al.* have assembled 100 µm and 10 µm glass cycles in a microchannel to perform dead-end filtration. The yield achieved from a 5 µl whole blood drop was of 7% (Shim & Ahn 2012). Crowley *et al.* report a crossflow filter microfluidic system for blood filtration. The filtration pores were 500 nm in height and excluded by this dimension alone the passage of

cells (Crowley & Pizziconi 2005). Blood samples of 20% or 40% hematocrit were used with little difference in observed flux of plasma. The yield observed was shown to be 0.28% to 0.9% from a 5 µl blood drop. No cells were observed by microscopic inspection but the high pressure through the pore caused a strong hemolysis in certain configurations. Chen *et al.* explored weir and pillar structures for isolation of leucocytes from whole blood and showed pure plasma separation solutions (Chen et al. 2008; Chen et al. 2007). Sollier *et al.* reported serpentine and U-shape cross flow filter for filtration of 1:10 diluted whole blood with 5% plasma retrieved (Sollier et al. 2009). If flow rates can be high, in general, clogging is the main limiting factor when using microfiltration methods. The filter after a limited operation time is saturated and the extraction stops. Strategies for unclogging and limiting the saturation time of the filter were devised, such as back pulsating flows (Vandelinder & Groisman 2006) but only marginally limit the clogging. The small pore geometry and the high viscosity of undiluted whole blood usually require an operation of the chip at high pressures. Cells trapped in the filter experience high mechanical stress and consequently hemolysis is a very common problem. Depending on the pore size, cell leakage through the filter can be an issue when the highly deformable blood cells experience a high mechanical stress. In microfiltration devices, the surface to volume ratio is high due to the high porosity and small pore size. These areas, depending on their affinity, could strongly deplete the retrieved plasma in certain molecules, drugs or proteins.

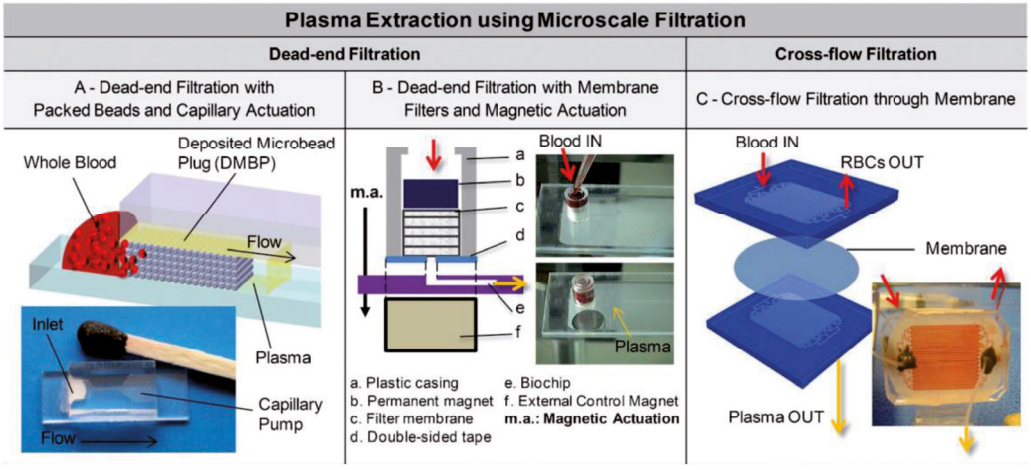

Figure 1:6 : Plasma Extraction using microscale filtration. Reprint from (Kersaudy-Kerhoas & Sollier 2013)

Cells flowing in microfluidic systems are subjected to forces that naturally or artificially create a deviation of the cells and deplete them from a certain region of the flow. These phenomena can be used to separate plasma from whole blood, as illustrated in Figure 1:7. In 2004, Huang et al. proposed the first Deterministic Lateral Displacement (DLD) device (Huang 2004). This device consists of a circular pillar array placed in the flow. Each pillar row is slightly offset laterally compared with the previous row. A thin lamina of flow passing near a pillar will go straighter through the array by going around the opposite side of the subsequent row. Flow further from this pillar, does not follow this zig-zag pattern and keeps on the same side of subsequent pillar rows. Small particles with geometrical center within this thin lamina will zigzag between the pillars, whereas bigger particles will go straighter through the array. Cell or liquid can be retrieve from different sections of the array outlet. If this structure is very convenient, for cell sorting, it is more rarely reported for plasma extraction. Davis *et al.* demonstrate two devices adapted for blood fractionation or plasma separation. The devices consist of three areas of decrease pillar pitches with an adjunct area for sorted element storage to prevent clogging of the subsequent thinner array. DLD devices are prone to clogging of the complex and thin pillar arrays by big cells present in blood. The flow regimes here usually require low flow rates. At Reynolds numbers lower than one, flows are laminar and free of turbulence. Forces on particles, in these regimes, are dominated by viscous forces. In microchannels, viscous lift forces tend to push cells towards the center of the channel and create a cell-free liquid layer against the wall: the Farhaeus effect (Fahraeus 1929). This cell-free layer is usually collected by creating a bifurcation. In a bifurcation, following Zweifach-Fung bifurcation law, if flow rate ratios are higher than 1:2.5 and the cell diameter is comparable to the channel size; all particles will go through the high flow rate channel (Zweifach & Intaglietta 1968; Fung 1973). Faivre *et al.* were the first to implement a device taking advantage of the Farhaeus effect and a constriction/expansion geometry to continuously separate plasma through side channels from whole blood diluted to 16% hematocrit with 12% yield (Faivre et al. 2006). The Zweifach-Fung bifurcation law was used specifically by Jaggi *et al.*(Jäggi et al. 2007). 2.5% yield and 92% purity were achieved with 1:9 diluted bloods. The quality of plasma reduced drastically with physiologic hematocrit: 4% yield and 31% purity were achieved with undiluted blood. Yang *et al.* showed a device based on 5 subsequent bifurcations extracting plasma from a whole blood

channel (Yang et al. 2006). The device yield was of 24% with 35% hematocrit blood. Fan *et al.* presented a similar device with an integrated barcode assay for protein detection based DNA-encoded antibody library technique (Fan et al. 2008). Works have shown the combination of such viscous phenomena with the apparition of other effect at intermediate Reynolds numbers. Sollier *et al.* reported the apparition of vortices in an enlargement (Sollier et al. 2010). Kersaudy-Kerhoas *et al.* showed a similar phenomenon when they combined a constriction/expansion area with a down-stream bifurcation (Kersaudy-Kerhoas et al. 2010). When Reynolds number (Re) increases to numbers higher then 1, inertial forces start to dominate viscous forces. In such systems, equilibrium position of particles is described for macroparticules in large pipes: in circular pipes, particles of same size focus on an annulus called the Segre-Silberg annulus (Segré & Silbeberg 1961). This phenomenon is also noticeable in microsystems (Di Carlo 2009). The focusing is the effect of two forces acting on the micro spheres: (i) a shear-gradient lift force, due to the parabolic flow velocity profile, that pushes particles towards the wall of the channel, (ii) a wall effect that directs the particles away from the wall, caused by the interaction of the particles wake with the wall. Therefore, depending on their size, particles tend to reach different equilibrium positions. This method is often used to separate, sort and extract particles of different sizes (Di Carlo 2009). This method was used by Mach *et al.* to extract bacteria contaminated plasma from a blood sample (Mach & di Carlo 2010). Samples used in this study were diluted 200x prior to running experiments. Contrary to Fahraeus effect based separation, the red blood cells tend to concentrate at a fixed distance from the wall leaving a large central flow portion containing low concentrated small particles. The yield achieved here is 40% but purity is limited to 82% with a significant hemolysis. The device performance is strongly affected by cell concentration and viscosity; hence the need to work with such strongly diluted samples. In bent or curved channels, in flow regimes where Re>1, vortices –called Dean vortices - appear perpendicularly to the global flow rate direction (Sudarsan & Ugaz 2006; Di Carlo 2009). This phenomenon is due to the difference in velocity between the fast channel center area and the slower near-wall areas. Due to inertial forces upon encountering the bend, the central part tends to flow to the outside of the curve. This movement creates two symmetrical secondary flows which form the Dean vortices. The vortices create a flow towards the outside of the bend in the middle of the channel that circulates back to the

inside along the top and bottom wall. In addition to inertial forces, particules are subjected to this flow and new equilibrium postions are generated (Carlo et al. 2008; Di Carlo et al. 2007). The advective transport involved in this process makes for a faster focusing. Blattert *et al.* proposed the combination of a single bend channel adjunct to a bifurcation for blood plasma separation (Blattert et al. 2005). Centrifugal forces increase the cell-free layer thickness and purity before the bifurcation. The sample purity had a strong dependence on hematocrit with approximately 40% purity for physiologic hematocrit and 90% for 10x diluted whole blood. The yield claimed is in the range of 5-10%. Morikawa *et al.* used a spiral structure before a bifurcation to separate plasma from blood (Morikawa et al. 2012). Experiments conducted with 400x diluted blood led to purity of approximately 90%. Nivedita *et al.* used a similar structure to extract plasma from 50x diluted blood (Nivedita & Papautsky 2013). Devices based on purely passive cell deviation in microfluidic system, suffer from a strong drawback: the need for strong dilution. The processes involved imply usually using low viscosity and low concentration to prevent particule-particule interactions. Yield and purity are usually a tradeoff in those systems: cascading such systems to perform the operation on ever less concentrated samples with each cascade seems to be a strong candidate for improvement. If those systems are not necessarily suited for extraction of blood from microsamples, the strong flow rate used in these methods (especially when operated at Re>1) makes them good candidates for separation of sample of volumes in the order of magnitude of milliliters or for continuous separations.

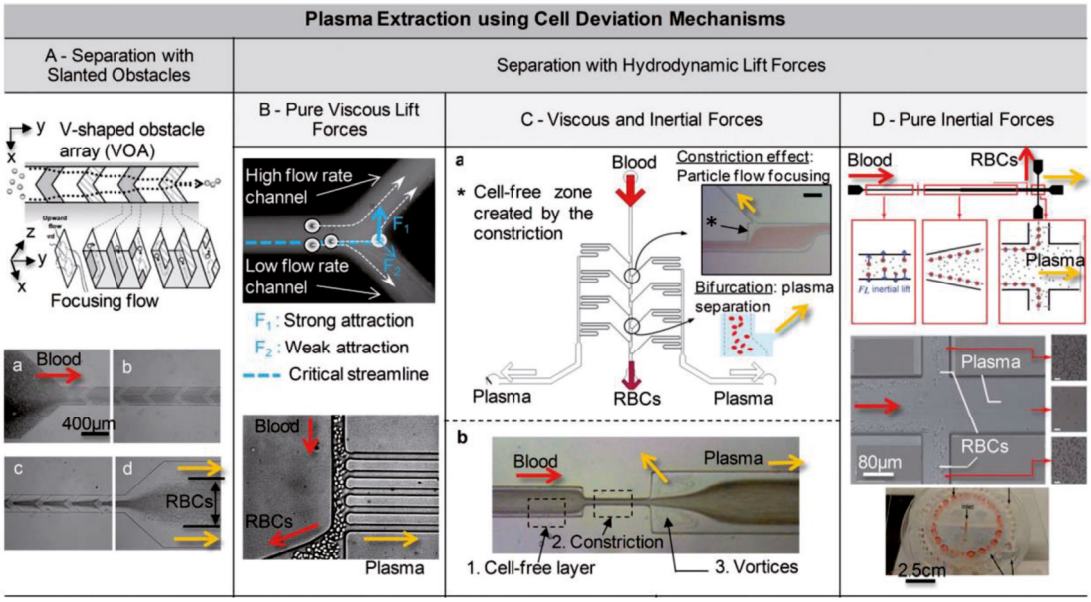

Figure 1:7 : Plasma Extraction using Cell Deviation Mechanisms. Reprint from (Kersaudy-Kerhoas & Sollier 2013)

If microfluidic systems described in this chapter are traditionally based on a channel configuration, paper-based devices are making a strong impact in the microfluidic applications. If lateral flow assays are common, new and innovative devices have been recently developed on paper support (Martinez et al. 2007; Bruzewicz et al. 2008; Martinez et al. 2010). Paper-based devices performing plasma separation rely not only on the paper matrix for performing filtration but also for being the matrix where liquid flow occurs: pumping the liquid through capillary forces. Chromatography paper used by Yang et al. has a pore size insufficient to exclude single RBC from the flow (Yang et al. 2012). Agglutinating antibodies are spotted and dried on the area of whole blood spotting. Upon blood dispensing on this area, RBC agglutinate and are thus excluded from the flow of plasma reaching the outer areas of colorimetric detection. Purity claimed is approximately 90%. Commercial membranes assembled to paper devices have been devised in different configurations. A filtration membrane and paper chip with wax channels was reported by Songjaroen *et al.* (Songjaroen et al. 2012). Blood is spotted on the filtration membrane and plasma is transported by capillary forces to an overlapping chromatography paper. On the chromatography paper, colorimetric protein detection is performed. Robinsion *et al.* use a similar approach, assembling filtration membranes and glassfiber pads to perform phenylalanine detection (Robinson et al. 2016). Commercial membranes have also

been assembled in a 3D layered structure (Vella et al. 2012). A stacked membrane and a wax-printed paper device are vertically assembled and colorimetric protein detection is performed. The waxprinting technique allows for defining hydrophilic and hydrophobic areas thus defining the absorbent detection areas. Kar *et al.* demonstrate a novel approach by creating H-channel structures (Kar et al. 2015). In this structure, buffer and whole blood are injected side by side in a channel where molecules diffuse to the buffer from the blood flow whereas cells tend to stay in the blood flow because of their low diffusion coefficient. Two outlets are placed at the distal end of the channel to form a cell suspension area and a clear liquid area containing an amount of plasma components depending on their diffusion coefficients. In general, paper-based devices for separation offer a low yield and low purity plasma. The ease of integration with other paper-based detection method is a clear advantage of these methods. However, the retrieval of sample for on-chip standard microfluidic analysis or off-chip analysis is difficult.

Active separation techniques use the application of an external field, usually by cumbersome off-chip equipment, to separate blood cells from their surrounding liquid. The field applied can be acoustic, electric or magnetic and, for non-conventional formats, centrifugal. In free flow acoustophoretics, an acoustic standing wave field is established by acoustic resonators. The particles in this field will be submitted to forces pushing them towards the nodes or anti-nodes of the system depending on their mechanical properties and those of the surrounding medium(Laurell et al. 2007; Lenshof & Laurell 2010). Free flow acoustophoretics has been used to focus efficiently the cellular components before extracting the surrounding plasma and cellular suspension in dedicated channels (Nordin & Laurell 2012). Manipulation of uncharged particles through non-homogeneous electric field is called dielectrophoresis. Depending on the polarizability of the particles and the frequency of the field, the particles will be pushed to high or low field concentration areas. This method was reported to be used to extract at low yield plasma from trapped cells (Nakashima et al. 2010). In a magnetic field, blood cells can be displaced either in a diamagnetic or a paramagnetic state(Pamme & Wilhelm 2006; Han & Frazier 2006). This separation method requires a complex sample preparation or the mixing of additives, which makes it inconvenient (Rodríguez-Villarreal et al. 2011). CD-based microfluidic systems use the centrifugal force generated in a CD player platform to generate liquid movement, mixing, valving, etc. The high centrifugal field in the system submits the blood

cells to strong inertial forces that lead to a migration of the cells to the outer part of the chip. A siphon design extracts generated plasma from the centrifugation channel. Purity and yield are relatively high in this technique. This process is fast but such strong forces tend to damage cells as demonstrated by the pink colored plasma retrieved, sign of a probable strong hemolysis.

The technologies presented here offer different characteristics summarized in Table 1:1. There is no universally more efficient method: depending on the requirements in terms of throughput, available sample volume, yield, purity or tolerance to hemolysis, a different method would be more adequate. As an example, for continuous separation, cell deviation techniques are more adequate due to the high flow rates in the systems. However, these methods require external pumping systems and sample dilution.

Table 1:1 : Performance comparison of microfluidic separation methods

Methods	Advantage	Disadvantage	Sample
Sedimentation	Low hemolysis No precise flow rate required No dilution	Time efficiency might be low Extraction rate low	Microsample
Microfiltration	High extraction rate	Clogging and low yield Hemolysis and low purity with pressure Membrane surface affinity with analytes Often dilution to reduce clogging	Microsample
Cell deviation	High extraction rate Continuous operation Flexible designs	Dilution needed Precise external pumping	Continuous
Paper devices	Simple and cost effective	No sample retrieval Limited testing	Microsample
CD devices	Adjustability of force	External equipment needed Hemolysis at high extraction rates	Microsample

Blood plasma separation microsystems have usually three major technical major shortcomings (Mielczarek et al. 2016) : (i) sample pretreatment requirements, often dilution thereby requiring a skilled operator with laboratory equipment, (ii)

complex designs inconvenient for mass-production or requiring external equipment such as external field generators, (iii) time consuming workflow rendering the devices non-competitive with operation times of bench-top equipment. These are the main technological barriers for the spreading of those technologies.

1.4 Proposed testing model: sample preparation at the point of collection

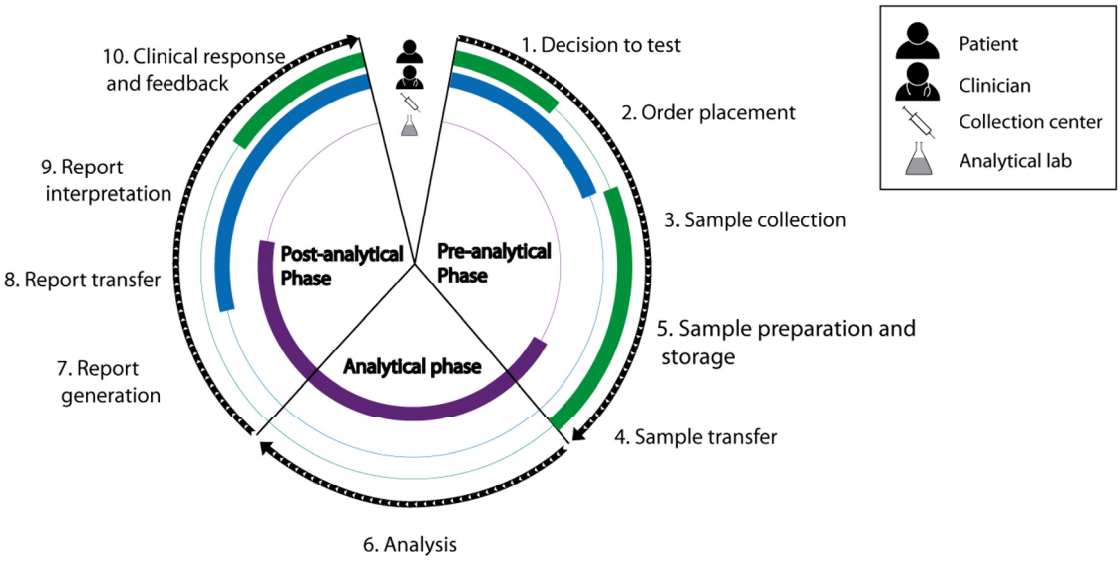

Figure 1:8 : Testing cycle with separation at the point of collection: a 3-actor testing scheme

The previous paragraphs exposed the shortcomings of different models of testing cycles. The traditional 4-actor model is complex and the pre-analytical steps are unreliable whereas the 2-actor and 1-actor µTAS models lack technical and/or medical interpretation and expertise, thus endure the low acceptance of professionals.

A 3-actor model, as illustrated in Figure 1:8, where sample preparation is run at the moment of collection (possibly by the patient himself), would solve those shortcomings. A microfluidic sample preparation device would integrate the necessary sample preparation steps such as blood separation and plasma volume metering in the particular example of this work. Running this operation at the moment of collection, before transportation, has the potential to improve preanalytical quality. Following the International Federation of Clinical Chemistry and Laboratory Medicine (IFCC) analysis tools (Plebani et al. 2014), such devices

would improve the quality indicators shown in Table 1:2. If pre-analytical steps are rendered more reliable, the robustness and expertise of the analytical laboratory is preserved in this model as well as the medical expertise.

Table 1:2 : Selected quality indicators impacted by a sample preparation in a microdevice at the point of collection (Plebani et al. 2014)

Quality indicator identifier	Symbol	Note
QI-10	Hemolysed sample	No cells for hemolysis
QI-11	Clotted	No cells for clotting
QI-12	Insufficient volume	On-chip metering
QI-13	Inadequate anticoagulation	No cells for clotting
QI-14	Damaged in transport	More stable samples
QI-16	Improperly stored	More stable samples

This scheme, with blood sample separation at the point of collection, also presents some drawbacks. The number of tests possible with such a separation step is reduced to chemistry tests: hematology test such as cell counts are not possible if cells are removed. This testing cycle, even though performable in in-house laboratories, would favor delocalized laboratories. The delocalized laboratories, now a tendency for 15 years, imply longer and thus riskier transports and a longer global turnaround time then in-house laboratories. They however have high throughput, high reliability and low costs of testing. Contrary to the 2-actor µTAS model that could make a single medical visit for the whole test cycle possible, the 3-actor approach would most probably require two medical visits. Also this approach requires the presence of an infrastructure for sample transportation and analysis that is not present in some environment such as developing countries where a 2-actor model is easier to implement.

1.5 Aim

The following work presents a device for blood microsample preparation. This device could be integrated to be operated with an adjunct on-chip analytical method to create a µTAS. However, as mentioned in paragraph 1.4, a 3-actor model where sample preparation is performed at the point of collection has many

advantages for the different actors in the market. Thus, the device is designed with this scheme in mind and allows separation and off-chip retrieval of the sample.

The device characteristics for sample preparation at the point of collection are established to be:

- Sample volume 25 µL : one large blood drop retrievable through skin puncture
- Plasma volume 2 µL : small DBS sample size (Harris & Polreis 2016; Kadjo et al. 2016)
- Operation time under 30 min : competitive with centrifugation operations
- Operation free and dilution free : useable by the patient himself or unqualified personnel
- Pumpless design: useable with minimal infrastructure.
- Off-chip ejection of metered sample : for versatile, gold standard off-chip analysis
- Low lysis, high purity : allows a high number of chemical analysis
- Cost-effective design : single depth designs without complex features. Design compatible with high throuput manufacturing methods. Possibly high flexibility in material choice.

Considering these requirements, a capillary-driven pumpless device using sedimentation was devised. Sedimentation is preferred here as it requires no external equipment and can be operated without prior dilution : this method can be compatible with the 30min operation time frame. The device uses capillary valving to allow for the ejection of a segmented plug of volume-controlled plasma. The following chapters will describe the separation phenomenon, the device fluidic characteristics, the retrieved sample quality and a clinical study aimed at an obese population will present an implementation of a testing cycle.

Chapter 2 Sedimenting suspensions in microchannels: Analytical description and numerical modeling

This chapter presents a unidimensional model for sedimentation-based separation of suspensions in microchannels. The separation relies on velocity differences caused by the sedimentation process. The model is applied to blood in a numerical implementation : it describes a plasma extraction mechanism. The effect of important parameters is established.

2.1 Introduction

Blood is a suspension containing a high volume fraction of cells. Those cells form the solid fraction: the dispersed phase, whereas the plasma forms the liquid fraction of blood: the dispersion medium. With any suspension containing micrometer sized particles, particles settle. Erythrocyte sedimentation rate (ESR) is the measure of settling speed of red blood cells (RBC). It has been used for almost a century and is still today a common clinical test (Saadeh 1998). The protocol established by Westergren in 1921 requires the measurement of the distance traveled in an hour by the upper layer of RBC in a tube filled with anticoagulated whole blood. This test is unspecific: an elevated ESR might be caused by inflammation, blood cell diseases or even cancer. Typical values are in the range of 6-15 mm/h for women and of 2-7 mm/h for men. These values tend to increase with age: even in healthy patients, ESR increases of about 0.1-0.2 mm/h every year.

Blood flowing in horizontal tubing at moderate velocity, where mixing is negligible, has been observed to form what was described as "layered flow" (Schmid-Schönbein 1988), which can be described as a 2 phase system: a clear plasma layer above a concentrated cell suspension layer, as illustrated in Figure 2:1. Over time, the concentration of the sediment reaches high values and its high viscosity was observed to create clogging in channels.

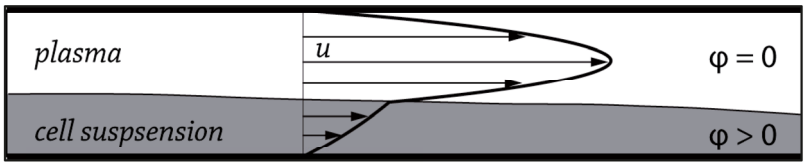

Figure 2:1: Layered flow illustration

The concentrated cell suspension and the supernatant plasma have different viscosities. Upon application of a pressure gradient, the two viscosity zones have different velocities. This phenomenon can be taken advantage of to create a spatial separation of plasma and cellular suspension which is the subject of the present work. The flow distribution forms a downstream plug of thinner liquid that can be retrieved. The separation device designed around this phenomenon is presented in Chapter 3.

This chapter presents a model combining Kynch sedimentation theory and Quemada viscosity model in a laminary flow situation. A general analytical solution for the velocity profile of pressure-driven flows of varying viscosities is described. The solution, in integral form, can be applied to arbitrary viscosity profiles, continuous or discontinuous. A finite difference implementation is then documented. The effect of relevant parameters is analyzed and discussed.

2.2 Sedimentation

In a suspension, volume density of the particles and volume density of the dispersion medium are typically different. Thus, due to buoyancy and gravity forces, particles are subject to a total net force. Depending on the volume densities, particles move along gravity towards the bottom of their container or against gravity towards the top of the container. Most commonly, particles settle following gravity. Against a physical barrier such as the container bottom, particles create highly concentrated layers. This process is called sedimentation and is at the core of the separation mechanism studied in this work.

2.2.1 Kynch sedimentation

Sedimentation has been described using two approaches: the discrete and the continuum approach. The discrete approach describes the laws of mechanics that apply to each particle. If this approach can precisely describe the local behavior of individual particles, it is very impractical to determine behavior of large quantities of particles in large volumes. The continuum approach considers the suspension as one liquid with properties depending on the individual particle and medium properties.

The continuum approach to sedimentation was pioneered by Kynch in 1952 (Kynch 1952). He assumed an ideal suspension to allow for an effective continuum theory to be applied. The following assumptions were made (Concha A. 2014) :

1. All particles are the same size, shape and density and are small compared to the dimensions at play.
2. Incompressibility of the particles and the medium
3. No-mass transport between particles and medium
4. Velocity of particles only depends on the local density
5. Concentration is homogenous along the cross-section of the container.

Assumption 2 was addressed by later works that extended the theory to compressible particles (Concha & Bustos 1987). Assumption 4 describes an ideal situation where wall effects are neglected (Bustos et al. 1990). Assumption 5 allows neglecting shear that might be induced in settling layers. Combined assumptions 4 and 5 allow reducing the problem to a unidimensional description: the concentration varies only along the vertical direction y as illustrated in Figure 2:2.

Two configurations are described for sedimentation: batch and continuous sedimentation. Continuous sedimentation is performed in tanks where flows are continuously pumped in and out of the container. The batch sedimentation is performed in a container with a closed bottom where no in- or out-flows are present. Kynch theory was built around batch sedimentation description.

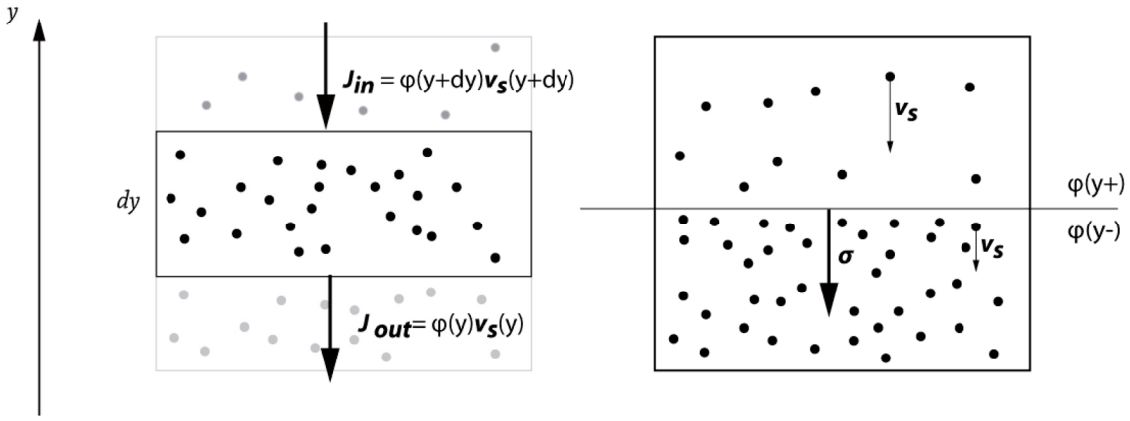

Figure 2:2 : Governing regimes in continuum sedimentation. On the left : continuous case. On the right : Discontinuous case.

Sedimentation is governed by the continuity equation presented in Equation 2:1. This equation describes the flux of solid volume fraction in the settling column.

$$\frac{\partial \varphi}{\partial t} + \nabla \cdot (\varphi \boldsymbol{v_s}) = 0$$

Equation 2:1 – Continuity equation

where φ is the solid volume fraction and $\boldsymbol{v_s}$ is the particle sedimentation speed. Bold symbols represent vectors. $\boldsymbol{J} = \varphi \boldsymbol{v_s}$ defines the solid flux density in the system. Its continuous implementation is illustrated in Figure 2:2a.

Such systems, even with continuous initial conditions, typically present discontinuities. At those discontinuities, Rankine-Huginot equations apply. In this

particular system, they translate to the mass jump conditions presented in Equation 2:2.

$$\boldsymbol{\sigma}[\varphi] = [\varphi \boldsymbol{v_s} \cdot \boldsymbol{e_i}]\, \boldsymbol{e_i} \;\rightarrow \sigma(\varphi^+, \varphi^-) = \frac{\varphi^+ v_s(\varphi^+) - \varphi^- v_s(\varphi^-)}{\varphi^+ - \varphi^-}$$

Equation 2:2 – Mass jump conditions at discontinuities

where σ is the speed of propagation of the discontinuity, $\boldsymbol{e_i}$ is a unit vector normal to the discontinuity surface, [°] is the difference of the variable on each side of the discontinuity, φ^+ and φ^- are the volume fractions on each side of the discontinuity. This solution is illustrated in Figure 2:2b.

Thus, the system describes changes in local viscosity that might happen continuously or not. Continuous increase of local concentration is called rarefaction wave.

2.2.2 Structure of a batch sedimentation process

In a batch sedimentation experiment, the container is filled with homogenous suspension at initial volume fraction $\varphi = \varphi_0$ at time $t = 0$. The sedimentation process starts and layers form. On the top, a medium-suspension interface is created and clear medium layers form on top of the container (Zone 1). This region grows towards the bottom of the container. The particles under the interface are in the hindered settling zone (Zone 2), commonly at initial volume fraction. The particle reaching the bottom of the container concentrate and form a thick sediment (Zone 4) at volume fraction $\varphi = \varphi_\infty$. This region grows towards the top of the container. The concentration reaches the sediment concentration through a transition zone (Zone 3) where a continuous and/or discontinuous process leads to the increase. At the critical time t_c, for all sedimentation experiments, the final state is reached and a sediment is formed with clear medium on top; no transition nor hindered settling zones are present.

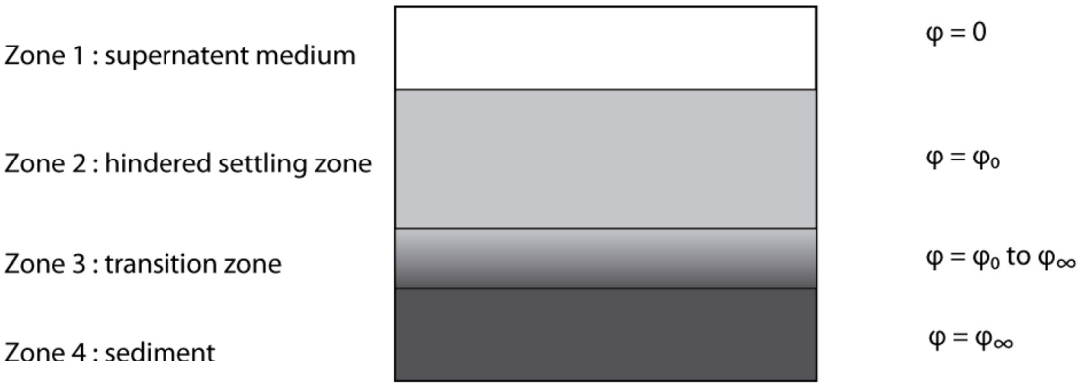

Figure 2:3 : Batch sedimentation structure

2.2.3 Modes of Batch Sedimentation

Different cases have been described in literature and, from the mathematically possible solutions, 7 Modes of Batch Sedimentation (MBS) have been presented for a solid flux density function containing at most 2 inflection points (Bustos et al. 1999). In the case of blood, the solid flux density function has one inflection point at $\varphi = a$ as illustrated in Figure 2:4.

Two definitions are necessary to solve batch sedimentation problems : i) φ_∞^{**} is defined as solid fraction at the intersection between the solid flux density function and the tangent to the curve at $\varphi = \varphi_\infty$, ii) φ^* is defined as the highest value w such as $\sigma(\varphi, v) < \sigma(\varphi, w)$ for $v \in [\varphi, w]$.

Depending on the original solid fraction (φ_0), there are three possible MBS :

a) If $0 < \varphi_0 < \varphi_\infty^{**}$, the process is a MBS-1 as illustrated in Figure 2:4a

   MBS-1 is described by a system comprising two discontinuities meeting at the critical time. The first discontinuity is between the clear medium at $\varphi = 0$ and the hindered settling zone at $\varphi = \varphi_0$. The second defines a transition zone bringing the suspension directly from $\varphi = \varphi_0$ to $\varphi = \varphi_\infty$.

b) If $\varphi_\infty^{**} < \varphi_0 < a$, the process is a MBS-2 as illustrated in Figure 2:4b

   MBS-2 comprises two discontinuities and rarefaction wave. As with MBS-1 the first discontinuity separates the supernatant medium and the hindered settling zone at $\varphi = \varphi_0$.The transition zone comprises a discontinuity with a drastic change from $\varphi = \varphi_0$ to $\varphi = \varphi_0^*$. A

rarefaction wave continuously brings the viscosity from $\varphi = \varphi_0^*$ to $\varphi = \varphi_\infty$ in the sediment.

c) If $a < \varphi_0$, the process is a MBS-3 as illustrated in Figure 2:4c

MBS-3 comprises one discontinuity and one rarefication wave. The discontinuity that separates the supernatant from the hindered settling zone is similar to the one described for MBS-1 and MBS-2. The transition zone consist only of a rarefication wave: the whole sediment concentrates continuously from $\varphi = \varphi_0$ until reaching $\varphi = \varphi_\infty$.

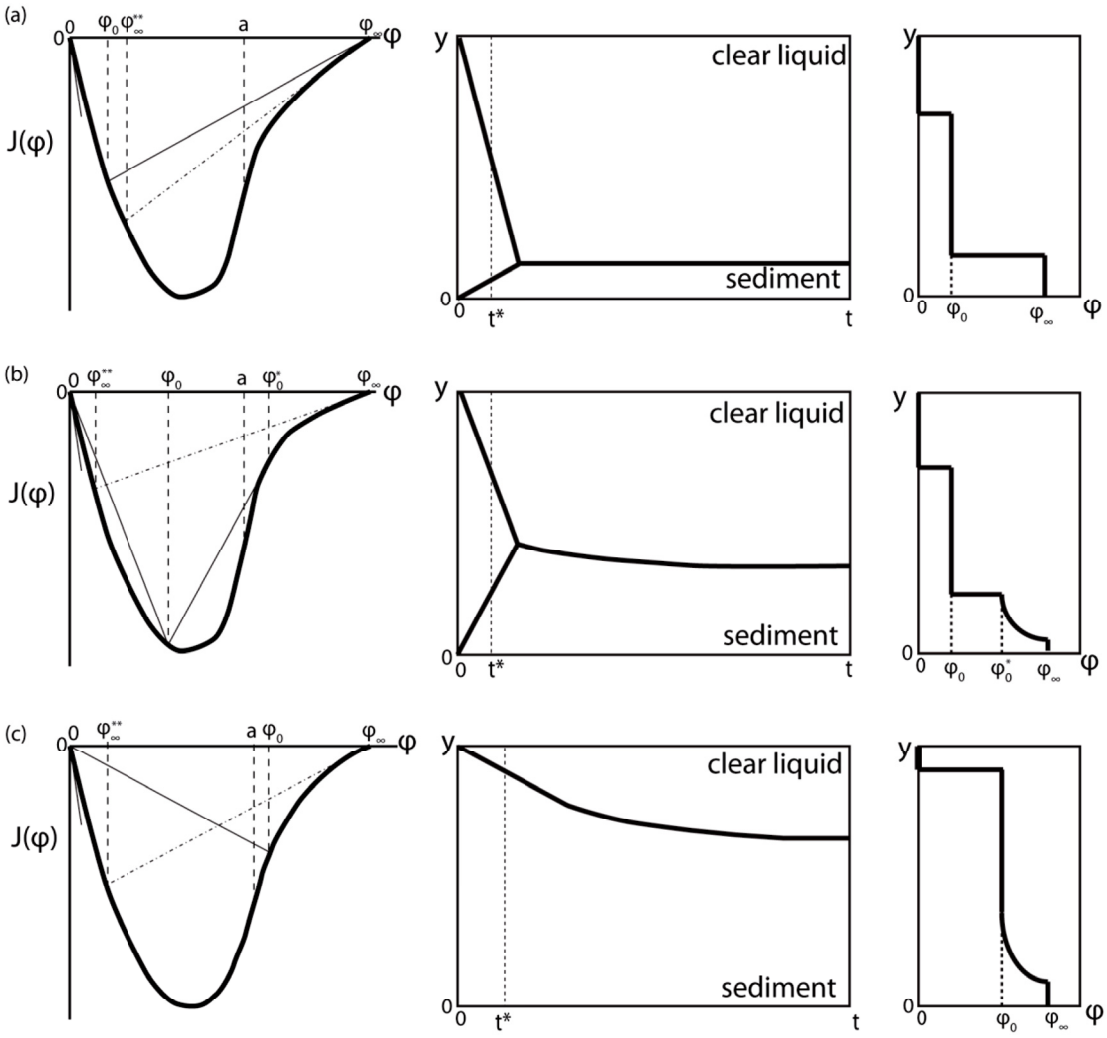

Figure 2:4 : Modes of batch sedimentation a) MBS-1, b) MBS-2, c) MBS-3. (left) Solid flux density function (center) position of the discontinuities as a function of time (right) solid fraction as function of vertical position at arbitrary time t*.

2.2.4 Sedimentation velocity of a particle

The sedimentation velocity of a particle is central in Kynch description of sedimentation, as visible in Equation 2:1. Models for computing this velocity are discussed in this section.

The stationary velocity $\boldsymbol{v_s}$ of a particle settling in a viscous medium is determined by an equilibrium between gravity, buoyancy and drag forces. The velocity of a hard sphere at such an equilibrium is described by Equation 2:3. This simple model will be used to compute settling speed in the subsequent paragraphs.

$$\boldsymbol{v_s} = \frac{2}{9}\frac{\Delta\rho}{\mu(\varphi)}\boldsymbol{g}R^2$$

Equation 2:3 – Stokes terminal velocity for a sphere

where $\Delta\rho$ is the difference of volumetric density between the particle and the suspension medium, $\mu(\varphi)$ is the viscosity of the suspension dependent on the volume fraction of particles φ, $\boldsymbol{g}$ is the standard gravity, R is the hydraulic radius of the particle.

Alternative empirical models for the settling velocity of a particle in a suspension directly consider the changes in settling speed with the concentration of the surrounding suspension (Sartory 1974).

$$v_s = -v_0(1-\varphi)^2\exp[-\frac{2.5\varphi}{1-\left(\frac{39}{64}\right)\varphi}]$$

Equation 2:4 – Hawksley-Van settling velocity

where v_0 is the Stokes velocity.

2.2.5 Influence of diffusion

The Peclet number Pe is a dimensionless number defined as the ratio of advective to diffusive transport rates (Kirby 2010). In the case of sedimentation, Peclet number is given by Equation 2:5 and is the ratio of sedimentation and diffusive transport rates (Benes et al. 2007).

$$Pe = \frac{v_s R}{D}$$

Equation 2:5 – Peclet number for sedimenting particules

where D is the Stokes-Einstein diffusion constant for individual particles. This constant is given by Equation 2:6.

$$D = \frac{k_B T}{6\pi\mu R}$$

Equation 2:6 – Diffusion constant

where k_B is the Boltzmann constant and T is the temperature.

For blood conditions, $Pe \cong 60$ and shows the dominance of sedimentation on diffusive transport. For this reason, the diffusive transport is neglected in the description of sedimentation processes.

2.3 Viscosity of suspensions

This section presents the basic mechanisms and some common Newtonian models for viscosity of a suspension. The viscosity directly impacts sedimentation velocity of a particle as visible in Equation 2:3.

Newtonian behavior is a characteristic of liquids which don't change viscosity upon the application of a mechanical stress. A suspension can be considered Newtonian if i) the dispersion medium is Newtonian ii) the particles are incompressible. This Newtonian behavior was demonstrated in altered blood: hardened RBC acting as hard particles in blood plasma (Chien 1970). For low pressure gradients in a microchannel, whole blood is expected to behave as a Newtonian liquid. For higher mechanical stresses, whole blood will behave as a Non-Newtonian liquid.

The viscosity of a particle suspension depends on the concentration of particles in the dispersion medium (Yilmaz & Gundogdu 2008). The effective viscosity of the suspension is higher than the viscosity of the suspension medium. The relative viscosity is defined by Equation 2:7.

$$\mu_r = \frac{\mu}{\mu_0}$$

Equation 2:7 – Relative viscosity definition

where μ_r is the relative viscosity, μ is the effective viscosity of the suspension and μ_0 is the viscosity of the dispersion medium.

The increase in viscosity of the suspension is the consequence of forces created by the movement of the particles in the medium. At low concentration, the particle movement is mainly hindered by viscous drag forces (Einstein 1911). Einstein's model describes such conditions and is reported in Equation 2:8

$$\mu_r = 1 + 2.5\varphi$$

Equation 2:8 – Einstein's equation for viscosity of a suspension

This linear model is not valid for high concentrations. When concentration is high, particle-particle hindering mechanisms dominate. Krieger-Dougherty's empirical model describes such case and is presented in Equation 2:9 (Krieger & Dougherty 1959).

$$\mu_r = \left(1 - \frac{\varphi}{\varphi_{max}}\right)^{-[\mu]\varphi_{max}}$$

Equation 2:9 – Krieger-Dougherty's equation for viscosity of a suspension

where φ_{max} is the maximal packing fraction and $[\mu]$ is an instrinsic viscosity parameter.

This model has got a vertical asymptote placed at the maximal packing fraction: as both the viscosity and the rate of increasing of viscosity with concentration tend to infinite at maximal packing fraction.

A model was built by Quemada (Quemada 1977) and describes the viscosity of a fluid in Newtonian conditions. This model is similar to Equation 2:9 with $[\mu]\varphi_{max} = 2$.

$$\mu_r = \left(1 - \frac{\varphi}{\varphi_{max}}\right)^{-2}$$

Equation 2:10 – Quemada's equation for viscosity of a suspension

Even though, reduced to the bare minimum in terms of parameters, this model fits the viscosity of blood over a wide range of volume fractions. This simple model will be used to compute viscosity in the subsequent paragraphs. A comparison of the three proposed viscosity models is shown in Figure 2:5.

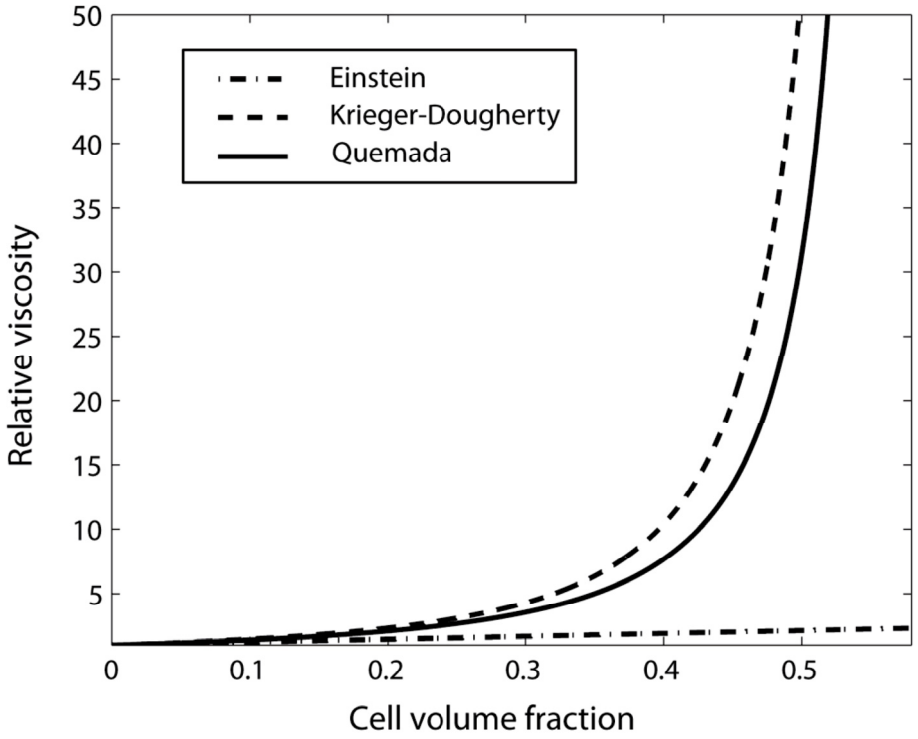

Figure 2:5 : Newtonian viscosity models. Comparison of Einstein, Krieger-Dougherty and Quemada models for parameters $[\mu] = 3$ and $\varphi_{max} = 0.75$.

2.4 Generalized stratified Poiseuille flow

2.4.1 Stratified flows

Since the 1950s, the behavior of 2 phase flows in pipes has been described (Baker 1954). This description was central in the mining industry where gas and oil often flow simultaneously in pipes. The notion of stratified flow was introduced as one of the flow configurations possible. This configuration is characteristic of low flow rates. The two phases organize in a layered fashion in the horizontal pipe and the interface doesn't have any vertical motion. At higher flow rates, waves, bubbles or an annular configurations might form.

Since the 1960s, the flow velocity profiles were computed for stratified flows in pipes under laminar flow conditions. The flow configurations were limited to a two-layer structure with a sharp phase transition between layers. Using simple geometries, explicit velocity profiles were computed for rectangular duct (Tang & Himmelblau 1963) or round channels (Ullmann et al. 2004; Das et al. 2011). The apparition of instabilities in the interface was studied using numerical models (Cao et al. 2004). For microfluidic systems, stratified flow configurations were also

described and the velocity profile computed (Finlayson & Shaw 2010; Finlayson 2012). For blood samples, Murata computed flow velocities in a stratified flow consisting of a clear supernatant layer and a thicker cell suspension layer (Murata 1996). In this study, the thicknesses and solid fractions of the layers were fixed arbitrarily.

The stratified flow models are limited to a two-region problem: viscosity is constant in each layer and changes abruptly at the interface. However, these models lack the possibility to describe more complex phase and viscosity arrangement; flow of mixtures or sedimenting suspensions cannot be described by two-phase stratified flow models.

2.4.2 Analytical resolution

The following sections will present a general uni-dimensional solution, in integral form, for Poiseuille flow of continuously and non-continuously varying viscosity layers. The model describes the system only as a function of height, as this is the dominant dimension for channel geometries where height is significantly smaller then width. The model will yield the velocity and shear stress profiles of a pressure-driven flow, as illustrated in Figure 2:6 for a two-phase stratified flow configuration.

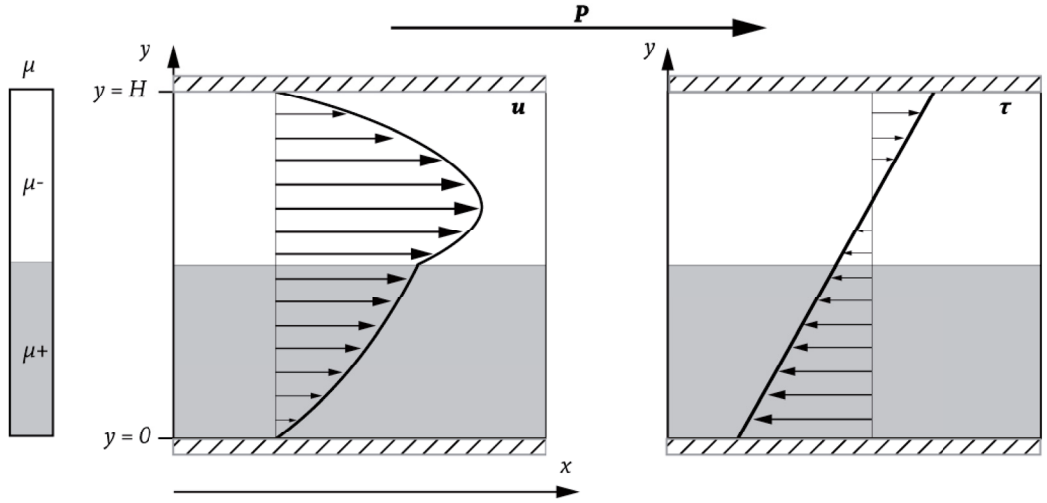

Figure 2:6 : Illustration of the velocity field u and the shear stress τ for a stratified Poiseuille flow. H denotes the channel height. Phase viscosities are μ - and μ + for the upper and lower layers respectively. P is the pressure.

The momentum equation of viscous incompressible liquids is described by Cauchy momentum equation (Equation 2:11). This equation supposes the absence of

external force fields. However, flow is driven by a pressure application (Kirby 2010).

$$\frac{\partial \rho \boldsymbol{u}}{\partial t} + \rho \boldsymbol{u} \cdot \nabla \boldsymbol{u} = -\nabla \boldsymbol{P} + \nabla \cdot (\boldsymbol{\tau})$$

Equation 2:11 – Cauchy momentum equation

with u describing velocity, P pressure, t time and ρ the volumetric density and $\boldsymbol{\tau}$ the shear stress tensor.

In this unidimensional mode, flow is supposed to be co-directional with the channel: absence of flow in the y direction. Thus imposing the forms presented in Equation 2:12 to the velocity and the pressure

$$\boldsymbol{P} = \begin{pmatrix} P_x \\ P_y \end{pmatrix} = \begin{pmatrix} P \\ 0 \end{pmatrix} \text{ and } \boldsymbol{u} = \begin{pmatrix} u_x \\ u_y \end{pmatrix} = \begin{pmatrix} u \\ 0 \end{pmatrix}$$

Equation 2:12 – Unidirectional flow

The incompressibility of the fluid allows a simplification of the shear tensor $\boldsymbol{\tau}$

$$\boldsymbol{\tau} = \begin{pmatrix} 0 & \tau_{xy} \\ \tau_{yx} & 0 \end{pmatrix} = \begin{pmatrix} 0 & \tau \\ \tau & 0 \end{pmatrix}$$

Equation 2:13 – Shear stress tensor simplification

Considering stationary state and laminary conditions, convective and time dependent terms can be cancelled. Thus, the left terms of Equation 2:11 are null. Applying the vectorial operators and projecting the resulting vectors on to the x-axis, Equation 2:11 simplifies to Equation 2:14. Such equation describes the laminar flow and can be applied in 2 major cases: Poiseuille or Couette flow. Poiseuille describes the flow in a conduct where liquid is driven by a pressure gradient, whereas Couette describes the flow between two surfaces where one is displacement comparatively to the other.

$$\frac{d\tau}{dy} = -\frac{dP}{dx}$$

Equation 2:14 – Simplified Cauchy momentum equation

In this model, it is assumed that the fluid behaves as a Newtonian fluid. For Newtonian liquids, the viscous shear stress τ is given by Equation 2:15.

$$\tau(y) = \mu(y)\dot{\gamma} \equiv \mu(y) \cdot \frac{du}{dy}$$

Equation 2:15 – Newton equation

where $\dot{\gamma}$ is the strain rate.

This model is built for viscosity profiles which can incorporate discontinuites as presented in Equation 2:16.

$$\mu \notin C^0$$

Equation 2:16 – Imposed discontinuity of viscosity

At each point and at each interface in the flow, because of the absence of slip in this model, the shear stress is continuous as well as the velocity as shown in Equation 2:17 and Equation 2:18. Considering Equation 2:15 and Equation 2:16, since the shear stress is continuous and the viscosity is not, the strain rate is discontinuous. Thus, the velocity is not differentiable at all point.

$$\tau \in C^1$$

Equation 2:17 – Condition on continuity of shear stress

$$u \in C^0$$

Equation 2:18 – Condition on continuity of velocity

With Poiseuille flow conditions and because of the no slip conditions, the boundary conditions impose the absence of velocity on the walls.

$$u(0) = 0$$

Equation 2:19 – Boundary condition bottom channel side

$$u(II) = 0$$

Equation 2:20 – Boundary condition top channel side

where H is the height of the channel.

Through the integration of Equation 2:14, the shear stress is described by Equation 2:21. The shear stress increases linearly with the position in the channel.

$$\tau(y) = -\frac{dP}{dx}y + C_1$$

Equation 2:21 – Shear rate profile

Where C_1 is a constant of integration.

By integrating Equation 2:15 and replacing the shear rate by its expression presented in Equation 2:21.

$$u(y) = -\int_0^y \frac{\tau(s)}{\mu(s)} ds = -\frac{dP}{dx}\int_0^y \frac{s}{\mu(s)} ds + C_1 \int_0^y \frac{1}{\mu(s)} ds$$

Equation 2:22 – Velocity with constants

where s is the integration variable spanning the height of the channel along the y-axis.

Equation 2:22 fills the conditions described in Equation 2:19

Applying the condition described in Equation 2:20 to Equation 2:22, the constant is determined to be a ratio of two integrals over the height of the channel.

$$u(H) = 0 \rightarrow C_1 = \frac{\frac{dP}{dx}\int_0^H \frac{s}{\mu(s)} ds}{\int_0^H \frac{1}{\mu(s)} ds}$$

Equation 2:23 – Application of top side boundary condition

Substituting the constant (Equation 2:23) in Equation 2:22, the general solution for the velocity profile is obtained in Equation 2:24. This solution, although in implicit integral terms, is general and can be applied to a multitude of complex viscosity profiles.

$$u(y) = -\frac{dP}{dx}\int_0^y \frac{s}{\mu(s)} ds + \frac{\frac{dP}{dx}\int_0^H \frac{s}{\mu(s)} ds}{\int_0^H \frac{1}{\mu(s)} ds} \cdot \int_0^y \frac{1}{\mu(s)} ds$$

Equation 2:24 – General solution for velocity profile

Substituting constant in Equation 2:21, the general solution for the shear stress profile is obtained in Equation 2:25. The shear stress is linear and extremum values are found on the walls of the channels.

$$\tau(y) = \frac{dP}{dx}\left(y - \frac{\int_0^H \frac{s}{\mu(s)} ds}{\int_0^H \frac{1}{\mu(s)} ds} \right)$$

Equation 2:25 – Shear stress integration

The position of equilibrium of momentum highly depends on the viscosity profile and is described by Equation 2:26. At this point, the maximal velocity is reached.

$$\tau(y_{eq}) = 0 \rightarrow y_{eq} = \frac{\int_0^H \frac{s}{\mu(s)} ds}{\int_0^H \frac{1}{\mu(s)} ds}$$

Equation 2:26 – Momentum equilibrium point

where y_{eq} is the y-coordinate of the null momentum position.

2.5 Limitations and possible analytical improvements

2.5.1 Integral form of velocity

As viscosity profiles might contain continuous and discontinuous changes, differentiation steps were avoided. The resolution presented required only two integration steps on the shear stress. Double differentiation of velocity was avoided because of the restriction on the continuity of this function. The final solution contains several integral forms that might not be trivial to analytically solve: numerical resolutions might be preferable in a number of cases.

2.5.2 Non-Newtonian suspensions

Newtonian behavior was assumed both in the resolution of the flow profile as well as the sedimentation. This assumption is sufficient for situations were pressure gradients and thus mechanical stresses are low. However, under higher pressures and flow velocities, blood exhibits strong non-Newtonian characteristics. Blood exhibit amongst other behaviors shear thinning (Sochi 2013; Johnston et al. 2004). The model of viscosity of the suspension presented in section 2.3 does not account for these behaviors. If required, the model could be extended through non-Newtonian viscosity models.

A common model for Non-Newtonian fluid viscosity is the Carreau model presented in Equation 2:27.

$$\mu = \mu_{\tau=\infty} + (\mu_{\tau=0} - \mu_{\tau=\infty})[1 + (\lambda\dot{\gamma})^2]^{\frac{n-1}{2}}$$

Equation 2:27 – Non-Newtonian Carreau model

Where λ is the relaxation time, n is the index power, $\mu_{\tau=0}$is viscosity with no strain rate, $\mu_{\tau=\infty}$ is viscosity with infinite strain rate.

This model however doesn't describe the dependence of the non-linearities in viscosity with the change in hematocrit: pure plasma reacting more like a Newtonian fluid then highly concentrated cell suspensions (Zeng & Zhao 2011). Such system was described by the more complete model presented in Equation 2:28. It combines hematocrit-induced viscosity changes and non-Newtonian behavior and was described by Quemada (D. Quemada 1978; D Quemada 1978). It is a generalized case of Equation 2:10.

$$\mu = \mu_0 \left(1 - \frac{k_0 + k_\infty \sqrt{\dot{\gamma}/\dot{\gamma}_c}}{2\left(1 + \sqrt{\dot{\gamma}/\dot{\gamma}_c}\right)} \varphi\right)^{-2}$$

Equation 2:28 – Non-Newtonian Quemada model

where k_0 is a constant depending on the viscosity at zero shear rate, $k_\infty$is a constant depending on the viscosity at infinite shear rate, $\dot{\gamma}_c$ is a critical shear rate determining the transition between both regimes.The critical shear rate is typically $2s^{-1}$ in physiological hematocrit whole blood (D Quemada 1978)

2.6 Physiological blood parameters

In the following sections, if not stated otherwise, blood parameters listed in Table 2:1 will be used. The parameters corresponds to the normal values for the blood of a young male adult: these will be considered as the physiological parameters.

Table 2:1 : Parameter list for subsequent calculations

Parameter	Symbol	Value	Note and reference
Density cell	ρ_{cell}	1098 kg/m^3	(Yilmaz & Gundogdu 2008)
Density plasma	ρ_{plasma}	1025 kg/m^3	For 20°C (Trudnowski & Rico 1974)
Standard gravity	g	9.81 m/s^2	-
Cell Stoke radius	R	2.58 µm	(Groom & Anderson 1972)
Plasma viscosity	μ_0	1.8 mPa · s	For 20°C. Considering 1.25 mPa · s at 37°C (Yilmaz & Gundogdu 2008)
Max packing fraction	φ_{max}	0.75	In the interval 0.73-0.8 (Sartory 1974)
Initial hematocrit	φ_0	0.45	Physiological range 0.4-0.54 for men (H.Billett 1990)

Values reported for plasma density and viscosity were adjusted to 20°C. The values typically found in literature are at normal body temperature (37°C).

Studies have described the behavior of those parameters with temperature changes and the reported laws are applied to correct for room temperature experimental conditions (Yilmaz & Gundogdu 2008),(Trudnowski & Rico 1974).

This model considers each RBC as the sedimenting particle: the formation of aggregates is neglected. The single RBC orientation changes during fall with a bias towards an orientation with their narrow side first (Groom & Anderson 1972). Thus, the Stoke or hydrodynamic radius is not equal to any physical dimension of the cell morphology.

For blood samples, hematocrit is defined as the cellular fraction and is thus equivalent to solid fraction.

2.7 Mode of Batch Sedimentation in whole blood samples

The continuum approach described by Kynch was applied to blood samples in the 1970s by Sartory (Sartory 1974). He described the settling of blood both in batch and continuous sedimentation configurations. The description of MBS not yet having been completed, this study was limited and the description of the sedimentation process lacked generality as it was restricted to a MBS-3 configuration. The modeling and discussion of MBS in blood samples are extended in this section.

As described in section 2.2, the possible modes of batch sedimentation depend on the solid flux density function. This section describes the modes of sedimentation in blood by combining laws of sedimentation described in section 2.2 and viscosity of suspensions described in section 2.3. The solid flux density function is, in this particular case, described by Equation 2:29.

$$J(\varphi) = \varphi v_s = -\varphi \frac{2}{9}\left(1 - \frac{\varphi}{\varphi_{max}}\right)^2 gR^2$$

Equation 2:29 – Explicit solid flux density function

Upon application of the parameters reported in section 2.6, the flux density function is depicted in Figure 2:7. The function is null for both $\varphi = 0$ and $\varphi = \varphi_\infty = \varphi_{max}$. As one can observe from Equation 2:29, $\left.\frac{dJ}{d\varphi}\right|_{\varphi=\varphi_\infty} = 0$, thus implying $\varphi_\infty^{**} = 0$ (intersection between the tangent at φ_∞ and the curve). With such a solid flux density function, MBS-1 is not present for any initial hematocrit.

The solid flux density function has one inflection point placed at $\varphi = a = \frac{2}{3}\varphi_{max} =$ 0.5. This point defines the hematocrit at which the modes of batch sedimentation transition between the second and the third mode:

- MBS-2 if $\varphi_0 \in [0, a = 0.5]$
- MBS-3 if $\varphi_0 \in [a = 0.5, \varphi_\infty = 0.75]$

In MBS-2, as shown in Figure 2:7, the transition is composed of a discontinuous jump between φ_0 and φ_0^* before a rarefaction wave brings the sediment solid density to φ_∞. The difference between levels φ_0 and φ_0^* decreases as φ_0 approaches a, as shown in Figure 2:7a to d. The divergence between the solid flux density curve and the discontinuity line is strongest at low hematocrits. At hematocrits nearing $\varphi = a$, the difference between the curves is minimal thus the difference between the discontinuous solution and the continuous process is minimal. The relation between φ_0 and φ_0^* obtained through numerical implementation is linear as shown in Figure 2:7e. It is determined to be described by the following Equation:

$$\varphi_0^* = 0.75 - 0.5\,\varphi_0$$

Equation 2:30 – Relation between initial hematocrit and discontinuity mass jump

At the transition point between MBS-2 and MBS-3, hematocrit is $\varphi_0 = a$ and $\varphi_0 = \varphi_0^*$: the discontinuous jump becomes null and the transition to a purely continuous accumulation is smoothly performed. The continuity between both regimes and the low deviation between the solid flux density function and the discontinuity line renders the experimental observation of the transition between modes difficult, even though it occurs in the physiological range. Sartory already explains that a discontinuous jump might occur for low hematocrits but his experiments and calculations show little to no discontinuities at physiological hematocrit (0.46), close to $\varphi = a$ (Sartory 1975). The importance of this discontinuity is predominant for low hematocrit samples and diluted samples.

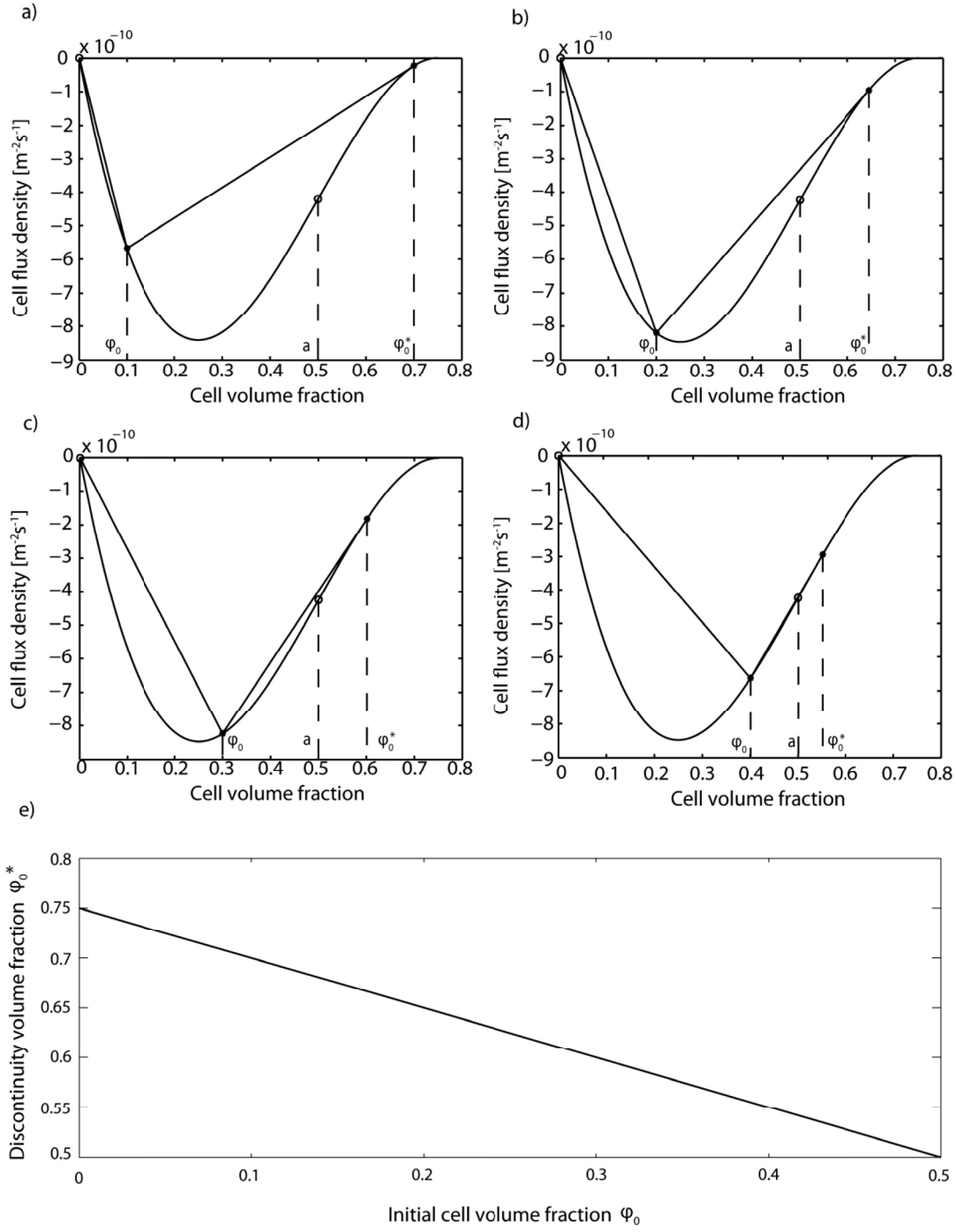

Figure 2:7 : Mode of Batch Sedimentation n°2 in blood samples, for hematocrit under $a = 0.5$. a) Solid flux density and graphical resolution for initial hematocrit 10% b) 20% c) 30% d) 40% e) Discontinuity volume fraction as a function of initial volume fraction

2.8 Numerical implementation of velocity model

The problem exposed in this chapter is solved numerically using a finite difference method. This discretization method simplifies differential resolution by applying

difference approximations. Therefore, temporal differentiation $\partial\varphi/\partial t$ (from Equation 2:1) is approximated by $\Delta\varphi/\Delta t$ where $\Delta\varphi$ is the difference of solid volume fraction occurring during a time step Δt.

This unidimensional model relies on a regular Cartesian grid with constant spatial step Δy to discretize the domain between channel bottom and channel top as illustrated in Figure 2:8. The total number of elements is $N = H/\Delta y$. Boundary conditions are applied to elements 1 at $y = 0$ and element N at $y = H$.

For each time iteration, the problem is solved as follows: first the numerical differential sedimentation system is solved (Equation 2:1 and Equation 2:2) and second the associated velocity profile is computed through numerical integration (Equation 2:24).

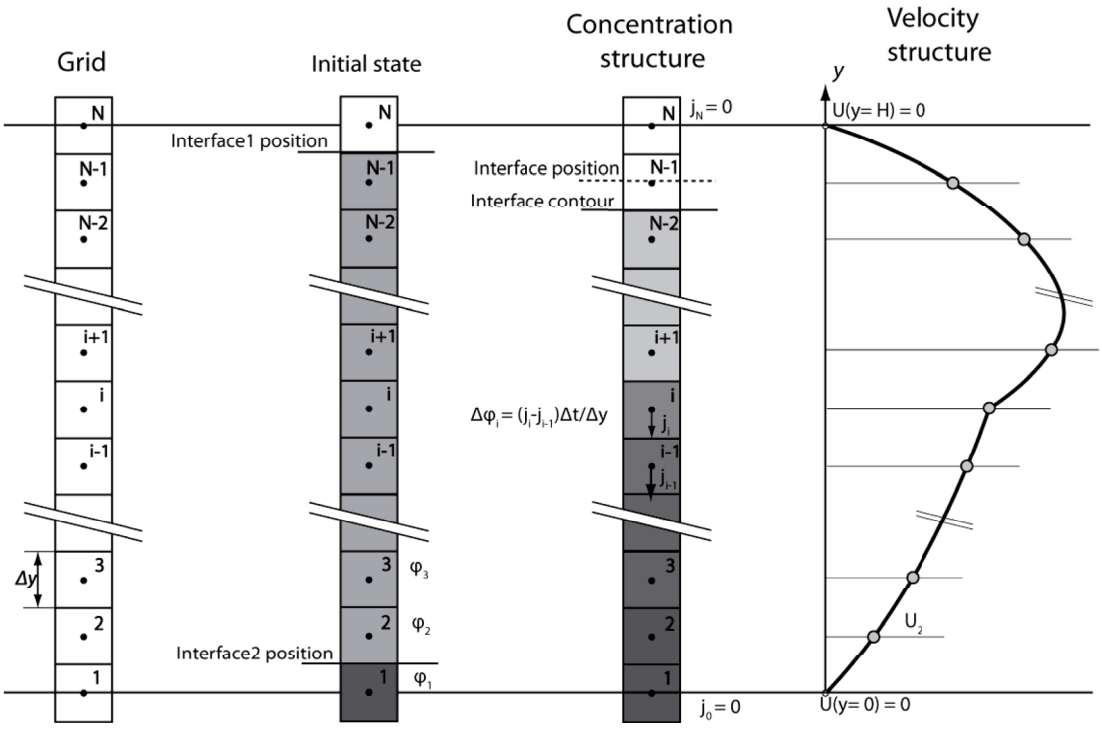

Figure 2:8 : Illustration of the numerical implementation structure. A Cartesian grid of N element is implemented for discretization. Initial state contains seeded layers of supernatant and sediment. For each time step, the model computes the solid fraction in each element and the velocity associated.

At t = 0, the initial state is established. All elements are set at solid fraction φ_0 (equivalent to hematocrit). The supernatant layer is seeded by imposing $\varphi_N = 0$ and the position of the discontinuity position is placed at position N. If the system

follows MBS-1 or MBS-2 behavior, an additional layer is seeded by imposing $\varphi_1 = \varphi_0^*$ and the second discontinuity position is placed at position 2.

The position of the interfaces is defined precisely and might be placed at a non-integer position. However, the contour, and thus the discontinuous change position, is set by flooring the element coordinate that contains the discontinuity, as illustrated in Figure 2:8. The speed of propagation σ of the discontinuity placed in element k is computed using the solid fraction either side of the contour ($\varphi_k = \varphi_+$ and $\varphi_{k-1} = \varphi_-$). In a single time step, the interface contour might not have moved even though its stored position was altered. This creates a small oscillation of the total particle volume in the system as the particle volume in the element of the contour is neglected. This oscillation depends on the proportion of the element neglected by the contouring, the size of the elements and the solid fraction in this element (approximately φ_-).

The continuity equation is applied between the channel bottom and the first encountered discontinuity regardless of the MBS. In MBS-1, 2 and 3, the supernatant and the hindered settling zone, if present, stay at a constant solid fraction as the solid flux is constant in those areas. Therefore, only the area corresponding to the transition zone and the sediment require the application of those equations. The finite difference implementation of Equation 2:1 was performed as a backward difference as shown in Equation 2:31.

$$\varphi_{i,t+1} = \varphi_{i,t} + \frac{J_{i,t} - J_{i-1,t}}{\Delta y}\Delta t$$

Equation 2:31 – Backward difference implementation of continuity equation

In this system it is imposed that $J_N = 0$ and $J_0 = 0$. Leading to equations on the boundaries: $\Delta\varphi_1 = j_1/\Delta y * \Delta t$ and $\Delta\varphi_N = -j_{N-1}/\Delta y * \Delta t$.

For the flow profile, the boundary conditions are already applied in Equation 2:24 and Equation 2:25. For each time step, the integrals are performed using numerical trapezoidal integration calculations.

2.9 Results at physiological values

Using parameters established in section 2.6, the numerical implementation described in section 2.8 allows to determine the behavior of blood sample undergoing simultaneously sedimentation and Poiseuille flow. Time step is 0.5 s and spatial step is 500 nm. The pressure gradient is set at 100 Pa/m that is in the

correct order of magnitude with values discussed later in Chapter 3 for channels of 200 µm of height. Figure 2:9 shows the evolution of cellular volume fraction and velocity in the channel with time. The channel is supposed to be placed horizontally and thus gravity has no component along the x-axis.

Figure 2:9a shows the initial state of the numerical model. The volume fraction is homogeneous in the channel height at initial hematocrit $\varphi_0 = 0.45$. The velocity profile is purely parabolic as expected in Poiseuille flow. The velocity maximum (or momentum equilibrium) is situated at the centerline of the channel and is approximately 45 µm/s. Some slight asymmetry in the parabola is noticeable due to the seeding of a single element of supernatant and another of sediment.

Figure 2:9b shows the situation at time t = 300 s. A layer of 29 µm of cell-free liquid is present in the top part of the channel. A layer formed by the sediment is also present at the bottom and is 59 µm thick. As described in section 2.7, for whole blood samples at hematocrit 45%, the samples transition discontinuously to hematocrit 52.5%. This is visible in Figure 2:9b on the top layer of the transition phase situated at 59 µm of channel height. The packed sediment forms slowly: solid flux density is low for high hematocrit. As visible in the velocity profile, the highly concentrated layers have a low velocity. The maximum velocity point is, at this time point, still in the hindered settling zone, at initial hematocrit. Thus, the separation has not yet begun and plasma does not flow faster than the cellular suspension.

Figure 2:9c shows the situation at time t = 600 s. A layer of 58 µm of cell-free liquid is present in the top part of the channel. The layer formed by the sediment is also present and is 118 µm thick. The hindered settling zone has greatly shrunk and now occupies a small fraction of the channel thickness. The maximum velocity point is, at this time point, in the supernatant cell-free layers. Thus, the cell-free supernatant has started to flow faster than the cellular suspension: cell-free liquid extraction has started.

Figure 2:9d shows the situation at time t = 900 s. A layer of 72 µm of cell-free liquid is present in the top part of the channel. The layer formed by the sediment is also present and is 128 µm thick. The hindered settling zone has disappeared and the top layer of the sediment is now at 0.63 volume fraction. The sediment is slowly concentrating with a gradual reduction in thickness. The velocity of the

sediment is very low and most of the supernatant is flowing faster than the sediment.

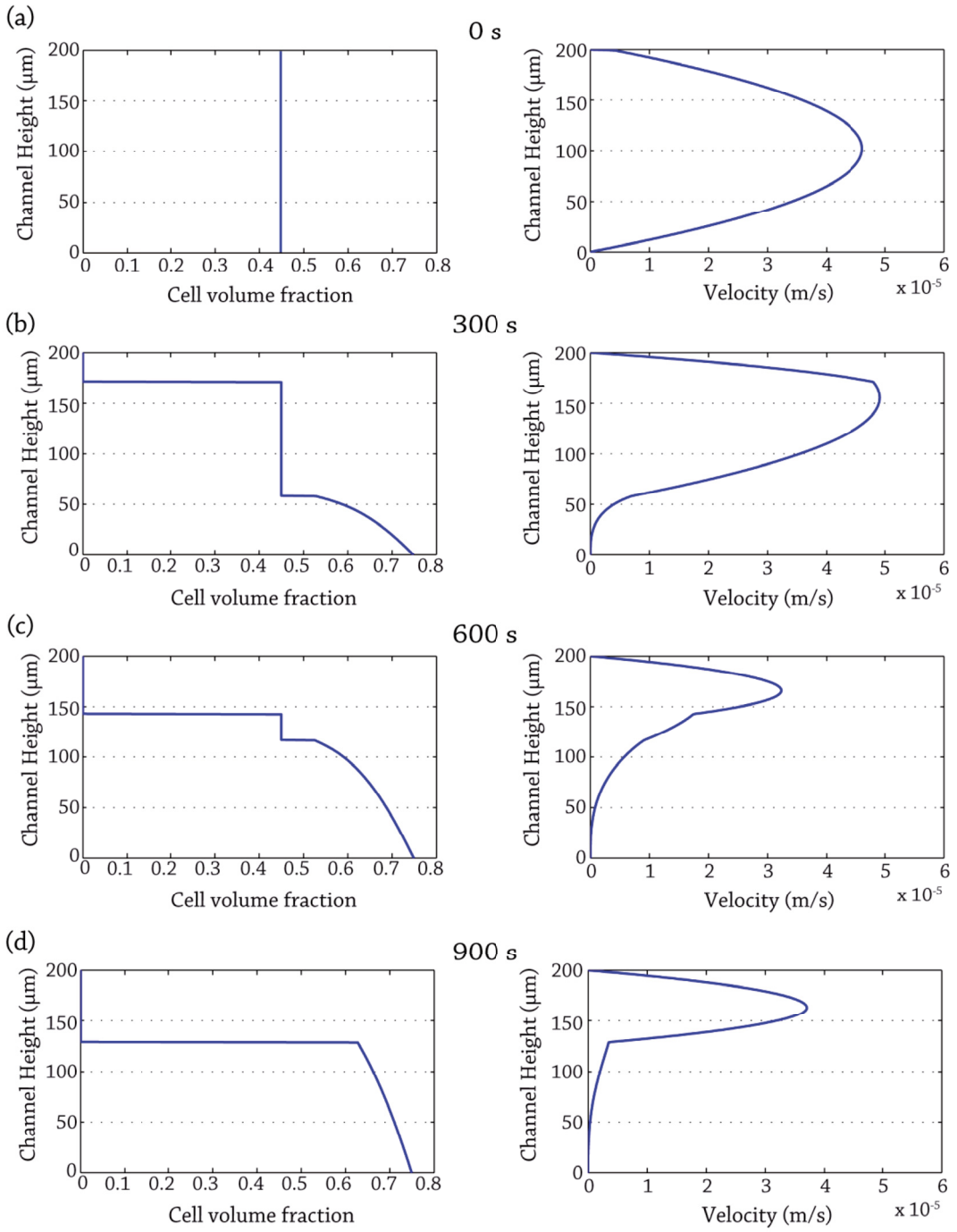

Figure 2:9 : Time evolution (time step : 300 s) of the cell volume fraction in the channel height and associated velocity profile (a) Initial conditions with parabolic velocity profile (b) Generation of the supernatant and sediment portions while velocity is still maximum in the cell suspension (c) Velocity maximal in the supernatant cell free liquid: extraction has started (d) Disappearance of the hinder settling phase. Only remains a high velocity supernatant and low velocity concentrating sediment.

The description made above allows describing different time points: t_{sep} the separation delay and t_1 the time when both interfaces (discontinuities) meet. As shown in Figure 2:10a, the position of the phase interfaces and the maximum velocity evolve with time. The point when supernatant starts flowing faster than the cellular suspension represents t_{sep} and is defined by the intersection of the maximum velocity curve and the supernatant interface. This point is at $t_{sep} = 403\ s$ as visible in Figure 2:10a. The extraction phase starts from this time point. The point t_1 is reached at 693 s when the interfaces meet. After this point, the sediment concentrate slowly and the top sediment layer concentration increases. Previous to t_1, the sediment top layer remain at φ_0^*.

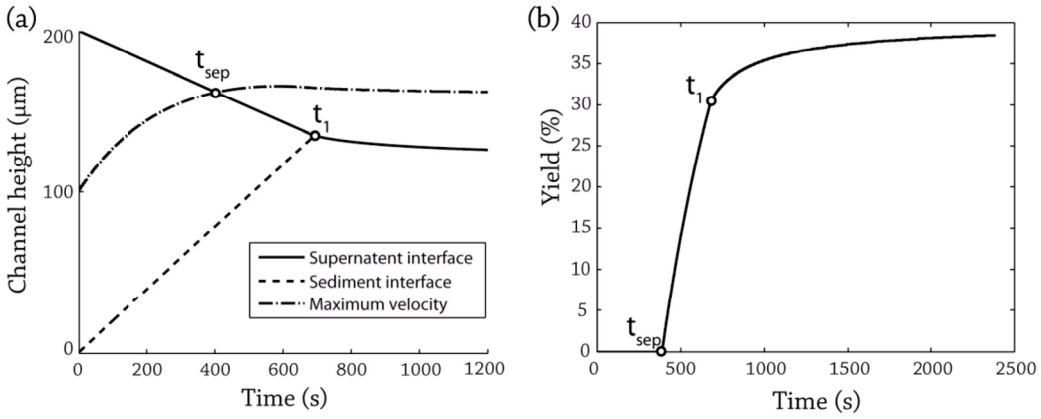

Figure 2:10 : Physiological values interface and yield evolution (a) Position of interfaces and characteristic times (b) yield time evolution

The supernatant liquid flowing faster than the cellular suspension is extracted. This extracted liquid flows at a velocity higher than the maximal cell suspension velocity. The yield is here defined as the thickness of this extracting supernatant divided by the total channel height and is represented in Figure 2:10b. The yield is null until reaching the separation delay. At this point the yield increases rapidly until the t_1 point. It changes from 0 % to 30% in 290s. This rapid change is due to the rapid increase in supernatant thickness. The amplitude and rate of this increase depends mainly on the difference between φ_0 and $\varphi_0 *$. After t_1, the yield increases slowly, reflecting the slow concentration of the sediment. The yield tends to 40% (90% of the total plasma volume). This value corresponds to the thickness of supernatant plasma in the completely sedimented samples. The remaining plasma is in the sediment that is composed at maximum packing of 75 % particles and 25% of plasma.

2.10 Effect of channel height

The effect of channel height on separation delay is shown in Figure 2:11a. The relationship is purely linear for all channel heights with a sensitivity on separation delay of 2 s/µm. The linearity is expected here as, for a given hematocrit, changing channel height changes proportionally sedimentation distances.

Figure 2:11b shows the yield as a function of time. Changing channel height, changes not only t_{sep} but also t_1 linearly. Thus, it creates a temporal dilation of the curves shown in Figure 2:11b. All curves still tend to the same value of 40% yield.

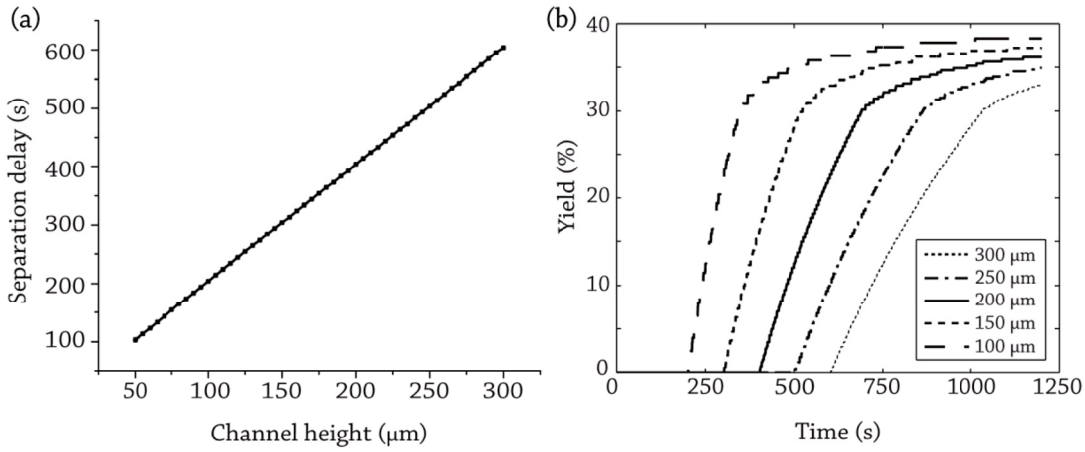

Figure 2:11 : Effect of channel height (a) Separation delay as a function of channel height (b) Yield as function of time for different channel heights

This factor is a key design parameter to the separation phenomenon. However, for small heights, the assumption made in the model and reported in section 2.2 does not hold: the cells are not small compared to the dimensions at play anymore. This is a limitation in the possible heights: for small channel heights, wall effects become predominant and hinder the sedimentation mechanism exposed in this work.

2.11 Effect of hematocrit

The effect of initial hematocrit (φ_0) on separation delay is shown in Figure 2:12a. The relationship between hematocrit and separation delay is mainly linked to the changes in viscosity and thus sedimentation speeds with hematocrit. As discussed in 2.3, the viscosity increases drastically for hematocrits close to maximal packing

fraction (75%). This effect is obvious in Figure 2:12a. Around physiological hematocrit of 45%, the sensitivity of separation delay to hematocrit is 12.5 s/%.

Figure 2:12b shows the yield as a function of time for different hematocrits. Initial hematocrit (φ_0) has a direct effect on the plasma proportion in the sample: the lower the hematocrit, the more plasma in the sample. Thus, for low hematocrits, yield tends to a higher value, as shown in Figure 2:12b. Altering initial hematocrit also has an effect on the sedimentation mechanism, as described in section 2.7. For hematocrits under 0.5, the solid fraction at the sediment interface transitions directly from φ_0 to φ_0*: the smaller the initial hematocrit, the bigger the hematocrit difference. Thus, for low hematocrits, sediment formation is mainly discontinuous and thus globally faster. For hematocrit values 0.3, increase in yield between t_{sep} and t_1 is more than 90% of the maximal yield, whereas for initial hematocrit value of 0.45, this increase only corresponds to 75% of the maximal value. For initial hematocrit values over 0.5, the samples only concentrate continuously and the yield increases slowly after the separation delay is reached.

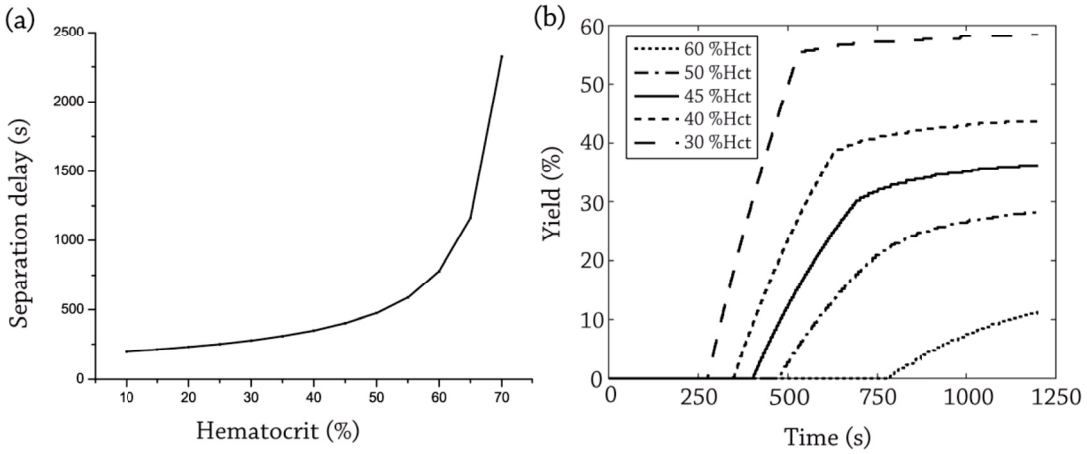

Figure 2:12 : Effect of hematocrit (a) Separation delay as a function of hematocrit (b) Yield as function of time for different hematocrits

Hematocrit has a strong effect on the sedimentation characteristics encountered : for low hematocrit values the separation will both be faster and have a higher yield. Sedimentation-based devices using sample dilution before operation typically benefit from these phenomena. Separation of blood samples with low hematocrits, such as infant or anemic patient samples, is expected to be of better efficiency. Extremely high hematocrits are rarer and are usually caused by severe dehydration or blood diseases. Thus, a device functional with healthy male-patient blood of

hematocrit 45-50% should be effective for the immense majority of hematocrit encountered.

2.12 Effect of particle size

In this section, cell radius will refer to cell Stoke radius as this is the parameter of importance in sedimentation processes. Considering the shape of erythrocytes, the Stoke radius depends both on the cell size and its orientation: a standard value for Stoke radius of erythrocytes is approximately 2.5 μm, as discussed in section 2.6. The effect of cell Stoke radius on separation delay is shown in Figure 2:13a. This relationship is mainly influenced by the changes in sedimentation speeds with cell stoke radius as discussed in section 2.2. As speed increases quadratically with cell radius in Equation 2:3, the separation delay decreases inversely with the cell radius. Around the physiological cell radius of 2.5 μm, the sensitivity of separation delay to cell radius changes is -373 s/ μm.

In Figure 2:13b, the yield as a function of time is shown for different cell radii. Changing cell radius, changes sedimentation speeds equally for all local volume fraction. Thus, it creates a temporal dilation of the curves shown in Figure 2:13b. All curves still tend to the same value of 40% yield.

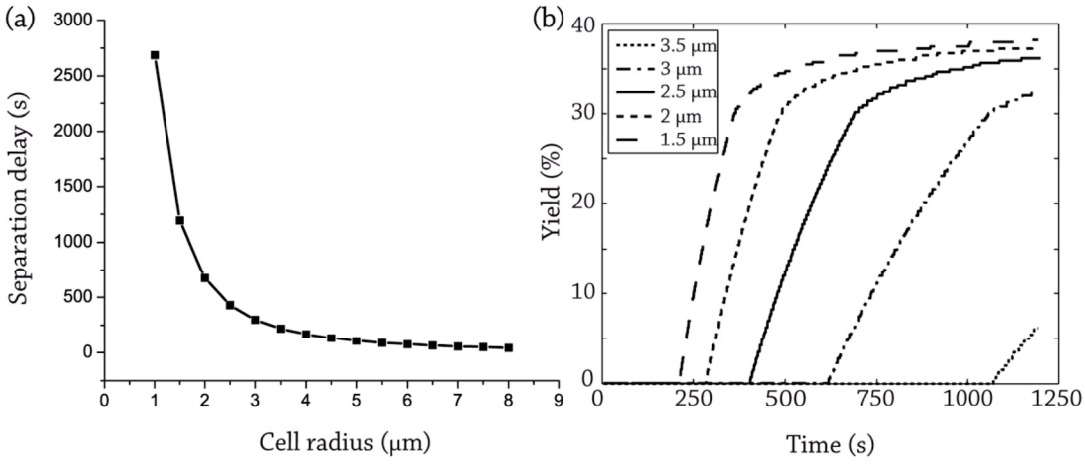

Figure 2:13 : Effect of cell Stoke radius (a) separation delay as a function of cell radius (b) Yield as function of time for different radii

This factor influences greatly the separation process. Blood samples with pathological small cells, common in sickle cell disease, are expected not to separate during device operation. Cell dimensions are also influenced by the additive used on the blood samples: anti-coagulation often creates swelling or shrinkage of the cells (Rosenblum 1968). Additionally formation of aggregates (natural such as

rouleaux or artificial such as triggered by an additive) should make the separation process faster.

2.13 Effect of temperature

In this section the effect of temperature on the separation process will be discussed considering the temperature-induced variation in plasma viscosity. Other effects, such as variations of cell density or plasma density, are dominated by the changes in plasma viscosity. The change in plasma viscosity with temperature is governed by the following equation.

$$\mu_0 = \mu_{37°C} e^{0.021(37-T)}$$

Equation 2:32 – Plasma viscosity dependence on temperature

where μ_0 is the medium viscosity, $\mu_{37°C}$ is the medium viscosity at 37°C, T is the temperature

The effect of temperature changes on the separation delay is shown in Figure 2:14a. The relationship is exponential as expected from Equation 2:32. Around room temperature, the sensitivity of separation delay to temperature is -8.5 s/°C.

The plasma viscosity influences the overall viscosity of the suspension and thus the sedimentation speeds. Similarly to the influence of size, temperature changes create a temporal dilation of the yield curves in function of time presented in Figure 2:14b.

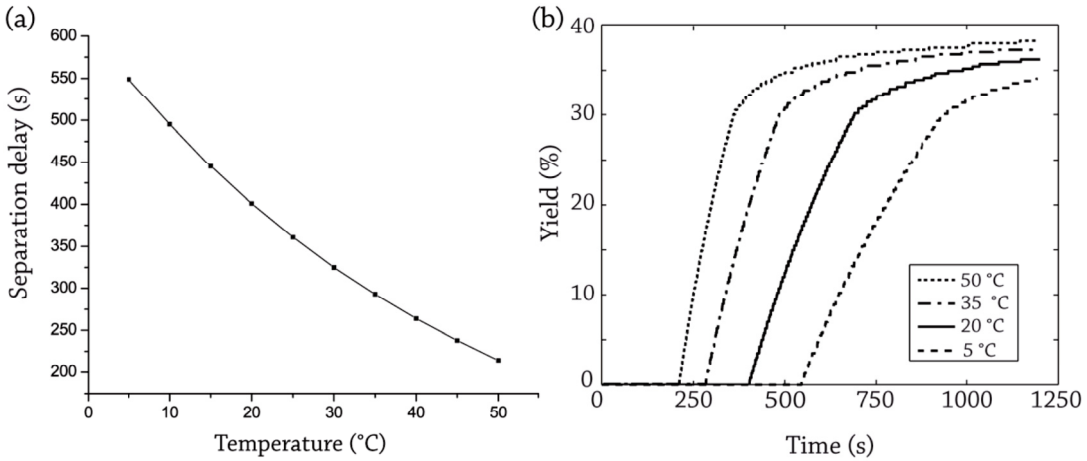

Figure 2:14 : Effect of temperature (a) separation delay as a function of temperature (b) Yield as function of time for different temperatures

The temperature influences greatly separation kinetics. Considering that room temperature encountered in a laboratory setting might oscillate in between 20-25°C, the separation delay corresponding change is about 45 s: more than 10 % change. The separation will be greatly influenced, in field use, by temperature conditions: separation delay on a cool winter day is twice that on an extremely hot summer day.

2.14 Strain-rate

In this numerical model, pressure gradient is 100 Pa/m and yields a linear velocity of approximately 45 µm/s. These values are close to the values reported in Chapter 3. With such a pressure gradient, the maximum strain rate in the cell suspension is reported in Figure 2:15. The maximal strain rate is situated at the channel wall, at first, and then moves to the supernatant interface, as sediment is formed.

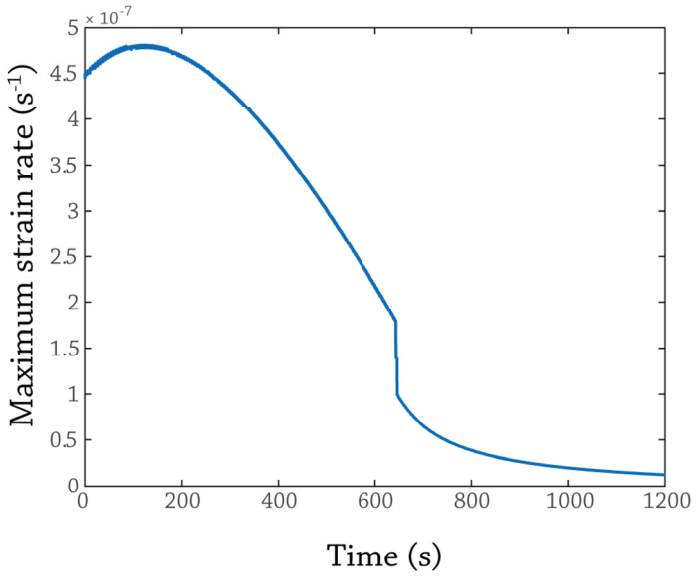

Figure 2:15 : Maximal strain rate in the cell suspension as a function of time for physiological parameters

The strain rate is the derivative of the velocity as defined by the equivalence in Equation 2:15. At high strain rates, a non-Newtonian liquid exhibits a change of viscosity as described in section 2.5. As the plasma is a Newtonian liquid, the maximal strain rate in the cellular suspension was extracted to assess the importance of a possible non-Newtonian behavior. The values reported here are much lower than the critical strain rate $\dot{\gamma}_C \cong 2\, s^{-1}$ described in section 2.5. This value is typical of whole blood at physiological hematocrit (D Quemada 1978).

The non-Newtonian behavior of blood samples is irrelevant for the strain rate in the system. The low velocity and low pressure gradients result in a low strain rate that allows considering the blood samples as a Newtonian liquid.

2.15 Conclusion

This chapter presented a model for sedimentation-based separation of suspensions in microchannels. Such suspensions can be described by Kynch sedimentation theory. Continuous and non-continuous dynamic changes in local particle volume fractions are described in a continuum framework. The volume fraction changes induced by the sedimentation process generate viscosity difference dominated by particle-particle interactions. The viscosity of the high volume fraction suspension is modeled following Quemada law. The combination of these models describes a system where the sedimentation creates a separation between a supernatant low viscosity particle free liquid and an underlying high viscosity particle sediment. The application of a pressure gradient creates flowrate in the microchannel containing the sedimenting suspension. An integral form of velocity and shear rate is presented for arbitrary conditions of local changes of volume fraction. This allows the description of the mechanisms at play upon simultaneous sedimentation and capillary flow of suspension.

The sedimentation mechanisms of blood samples were described using the established laws: hematocrit-dependent modes of sedimentation are presented. The described model was implemented in a unidimensional numerical finite difference manner. This allows describing the mechanism through which the cell-free supernatant flows at a greater velocity than the sediment and creates a clear plug. The separation delay is defined here as the time needed for the extraction to start: time point at which clear supernatant flows faster than cell suspension. The yield is also defined as the proportion of cell-free liquid extracted from the whole channel height. For physiological conditions, the separation delay is computed to be 403 s. Moment at which, the yield increases rapidly to 30% then slowly tends to 40%. The effect of different blood and design parameters is studied and their effect on separation delay is summarized in Table 2:2.

Table 2:2 : Model parameter and associated sensitivity of separation delay

Parameter	Nominal value	Sensitivity
Channel height	200 µm	2 s/µm
Hematocrit	45%	12.5 s/%
Particle radius	2.58 µm	-373 s/µm
Temperature	20 °C	-8.5 s/°C

The strain rate obtained in this model shows the non-importance of the non-Newtonian behavior of the suspension. For higher pressure gradients, models to extend the theoretical developments are proposed.

The main limitation of this model is its unidimensional nature. The differences in velocity should allow, in a 2 dimensional model, upstream cell suspension to flow over downstream sedimented cells. Thus, reaching a steady state where the cell suspension progresses at a fixed rate and cell free liquid at a higher rate. The yield should in this configuration reach stable lower values. This rolling motion is at the heart of the separation process as observed and described in chapter 3. If yield might be more precisely described in a two-dimensional model, the separation delay should be sufficiently described by this unidimensional model.

Chapter 3 will present a system based on the separation mechanism discussed here. The measured separation delay and yields for different blood samples are presented.

Chapter 3 Capillary-driven microfluidic device for sedimentation-based separation of finger prick blood microsample

This chapter presents a device for blood microsample separation based on sedimentation. The device has two functions: the extraction of plasma and the ejection of a volume-controlled separated sample. The device is presented and its function is characterized.

3.1 Introduction

The microfluidic device presented here is designed for blood sample preparation at the point of collection, while still being a candidate for integration in µTAS. Figure 3:1 illustrates its operation scheme. As illustrated in Figure 3:1a, the chip is devised to be used with finger prick capillary blood samples. These samples are convenient and require little to no skill to be taken as discussed in Chapter 1. The separation relies on sedimentation, as described in Chapter 2, to perform the blood liquid fraction extraction. The chip, as illustrated in Figure 3:1b, is of simple structure. The separated samples are retrievable off-chip in a volume-controlled fashion via an ejection mechanism, illustrated in Figure 3:1c, and can be used in a dry or liquid form for subsequent operations or analysis.

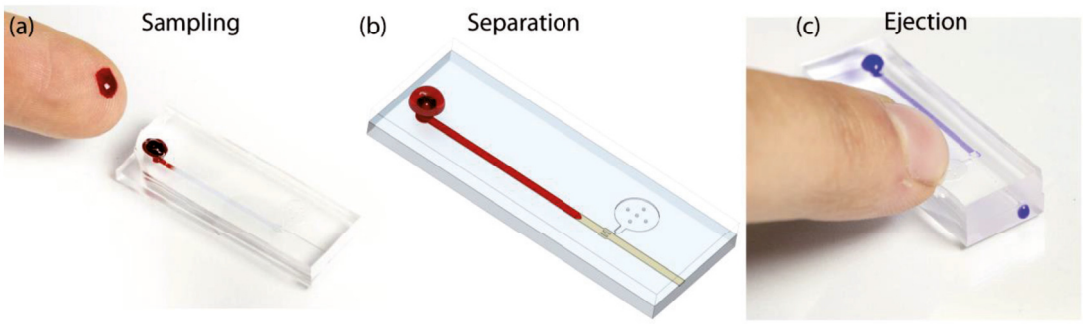

Figure 3:1: The device operation (a) Sampling of fresh whole blood and loading in the device (b) Separation and metering of the cell-free sample (c) Subsequent analysis performed in bench-top gold-standard equipment

3.2 Microfluidic device

3.2.1 Device structure

The device is illustrated and imaged in Figure 3:2. In following representations, devices are oriented with flow going from left to right. Extracted cell-free liquid is represented in a clear blue color to coordinate with the color of plasma obtained from stained whole blood separation : staining is used for easy visualization of extracted samples.

The device presented here consists of a microfluidic system containing a separation area and an ejection area, as illustrated in Figure 3:2a. The device is loaded through an inlet port with whole blood. Upon entering the device, the blood penetrates in the separation area. This straight channel section allows for the

sedimentation to create the desired viscosity contrasts. The process is detailed in section 3.3 and modeled in Chapter 2. This channel area contains neither trench nor complex structures: it is a simple single depth channel. Upon reaching the end of this area, a cell-free liquid plug is generated. The second part of the device consists of an ejection area detailed in section 3.4. The ejection area defines a 2 µL volume-metered output sample that is expelled from the chip upon actuation of a mechanism. The sample can be retrieved in liquid form with a pipette at the chip outlet or in a dry form in a dried plasma spot format. To form the dry sample, as the ejection mechanism is actuated an absorbent substrate is brought in contact with the outlet. The sample is sucked into the absorbent substrate by capillary action before it is allowed to dry in contact with air. The liquid or dry sample can be stored and used in subsequent analysis.

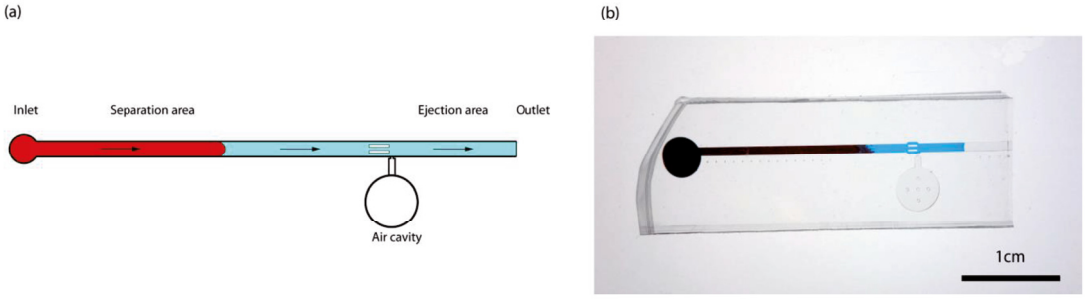

Figure 3:2 : Device structure containing two areas performing the main functions : separation and ejection (a) Illustration of the device structure (b) Imaging of the device

3.2.2 Fabrication process

The microfluidic device fabrication is based on a standard soft lithography polydimethylsiloxane (PDMS) process illustrated in Figure 3:3. The device consists of two parts: the top part contains the imprint of the structure while the bottom is modified with surfactant to obtain an adequate capillary pressure in the device.

The top part mold consists of a silicon wafer onto which a 200 µm SU-8 (GM 1070, Gerstelltec, Switzerland) layer is spincoated and photostructured. A 2 mm PDMS (Sylgard 184, Dow Corning, USA) layer is poured on the mold before degassing. The PDMS was prepared from a 1:10 mixture of curing agent and base. The structured PDMS layer is partly cured for 30 min at 80°C.

The bottom part mold consists of a bare silicon wafer exempt of structure. A 1 mm layer of PDMS with the addition of 0.58% of surfactant (Silwet 618, Momentive) is poured on the mold before degassing. The hydrophilic layer is partly cured for 30 min at 80°C.

Both the top and bottom layers are cured simultaneously. Each structured imprint in the top layer is cut to chip size and a 2 mm inlet is punched. The structured layer is put in contact with the hydrophilic part and the chip outlet is created by cutting the channel at the utmost end of the ejection area. The devices are stored at room temperature for at least 24 hours before use. This delay allows for complete polymerization of the materials and the establishment of some adhesion force resulting from cross-linking between the layers. This adhesion allows better handling of less fragile devices. Strong adhesion is not required for the operation of this device as the pressures at play are negative (capillary pressure in the channel) and thus no leakage occurs as long as layers are in contact.

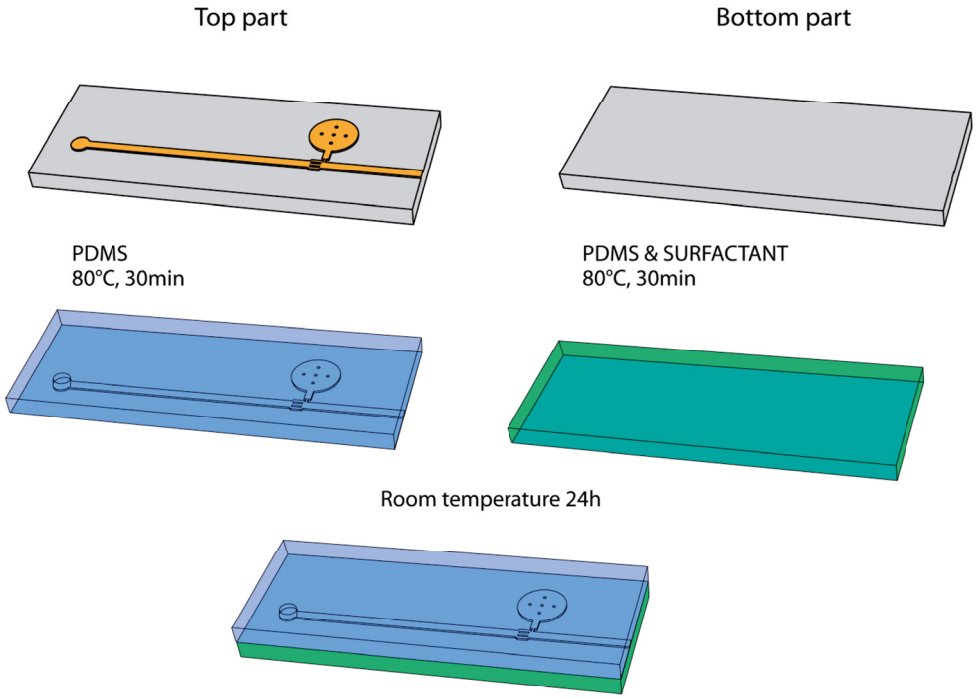

Figure 3:3 : Device fabrication process based on a PDMS soft lithography process. Top part is made of a PDMS while bottom part contains an additive to generate the necessary capillary effect.

3.3 Separation process

While flowing in the separation area, under the action of gravitational forces, the cells present in the sample sediment towards the bottom of the channel (Figure 3:4a). This sediment is at a high volume fraction (φ) of cells and is of higher viscosity than the cell-free supernatant because of hindering forces between particles. The simultaneous pumping of the liquid and the generation of the different sediment phases creates a velocity difference between the thinner supernatant and the thicker sediment.

Upon entering the channel, the sample's solid fraction is homogenous and cells loaded liquid flows. As the process of separation occurs, a layer of cell-free liquid appears on top of the cell suspension at the liquid-air interface. This region, shown in Figure 3:4b, is thickest at the air-liquid interface and gets thinner as the distance from the interface increases until disappearing. When the thickness of this layer reaches a threshold, the clear supernating plasma starts flowing faster than the sediment and a plug of cell-free liquid appears at the air-liquid interface. The time needed to start the separation is referred here as the separation delay. After this delay separation, the plasma occupies the entire height of the channel at the flow distal interface: a spatial separation of a cell-free liquid plug occurs along the channel length. As modeled in Chapter 2, the duration of this separation delay depends on blood parameters such as hematocrit or cell size. The height of the channel in the separation area of the device presented in this work is $h = 200$ µm, while its width is $w = 1$mm. Cell size is negligible compared to channel height. Thus, particle-particle and particle-liquid are the dominant interactions and wall effects that could hinder the mechanism are negligible. However, a bigger height increases sedimentation distances and thus the separation delay, as discussed in Chapter 2.

During the plasma extraction phase, the cell-free liquid plug grows continuously as blood enters the system. The air-liquid interface is positioned far from the cell suspension front. The cell suspension forms a high viscosity sediment visible in Figure 3:4c. This sediment progresses in the chip during extraction. Microscope observations have confirmed that, as illustrated in Figure 3:4a, the top layers in the cell sediment progresses faster than the underlying layers. This is due to the Poiseuille flow profile and the variations in solid fraction in the sediment. The top layers have not reached maximum packing fraction while bottom layers have, thus

creating a difference in viscosity. The velocity profile in the sediment makes for a progression mechanism where top layers flow over the still bottom layers. Thus, the top sediment layers settle in front of the underlying layers. This rolling phenomenon is totally absent in the unidimensional model presented in Chapter 2.

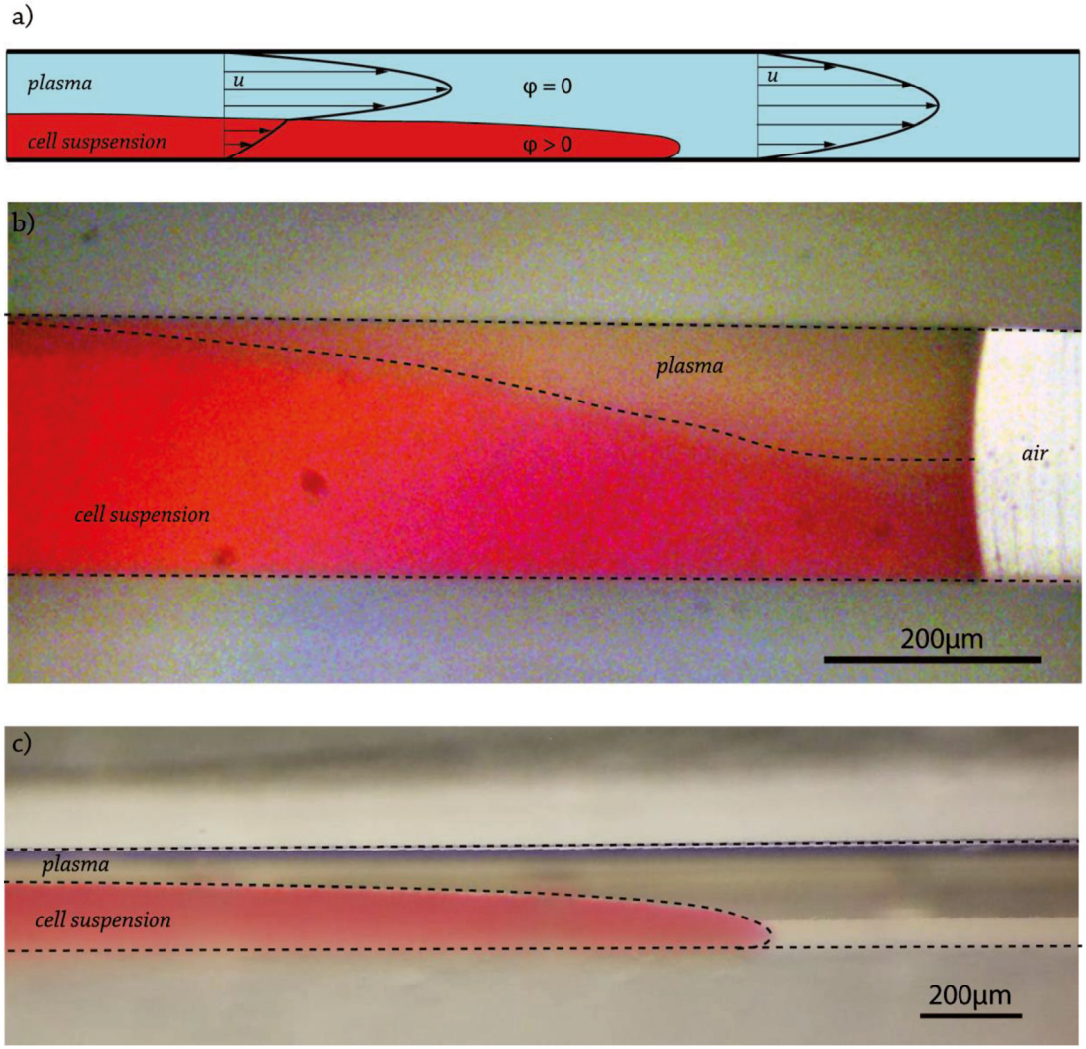

Figure 3:4 : Side views of the sedimentation-based separation (a) Illustration of the separation principle showing the expected velocity u distribution (b) Front with cell suspension before separation delay. The cell-free supernatant layer is forming but the plug has not formed yet (c) Cellular front during extraction phase showing the clear separation between sediment and supernatant

3.3.1 Separation of anticoagulated samples

To characterize the separation phenomenon, an experimental protocol was devised with an external fluidic control and anticoagulated blood samples. The external control allowed fixing constant flow rates and thus the pressure gradient along the

channel. Contrary to capillary-driven devices that operate at constant pressure as described in section 3.3.3. The stability of the fluids at play was ensured by applying anti-coagulation to the whole blood samples: small variations in manipulation delay and clotting dynamics are thus irrelevant. Separation of fresh samples using a capillary-driven flow is characterized in section 3.3.2.

A 200 µl sample of untreated skin-puncture capillary whole blood was mixed with 1.6% of 2% Coomassie blue in water for staining and observation convenience and with 0.18 mg/100 µL of dried K2EDTA anticoagulant. The dilution due to the staining is minimal and the anticoagulation doesn't induce any dilution. The samples are thoroughly mixed before use through tube inversion. A 20 µL sample of prepared blood was loaded in a portion of tubing with the pumping system (Nemesys, Cetoni). Tubing and syringes were previously filled with water and an oil plug (Perfluoromethyldecaline, Fluotec) to prevent any compliance effect or mixing. The tubing was inserted in the inlet of the device placed in a closed container, as visible in Figure 3:5a. The container inner atmosphere was saturated with humidity by using an open water container, thus mitigating evaporation.

Time lapse imaging with a digital camera (Panasonic, Lumix) was used to characterize front positions as well as plasma or total feeding flow rate. The chamber's bottom was lined with millimeter graph paper for dimension calibration purposes. Cellular suspension front and liquid-air front positions were measured, using software (ImageJ), from the center of the inlet through the center line of the channel to the desired front. Extracted volume is determined by computing the volume contained between the cellular front and the liquid-air interface. The infiltration distance is the channel length primed with liquid and it is measured from the inlet center to the liquid-air interface. The feeding rate of whole blood was measured on the time lapse imaging data by measuring the progression of the liquid-air interface, hence the changes in infiltration distance.

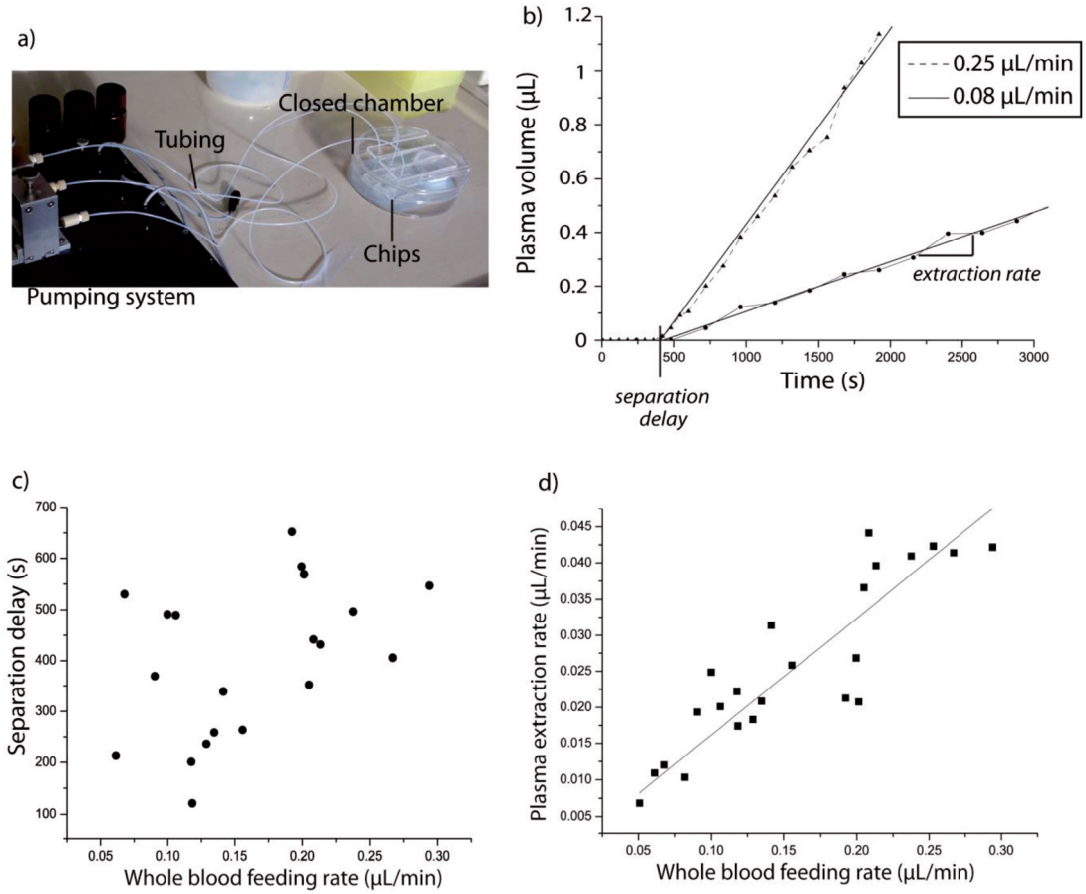

Figure 3:5 : Anticoagulated sample experiments (a) Experimental setup with external pumping system. (b) Typical extracted volume in time curve for 0.08 and 0.25 µl/min whole blood feeding rate. (c) Independence of separation delay with feeding flowrate (d) Dependence of extraction rate with feeding rate. A 16.8% yield is achieved during this phase.

To characterize the separation process, constant flow rates of 0.05 µl/min to 0.3 µl/min of stained anticoagulated whole blood were imposed in the separation channel. The separation process followed a pattern visible in Figure 3:5b: a separation delay that is followed by an extraction phase. Before the separation delay is reached, no separation is noticeable in the top view imaging. At this point, a rapid transition occurs to a steady state extraction phase. No transitional behavior was observed in the time lapse imaging data. During the extraction phase, the cell-free plug grows constantly with time during channel filling, as visible in Figure 3:5b. This region was observed to be linear at all time points and for all feeding flow rates (adjusted-$R^2 = 0.987 \pm 0.012$, $N = 23$).

The plasma extraction rate is computed by extracting the slope of a linear regression of non-zero extracted volume data points. The anticoagulated blood

separation delay is computed by using the time axis intercept of the linear regression.

The separation delay is represented against measured whole blood feeding rate in Figure 3:5c. For the separation delay computation, plasma extracted volumes with poor linearity (adjusted-R^2 <0.97) were excluded as well as low flow rates (feeding flow rates smaller than 0.05 µl/min). Low flow rates were excluded because the small difference in slope implies a high incertitude in intercept position. The separation delay shows little to no correlation with the imposed feeding flow rate (Pearson r − 0.43). The separation delay was determined to be 400s ±148s (N−20) for all feeding flow rates.

The extraction rate is represented against measured whole blood feeding rate in Figure 3:5d. The extraction rate is linearly correlated with feeding flow rate (adjusted-R^2 = 0.96, N = 23). The extraction yield achieved, defined here as the volume of plasma extracted compared to the total blood loaded in the chip during the extraction phase, was determined to be 16.8% ±3.6%. The yield can similarly be defined as the ratio between extraction rate and feeding flowrate. The process shows to be stable at least up to a feeding rate of 0.3 µl/min. Higher flow rates were not tested because the high volume filled during the separation delay would not allow a reliable determination of the flow rates: the extraction phase would not correspond to a sufficient channel length for reliable measurements.

3.3.2 Separation of fresh samples

To characterize the fresh blood separation mechanism, the devices were run using the capillary pressure as the driving mechanism. With such a design, pressure is constant in the system but flow rates vary with the accumulation of resistance : resistance increases as the liquid primes more channel distance. The fluidic control, discussed in section 3.3.3, is set by design, thus reducing experimental flexibility and stability. The fresh samples are intrinsically less stable during use and their properties alter during the experiment.

As for anticoagulated samples, a 200 µl sample of untreated capillary whole blood was mixed with 1.6% of 2% Coomassie blue in water for staining and observation convenience. This staining should not alter the blood sample that should behave as fresh unstained finger-prick samples. The samples are thoroughly mixed before use through up/down pipetting operations. A 25 µL of prepared blood was loaded with

a pipette in the chip inlet port. This quantity is in excess, as the chip total volume is 7 µL. The sample totally fills the inlet and creates a drop on the chips top part. The chips were, prior to loading, placed in a closed container with high humidity to mitigate evaporation.

Time lapse imaging with a digital camera (Panasonic, Lumix) was again used to characterize front positions.

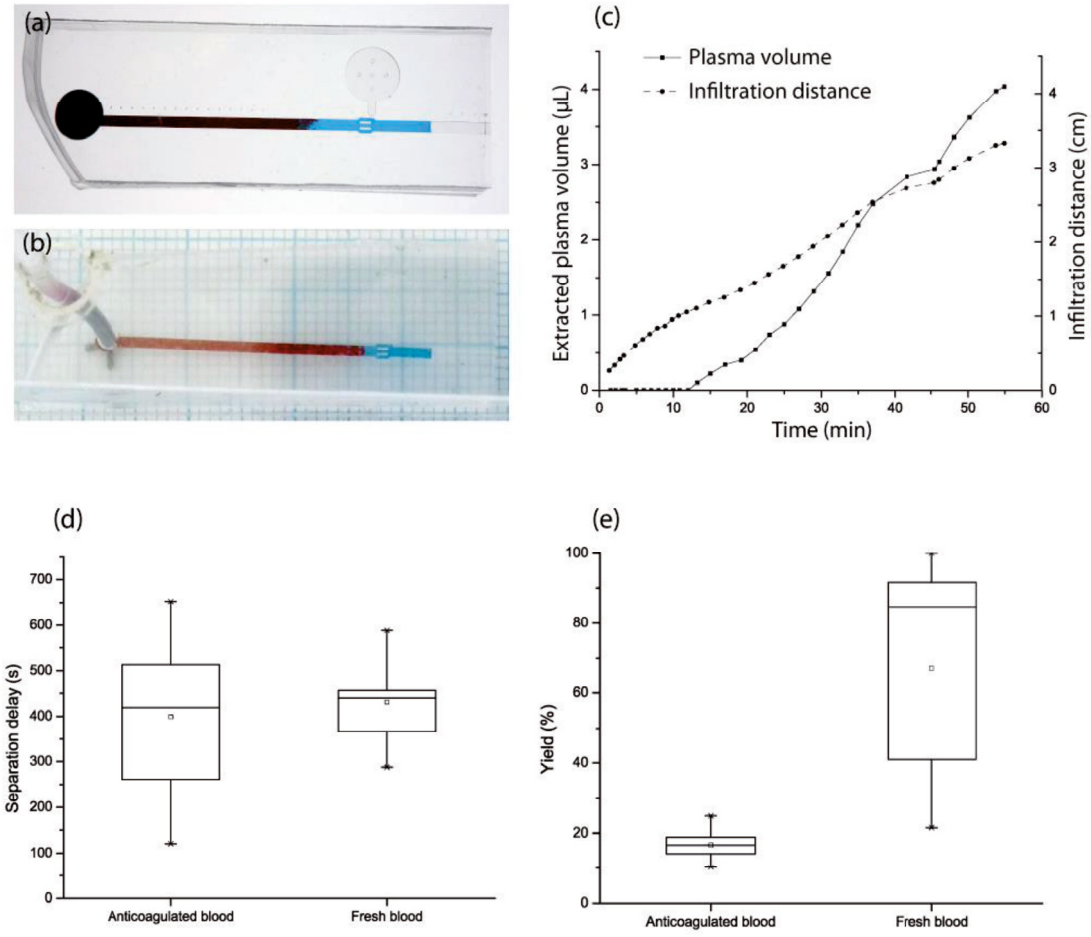

Figure 3:6 : Fresh sample separation experiments and comparison with anticoagulated samples (a) Device separating fresh sample exhibiting an irregular cellular front (b) Device separating anticoagulated samples exhibiting a smooth cellular front (c) Example of chip loading with extracted volume and infiltration distance with time (d) Comparison of anticoagulated and fresh sample separation delay. The separation delay show a strong similarity for both sample types (e) Comparison of anticoagulated and fresh sample yields. The yield show a strong dissimilarity for both sample

Imaging of the cell suspension front during operation showed a clear difference between anti-coagulated (Figure 3:6b) and fresh samples (Figure 3:6a). Anticoagulated showed a smooth slightly parabolic cellular front, whereas fresh samples showed an irregular and highly variable front shape as visible in Figure 3:6a.

As shown in Figure 3:6c, the separation behavior contains two regions, as with anticoagulated samples: a separation delay period and an extraction phase. Due to the non-constant nature of the capillary-driven flow rate in the device (see section 3.3.3) combined with the coagulation mechanism, the extraction rate is not constant.

The fresh blood separation delay is determined by identifying the first time point with a resolvable clear plug in the time lapse imaging data. The cell-free liquid extraction yield is computed in the following paragraphs by considering the total volume entering the chip during the extraction phase and the total generated clear liquid during the complete extraction phase. This value represents a time average yield during the complete extraction phase.

The fresh blood separation delay is 430s ±88s (N = 13). The fresh blood separation delay is represented in Figure 3:6d and compared to the anti-coagulated blood separation delay reported in section 3.3.1. No significant difference can be observed between both samples.

The fresh blood extraction phase yield obtained is 67.1% ±30% (N = 13). The fresh extraction yield is represented in Figure 3:6e and compared to anti-coagulated blood extraction yield reported in section 3.3.1. A significant yield increase is noticeable between anti-coagulated and fresh samples: a 4-fold increase in yield associated with a significant increase in variabilty. Thus, this experiment shows that the mechanism of separation of fresh samples and anti-coagulated samples are different, probably due to coagulation in the samples.

3.3.3 Capillary-driven flow

Experiments reported in section 3.3.2 were conducted using only the design-dependent capillary pressure to drive liquid in the separation channel. This section discusses the fluidic behavior expected.

The device is formed of two materials with different surface energies and thus contact angle. The contact angles on the surfactant-loaded modified material was characterized in a dedicated tool (DSA-30E, Krüss, Germany) using water as test liquid and the results was 78.1° ±0.6° (N=3). A 5 minute delay was implemented between dispensing and measurement to allow for stabilization of the contact angle. The surfactant-loaded surface contact angle showed reduction with time possibly due to surfactant solubilization dynamics: the drop would spread with time. For further calculation, raw PDMS contact angle is estimated to be 98.7° (Jo et al. 2011).

Surface tension creates a curvature of the air-liquid interface and a total net force. In capillary-driven devices of constant geometry, such as the presented device, capillary pressure is constant and highly depends on contact angle on each surface. The device has a surfactant-loaded channel bottom and raw polymer channel top and walls. For such conditions, pressure is given by Equation 3:1(van der Wijngaart 2014; Zimmermann et al. 2008).

$$P = -\frac{dU_t}{dV_t} = -\gamma_{la}\left(\frac{cos\theta_{mod} + cos\theta_{PDMS}}{h} + 2 * \frac{cos\theta_{PDMS}}{w}\right)$$

Equation 3:1 – Capillary pressure in microchannel

where P is the total capillary pressure, U_t is the total interfacial energy, V_t is the volume filled in the channel, $\theta_{mod}$is the contact angle on the hydrophilic modified PDMS, θ_{PDMS} is the contact angle on the PDMS, h is the height of the channel and w is the width of the channel. Considering the parameters of the device, the computed pressure is 0.1 Pa.

If pressure is constant across the whole structure, the fluidic resistance increases linearly with the liquid infiltration length in the channel. Considering the channel cross-section, the resistance by unit length is governed by Equation 3:2 (Kirby 2010).

$$R_{linear} = \mu \frac{12}{w\, h^3 (1 - 0.63\frac{h}{w})} \quad \text{if } \frac{w}{h} > 2$$

Equation 3:2 – Linear resistance of a microchannel

where R_{linear} is the resistance per unit length, μ is the dynamic viscosity. The resulting resistance per unit length is $1.7*10^{12}$ kg/m^{5}s

The accumulation of resistance and the constancy of pressure leads to a variation of flow rate : flowrate is high upon entering the channel and decrease as infiltration distance increases as shown in Figure 3:6c. The infiltration length is proportional to $\sqrt{t}$ as described by Washburn law (Masoodi & Pillai 2010). Considering the given parameters, chip complete loading should be 41min. This corresponds roughly to the observed behavior. However, the observed fluidic behavior shows a strong variability.

3.3.4 Discussion of separation mechanism

The separation of anticoagulated samples with external flow rate control showed good repeatability both in extraction rate and separation delay. The separation time delay showed no dependence with feeding flowrate. As expected from chapter 2 modeling, the separation delay depends solely on sedimentation parameters such as channel height, hematocrit or cell size and shows no dependence to feeding flow rate (or similarly to dP/dx). Changes in temperature or cell size due to anticoagulant mixing may explain the separation delay variability. It is expected that, at higher flow rates, inertial forces will disturb the sedimentation mechanism. Our experiments have however not shown this threshold. The separation delay obtained corresponds to the expected value computed in Chapter 2 for a young male adult: the model describes adequately the formation of the supernatant at the interface.

For anti-coagulated samples, the yield is constant during all the extraction phase as no transition is observed. This contradicts the model presented in Chapter 2. From this model, a transitional behavior is expected during 100-300s: the yield should increase almost linearly during this time period. The two dimensional separation mechanisms in the sediment could explain this divergence. This mechanism is also the reason for the stable 17% yield. The higher yields proposed in the unidimensional model do not take into account the constant renewal of the cellular front.

For anti-coagulated samples, the stability of extraction rate is excellent even for long experiments as shown by the temporal linearity of extracted volumes shown in Figure 3:5. Cells sedimentation in the inlet port seems not to impact the separation. If this process was of importance, the suspension entering the channel would be saturated with cells after approximately 1000 s considering the sediment

interface progression speed computed in Chapter 2. The yield would thus decrease drastically as saturated blood would enter the separation channel, with little plasma to be extracted. The drastic increase in resistance would also disturb the fluidic function of the device. This phenomenon is not observed and mixing in all or part of the inlet could explain this time constancy of extraction rate. Thus, blood supplied to the separation channel appears to be of constant hematocrit.

The maximum extraction rate observed for anti-coagulated samples was 0.05 µL/min for a feeding rate of 0.3 µL/min. In such conditions, the extraction time for 2 µL is 40min. The total operation time would be around 47 min for the separation of 2 µL considering separation delay and extraction time. Under these conditions, we have observed no mixing and the associated Reynolds number is given by Equation 3:3.

$$Re = \frac{Vm\, D_h}{\nu}$$

Equation 3:3 – Reynolds number

Where Vm is the characteristic flow velocity, D_h is the hydraulic diameter, and ν is the kinetic viscosity of initial hematocrit blood. Considering the parameters in our case : $D_h = 333\mu m$, $Vm = 25\mu m/s$, $\nu = 3.8 \cdot 10^{-6}\, m^2/s$. The corresponding Reynolds number is $Re = 2.2 * 10^{-3}$. Doubling feeding flowrate should allow reaching the target operation time of 30 min while still maintaining laminary flow in the channel. This computation does not take into account changes in viscosity in the channel.

The similarity between fresh blood and anti-coagulated blood separation delays, shown in Figure 3:6, results from clotting dynamics. The serum extraction protocol usually requires a 30min clotting time. The 6min40s separation delay here is much shorter than traditional clotting times: little clotting occurs and the sedimentation mechanism is similar with fresh and anticoagulated samples.

A key difference between anticoagulated and fresh samples is the clotting that occurs during the extraction phase. During the first instants of extraction, the separation mechanism is expected to be similar between anti-coagulated and fresh samples: plasma is extracted. However, if the separation phenomenon is stable for anti-coagulated samples, fresh samples exhibit a variable increase of yield with time: clotting in the sample occurs as shown by the difference in cellular front

shape. The clotting of the dense sediment creates a plug that filters the blood: serum is extracted through the clot. The high yield number show that blood entering the channel is filtered upon entry: thus concentrating blood cells in the inlet and loading the channel with already separated liquid. Fresh blood extraction yield is thus noticeably higher than expected plasma proportion in the sample. The variation in clotting dynamics explains the high variation shown in the yield. Coagulation is expected to increase variability due to its intrinsic patient-dependent and time-dependent nature (Mann et al. 2009). This filtration mechanism might increase hemolysis in the sample but allows a high yield. The sample is expected, for fresh samples, to be a combination of a majority of serum and a minority of plasma. This filtration phenomenon is not taken into account in the model presented in Chapter 2.

The low pressure and resistance encountered in this device contribute strongly to the variability of capillary-driven flow rates and filling times. The low capillary pressure makes the device sensitive to perturbations due to the importance of hydrostatic pressure, inlet drop pressure and evaporation in the low pressure and low resistance system. Pressure is also very sensitive to contact angle changes; as is the total chip loading time. The total chip loading time is very sensitive to contact angle on the hydrophilic wall : $3 \cdot 10^5$s per degree contact angle on the hydrophilic side. This high sensitivity to surface energies is the cause for observed local variation of flow rates. The reduction in hydrophilic surface contact angle, observed with time, possibly creates a dynamic equilibrium of pressure and flow rate thereby stabilizing the device and making the filling more reliable.

3.4 Ejection mechanism

The device is designed for off-chip sample retrieval for later downstream gold-standard bench top analysis. As established in Chapter 1, a common source of error in the pre-analytical phase is the inadequate volume of the sample. Thus, the device incorporates an ejection mechanism allowing retrieval of a volume-metered separated sample.

The channel distal part contains a metering area as illustrated in Figure 3:7. This area contains the 2 µL sample volume to be ejected. The volume is defined by two capillary valves placed on each side of the metering area: an in-channel capillary valve and the open outlet. The in-channel capillary valve contains narrow channels

of higher capillary pressure that create a delay upon channel flow but don't impede the liquid progression to the metering area. Upon complete filling of the metering area, flow in the device stops spontaneously as the outlet forms a capillary stop valve. This spontaneous end to the device operation allows for operating the device ejection with more time flexibility: no overflow or rapid failure can occur once full.

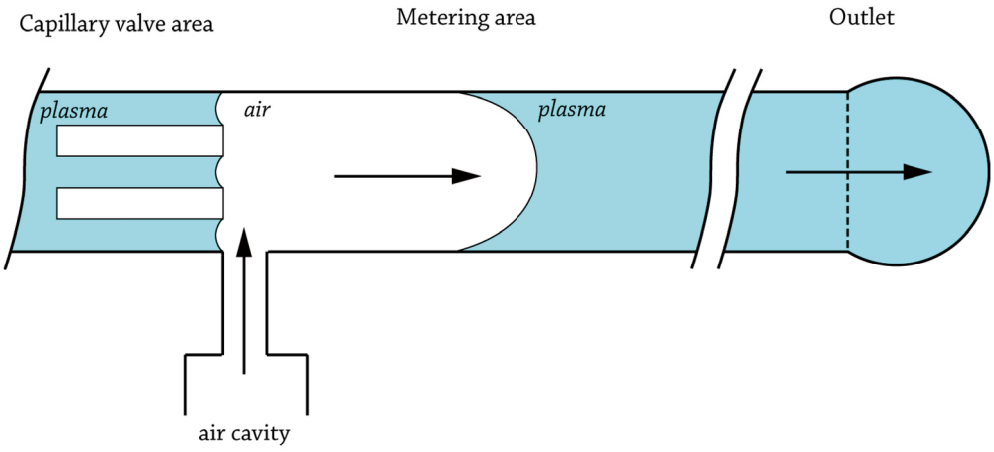

Figure 3:7: Ejection mechanism. Air injection allows the ejection of a 2 µL liquid sample from the metering area. The volume definition is performed by the capillary valves present in the channel and at the outlet.

The sample ejection is activated by collapsing, through external mechanical pressure, an air cavity in the chip. The air cavity is connected to the metering area next to the capillary valve. Upon collapsing the cavity, air is injected in the channel as shown in Figure 3:8a. There is a contrast in fluidic resistance between the capillary valve and the separation channel on the left side of the air injection channel and the metering area and the outlet on the right side. The difference between upstream and downstream resistance at the point of injection and the high capillary pressure in the valve orients the air flow entering the metering area towards the outlet. Surface tension in the capillary valve implies that the pressure generated upon collapsing the air cavity creates an air/liquid interface at the capillary valve distal end. The pressure generated is not sufficient to allow air to enter the capillary valve narrow channels. It is however sufficient to overcome the capillary pressure at the outlet and generate a drop outside the chip at the outlet as shown in Figure 3:8b. The cavity is collapsed until the metering area is emptied into the drop and air is allowed to exit the channel through the outlet. The drop generated at the outlet was retrieved in this work using a pipette. For proof of

concept purposes, samples were successfully transferred directly to DBS paper supports. The metering restricts the volume that is ejected and thus renders the system impervious to variation in extracted volume.

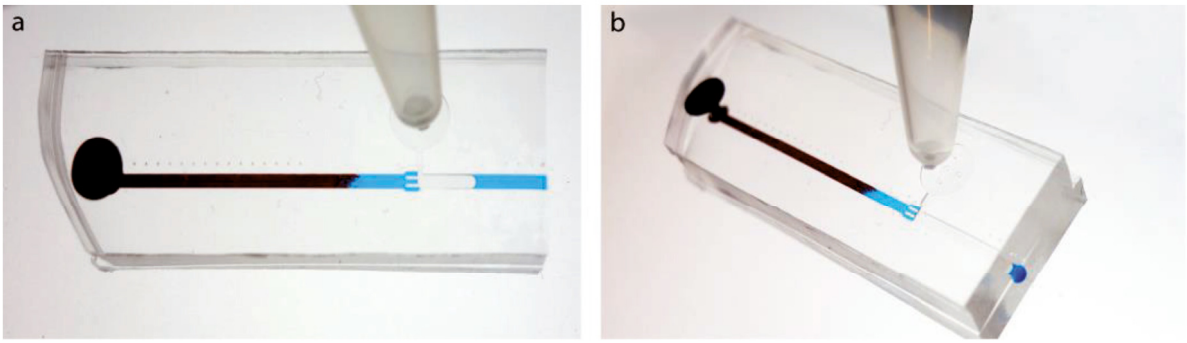

Figure 3:8: Ejection mechanism actuation (a) Air injection in the metering area upon collapsing of the air cavity (b) Drop formed at the outlet with empty metering area.

Two valve geometries were implemented. A narrow design, shown in Figure 3:9a, created a local increase in resistance by reducing the total width in the capillary valve and had a relatively high barrier pressure. The pressure barrier is different on the side channels than on the central one, due to the angle of surrounding structures. If the ejection was ensured, the resistance and pressure barriers lead respectively to a slow filling and a high delay (or a stop) in the capillary valve. An expanding/narrowing design was implemented to accommodate a resistance neutral valve, shown in Figure 3:9b. Also, to reduce barrier pressure, angles were altered after the valve: a narrowing of the channel to its initial width was implemented. The negative angle (narrowing) on the side channels improved priming performance by altering the energy barrier (Man et al. 1998). The air injection channel was placed in the wide part of the channel. This ejection showed satisfactory ejection performance, while having faster filling times and low delays.

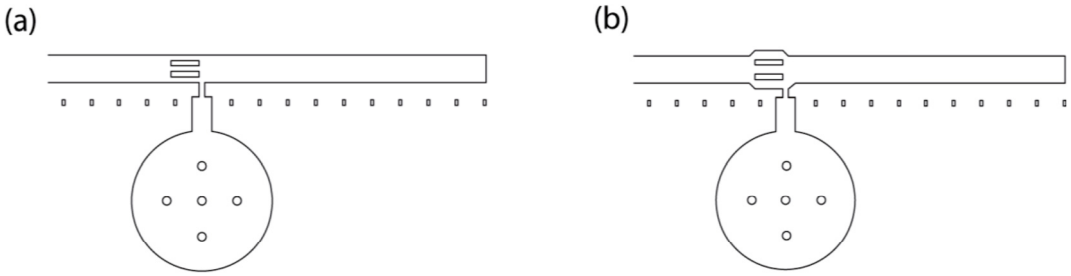

Figure 3:9 : Capillary valve designs (a) Narrow valve with higher fluidic resistance and energy barrier (b) expanding/narrowing valve with lower fluidic resistance and energy barrier

The main source of variability of the ejection volume is most certainly due to the cutting with a blade of the distal end of the channel. This operation was done manually under microscope. The parallax and the difficulty to precisely cut vertically in the high PDMS thickness are the cause of small volume variations: estimated to ±5% under microscope inspection. This variation is not inherent to the ejection mechanism and could drastically be reduce through fabrication changes. Alternatively, the inclusion of an in-channel stop valve could increase ejection volume reliability while still allowing some variations in the outlet position.

3.5 Device operation

The device was tested by different operators using fresh blood and capillary-driven flow. Failures were reported. Test batches included 16 devices with straight capillary valve and 51 devices with an expanding/narrowing capillary valve. The identified failure modes are reported and described in the Table 3:1.

Table 3:1 : Failure modes identified and description

Failure mode	Description
Blocked at restriction	Flow stopped at the capillary valve
Incomplete load	Flow stopped or slowed drastically before operation end (max wait time 1h15)
Cell front passes restriction	Cell visibly contaminated the metering area
Operator loading failure	Operator failed to load the inlet port correctly

The analysis of the incidence of these failure modes is reported in Figure 3:10. Failure mode incidence reported in devices with the narrow capillary valve are presented in Figure 3:10a. The success rate was 50%. The majority of errors reported were failures of the capillary valve system leading to a failure to fill the metering area. The air-liquid front was stopped at the distal end of the valve in 25% of case due to its design. The design of the valve also contributed to the failures due to incomplete load: the high resistance of the valve made for a slower filling of the metering area. The remaining failures were due to the flow rate instabilities of the capillary-driven device: local flow-rate increases that would

resuspend cell or not allow them to settle or clot. These accelerations resulted in the cell front passing the capillary valve.

Failure mode incidence reported in devices with the expanding/narrowing low resistance capillary valve are presented in Figure 3:10b. The success rate increased to 71%. External user testing of the devices led to the addition of a new source of failures: operator loading failures. These failures are due to the difficulty of priming correctly the 2 mm punched inlet and are greatly operator-dependent. The failures due to the liquid front being pinned at the capillary valve are reduced to a marginal incidence with the less stringent valve design. The lower resistance of the valve is an important factor in the reduction of incidence of the incomplete load failure mode. However, the fluidic stability issues resulting in the cell contaminating the separated samples remain unchanged and these issues also account for the remaining failures of incomplete loading of the channel.

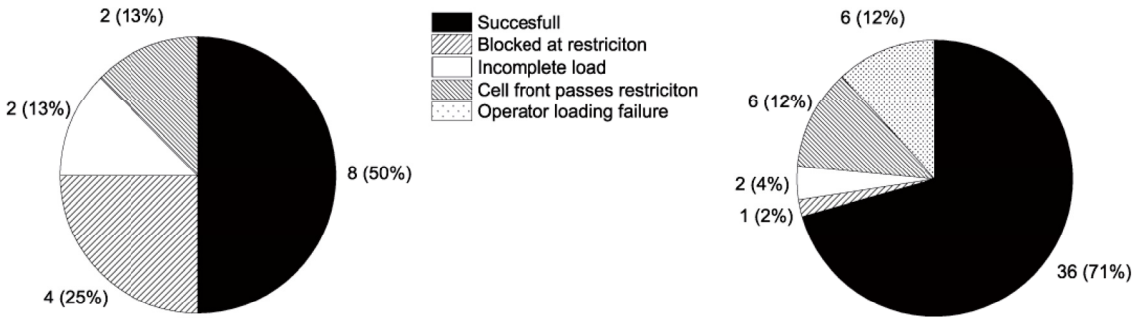

Figure 3:10 : Failure mode occurrence rate (a) Failure mode repartition for the devices having a straight capillary valve showing the strong failure rate of the capillary valve (N=16). (b) Failure mode repartition for the devices having a narrowing/expanding capillary valve. The success rate is not noticeably increased through the reduction in failures of the capillary valve passage (N=51)

The interface for loading the device with the sample is responsible for a significant portion of errors as shown in Figure 3:10b. The difficulty lies in dispensing the sample directly in the inlet with the liquid contacting the bottom surface of the inlet while not pressing the pipet tip in the inlet creating a seal and pumping liquid directly to the channel. The hydrophobic surface of the inlet means that air gets trapped in the inlet if the sample is not dispensed properly in the inlet and thus completely isolates the channel from any blood supply.

As mentioned in section 3.3.4, the stability of the fluidic behavior suffers from the low resistance and low pressure. It renders the device very sensitive to parameter

changes. This is the cause for the second significant failure group shown in Figure 3:10b: flow rate control instabilities creating cell front passing the restriction and incomplete load failures. The instabilities are due to local variations of infiltration speeds and thus flow rates due to local variation in contact angle or geometry. Local variations in contact angle could be due to local changes in surfactant concentration, local roughness change or contaminants. The local changes in geometry could be due to dust, debris or local changes in channel height. The 5:1 aspect ratio channel could allow for local collapsing that depends on the mechanical pressure applied in between layers upon assembly.

3.6 Design optimization considerations

3.6.1 Specific plasma and serum designs

In section 3.3, the important differences between separation of anticoagulated and fresh sample were investigated. Yield changes drastically between a separation relying only on the viscosity difference for anti-coagulated samples and a separation relying mostly on filtration through a packed clot for fresh samples. The device structure is operational for separating both types of sample. The nature of the separated liquid is expected to be different for each case: pure plasma for anti-coagulated samples, while fresh whole blood samples yield some plasma through pure sedimentation and larger amounts of serum after clotting. The subtle differences between plasma and serum mean that they are most often interchangeable for analysis. This difference yields the opportunity to create specific designs for each separated samples.

For fresh samples, the serum extraction device benefits from a much higher yield but suffers from the high variability of the clotting phenomenon. The timing of the process, in this particular case, depends not only on the sedimentation time delay but also on the clotting time. The formation of the clot and thus the yield could be rendered more reliable and repeatable through the addition of clot activator either at the moment of device loading or during flow in the channel. By design, the device presented previously has a total system yield (meaning ejected liquid compared to whole device volume) of 29%. This total system yield is thus functional for fresh samples separation.

For anticoagulated samples, the yield obtained is repeatable and should be taken into account for redesigning the separation area. The separation channel length depends on the volume of sample pumped during the separation delay to which 6 cm (12 µL) of channel length should be added for generating approximately 2 µL of cell-free liquid. This configuration should in average generate 0.35 µL of excess plasma plug in the separation channel that should account for the variability of the extraction process.

3.6.2 Fluidic design

As shown through several considerations throughout this chapter, the fluidic system suffers from obvious limitations that affect the reliability of the complete system. An interesting addition to the present device would be an initial flow resistor placed at the proximal end of the channel as illustrated in Figure 3:11a. The initial resistor dominates the channel resistance that accumulates with infiltration distance. This dominance stabilizes the flow rate as shown in Figure 3:11b: for high value resistors, the flow rate is constant. The addition of the capillary valve resistance is also negligible compared to the initial resistor, thus giving more flexibility in the design of these valves. The flow resistor would allow increasing drastically the pressure in the device thereby rendering it more stable towards local changes in surface energy.

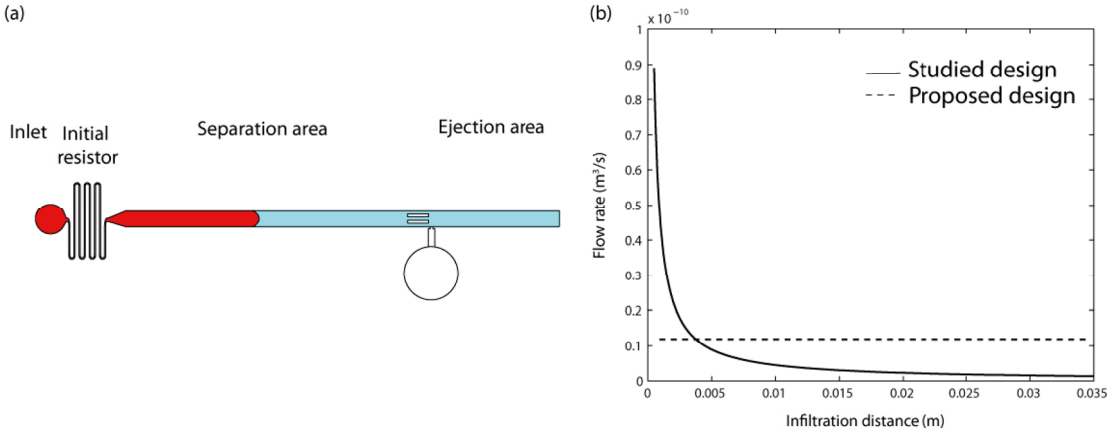

Figure 3:11 : Proposed fluidic design (a) Illustration of the initial flow resistor (b) Flow rate comparison between studied design and proposed design showing the constancy of the feeding flow rate in the proposed design.

As an example, a device with a 25° contact angle on the hydrophilic side has a capillary pressure of 284 Pa. A flow rate of 0.6 µl/min is achieved through the

addition of an initial flow resistor of $3*10^{13}$ kg/m^{4}s. Considering these parameters, for the generation of 2 µL of separated samples, the total device length would be 9 cm and the total sample volume required would be 18 µL. In this proposed design, the device operation would last 30 min and the total system yield would be 11.1%.

Such a design is, as mentioned, very tolerant to local changes in contact angle on the hydrophilic bottom: the sensitivity is 17 s/° on the filling time device. The sensitivity to a change in channel height is also low: 10 s/µm.

3.6.3 Ejection mechanism designs

The ejection mechanism implemented in the fabricated device has shown to be reliable. It is impervious to ejection speed differences or varying sample viscosities. Issues only arose, during preliminary testing, when the outlet was clogged either by samples or through a badly opened outlet during fabrication. Retention issues are absent of the expanding/narrowing valve design. The slight delay for exiting the valve could be further improved by modifying the angles of the structures present at the distal part of the valve that remain at a right angle. The initial resistor, discussed in previous paragraphs, would allow more flexible design as it does drastically increase the asymmetry in fluidic resistance of the device and renders the pumping of liquid towards the inlet more difficult.

3.7 Conclusion

The device presented in this chapter has two functions : separation of blood samples and ejection of a volume-metered output. The device successfully separates fresh and anticoagulated samples. In the case of anti-coagulated samples, after a separation delay of approximately 400s, the plasma is separated with a repeatable yield of 16.8%. The separation is driven by the establishment of a viscosity contrast in the channel that creates a clear liquid front progressing at higher speed than a cellular suspension front. For fresh samples, after a similar separation delay, the cell-free liquid is separated with a variable yield of approximately 67%. The high yield probably results from a combination of sedimentation and filtration (through the clot) separation, thereby yielding serum. The device allows the reliable ejection of a 2 µL clear separated sample when used with fresh blood.

The capillary-driven flow design allows the use of the device without external equipment. However, the low resistance and low pressure design showed here is very sensitive to change of capillary pressure during operation. This instability is the main cause of failure during operation.

Overall, the device shows a promising performance while still allowing room for optimization. The proposed addition of an initial flow resistor and the increase of capillary pressure would without doubt improve the reliability of the pumping phenomenon.

Chapter 4 Chip sample quality: off-chip characterizations

This chapter presents a cellular and a molecular off-chip characterizations of the liquid separated with the microdevice. In each case, a simple model is used to gain insight into the physical phenomena at play. Cellular analysis of the different separated liquids is performed using flow cytometry. Contamination is discussed in light of sedimentation speeds. Molecular analysis is performed using mass spectrometry proteomic profiling. Proteomic content is discussed and impact of surface adsorption and coagulation are assessed. Using these characterizations, sample quality and analytical reliability is established.

4.1 Cellular analysis and determination of separation efficiency

For separated samples, the contamination with cells can have an adverse effect on analytical results. Any remaining cells, most often RBCs, in the separated sample would affect the analytical reading or might lyse and contaminate the separated samples with their intracellular content (Kruszyna et al. 1977). As with hemolysis during separation, this contamination has a strong effect on analysis of high intra-cellular and low extra-cellular concentration analytes. In routine laboratory testing, the contamination is only assessed by rudimentary visual inspection of the turbidity of the sample (Kruszyna et al. 1977). In the following section, the cellular contamination of chip-separated samples is characterized using advanced flow cytometry.

4.1.1 Modeling of platelets contamination

The model developed in Chapter 2 describing the separation phenomena was limited to RBC sedimentation. However, blood is also composed of other cell types, among which platelets are the smallest (Hall 2010). For sedimentation-based separations, platelets might contaminate processed samples (Eastham 1963). A simplified model is described here to estimate the platelet contamination.

Sedimentation speeds are computed using Stoke velocity equation (Equation 2:3) for platelets; RBC sedimentation speed is computed for comparison purposes. RBC and platelets properties are summarized in Table 4:1. The separation is assumed to take place in a 200 µm high channel for a period of 45min. Using operation time and sedimentation speeds, sedimentation distance can be computed. Using the ratio of this distance to the channel height, the proportion of platelets separated is estimated.

Table 4:1 : Properties of RBC and platelets (Tandon & Diamond 1997; Hall 2010; Eastham 1963)

Parameter	Symbol	RBC	Platelets
Cell density	ρ_{cell}	1098 kg/m^3	1045 kg/m^3
Cell Stoke radius	R_{cell}	2.58 um	1.45 um
Concentration	C_{cell}	5 200 000 /µL	300 000 / µL

Considering plasma density $\rho_{plasma} = 1025\, kg/m^3$ and viscosity $\mu_{plasma} = 1.8\, mPa/s$, the sedimentation speed associated to RBC is 1276 nm/s and 55 nm/s for platelets. During operation, platelet sedimentation distance is 148 µm and an approximate 75 % depletion is expected. Thus, the contaminant concentration would be in the range of $1*10^5$ /µL, thus resulting in 97% purity : a significant platelet contamination is expected.

4.1.2 Quantification of contaminants

The capacity of the microdevice to separate particles in blood samples was tested. Fresh whole blood was separated in the device, diluted at 0.6% and used as experimental model. The samples originated from a single donor (young male adult) and were obtained through finger-prick capillary collection. Whole blood samples diluted at 0.06%, centrifuged serum and plasma samples (0.6%) were used as reference. The cellular components of each sample (302 µL) were analyzed using flow cytometry. The following parameters were measured: i) forward scatter (FSC), indicative of particle size; ii) side scatter (SSC), indicative of internal complexity and iii) number of events, indicative of particle count. Finally, particle concentration was determined as a ratio between total event count and original sample volume (corresponding to 0.2 µL or 2 µL for whole blood and separated samples respectively). Following Chapter1 definition, purity was calculated as the proportion of particles rejected when comparing separated and whole blood sample counts.

Experiments were carried out 5 times for each of the samples. A typical flow cytometry result of three separated samples is shown in Figure 4:1a. Particles are detected in each sample. Figure 4:1b represents the average particle concentration. Whole blood samples concentration was $3.6 \cdot 10^5$ particles/µL (coefficient of variation, CV = 17%). For reference samples, particle concentration was $1.1 \cdot 10^3$ particles/µL (CV = 48%) and $8.7 \cdot 10^2$ particles/µL (CV = 32%) for plasma and serum samples respectively. For the chip-separated liquid samples, particle concentration is $4.4 \cdot 10^2$ particles/µL (CV = 17%). Chip separated samples show significantly less particles than plasma (p-value = 0.012, Mann-Whitney U-test) or serum samples (p-value = 0.021, Mann-Whitney U-test). Plasma and serum do not yield significantly different particle counts (p-value = 0.067, Mann-Whitney U-test). Purity achieved for chip-separated samples was 99.987%. In comparison, lower purities were obtained for the reference samples (99.968% for plasma, and

99.976% and for serum samples). Thus, this experiment shows that the microdevice separates blood cellular components with a high repeatability and a high purity.

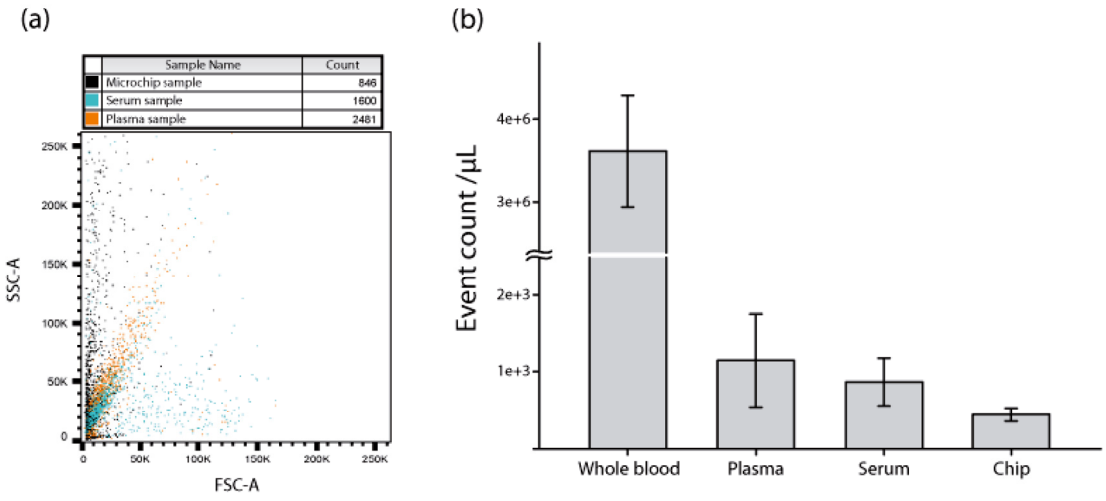

Figure 4:1 : Flow cytometry comparison of separated samples (a) FSC vs SSC scatter plot showing the low FSC distribution of events. Associated event counts are presented in the legend. (b) Event count per microliter of original sample. Chip-separated samples show a significantly lower event count and a better repeatability then centrifuged plasma or serum samples.

4.1.3 Determination of contaminant nature

Next, a further analysis of the flow cytometry data was conducted to understand the nature of contaminants. Particle size-based distribution was analyzed using the FSC data for the separated samples and compared to the whole blood samples. Figure 4:2a shows typical normalized histograms of FSC values for each sample type. For whole blood samples, the FSC values in the interval between 75K and 175K are strongly populated: this corresponds to the RBC population in the sample. This FSC range is absent in all separated samples, showing the strong rejection of RBC. The contamination of separated samples is of small size. Figure 4:2b shows the 5 chip-separated liquid results. Contaminants in chip-separated samples show repeatable small particle contamination with a strong rejection of RBC. Thus, this experiment shows that the chip-separated samples are marginally contaminated by particles smaller than RBC.

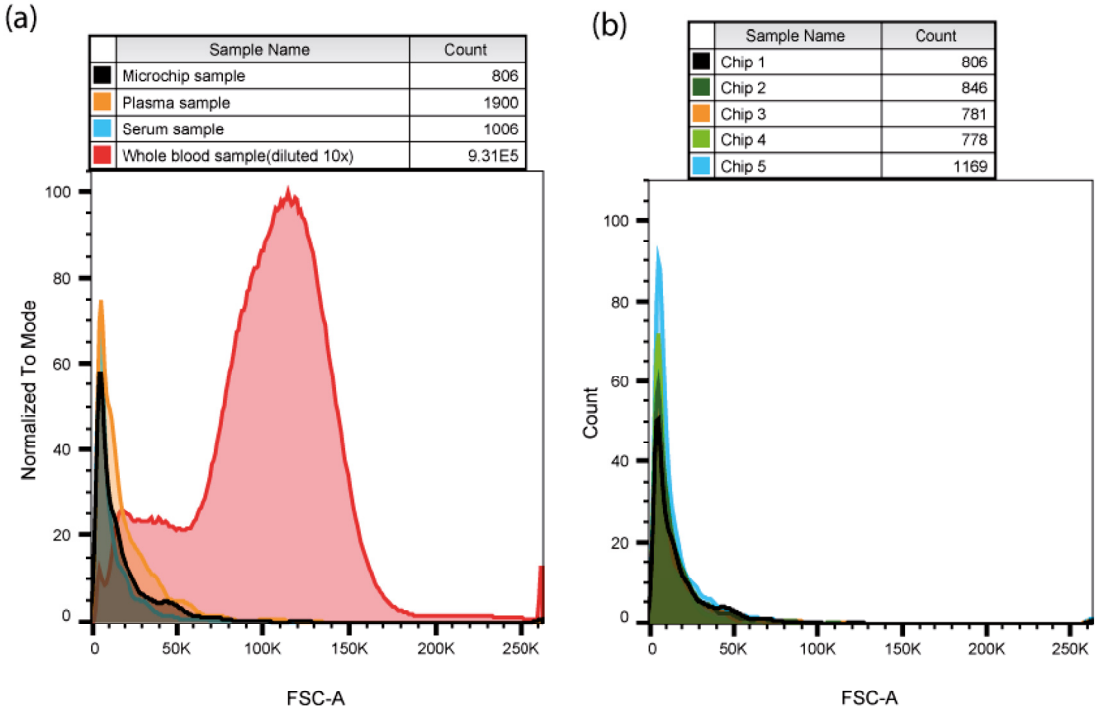

Figure 4:2 : FSC histogram comparison of separated samples. Values under 5K and over 265K are binned with the boundary value. (a) Comparison of whole blood and separated samples FSC histograms showing the high rejection of medium FSC RBC population in separated samples. (b) Comparison of the 5 chip-separated samples.

4.1.4 Discussion

The results of these experiments show that the microdevice separates fresh whole blood microsamples with a high purity. The remaining contaminants are constituted of small particles: cell debris and platelets. The on-chip separation is the most repeatable separation method characterized here: its CV is similar to the CV measured for the whole blood samples. The absence of manual operation or pipetting are certainly factors improving the repeatability of the proposed on-chip separation.

Considering that all contaminating elements are platelets, the chip-separated samples have rejected approximately 99.85% of the total platelet content. This rejection is much higher than predicted by the simple sedimentation model: the model showed only a 75% rejection. Considering platelets as individual cells is representative of their behavior in the blood flow; however, upon blood sampling, platelets start to participate to the coagulation phenomenon. Platelets aggregate by adhering to each other(Born & Cross 1963) : thus having a much bigger

hydrodynamic radius and sedimenting at higher speeds. Also, platelets adhere to channel wall where shear rate is maximal (Gutierrez et al. 2008) and to fibrin clots (Hoffman 2003). As shown in Chapter 3, coagulation occurs in the microdevice; it is thus expected that platelets constitute part of the clot and are thereby strongly depleted from the separated liquid.

Contaminants in centrifuged or chip-separated samples are particles of small size. If the contaminants of the three separated sample show little differences in size, chip-separated sample contaminants have a significant higher SSC value, as visible in Figure 4:1a. This might indicate the presence of a higher density of cell debris or particles resulting from the coagulation phenomena.

In skin-puncture whole blood samples, lower RBC count can be induced by Fahraeus effect (Fahraeus 1929) that causes hematocrit to decrease in small vessels or dilution by interstitial liquid (Lenicek Krleza et al. 2015). For a young male adult, the finger-prick whole blood count ($3.5*10^6$ /µL), reported in Figure 4:1b, is lower than expected venipuncture whole blood count ($5.2*10^6$ /µL) (Hall 2010). Physiological conditions were not tested and venipuncture hematocrit of the donor was not confirmed, thus a low systemic hematocrit value cannot be excluded.

4.2 Molecular analysis using proteomic profiling

The quality of separated blood samples is crucial for proper analytical biochemistry. Thus, alterations of the molecular content of the sample during separation could negatively impact the analytical output. Protein profiling is used in the following sections to characterize the protein content of chip-separated samples and compare its profile with reference samples.

4.2.1 Surface depletion model

When in contact with a polymer surface, partly due to its hydrophobicity, proteins tend to adsorb to the surface (Young et al. 1988a). This process is known as surface fouling. Microfluidic devices built in PDMS are known for the protein surface fouling they exhibit (Peterson et al. 2005). In presence of blood samples, PDMS surface show strong fouling of proteins such as fibrinogen or albumin (Anderson et al. 1995). If fibrinogen is impacted by coagulation, albumin levels are similar in plasma and serum samples. Albumin is very abundant in the blood stream and transports many different compounds (Fasano et al. 2005). Its

hydrophobic binding sites are an important factor in the ease of adsorption of this molecule to hydrophobic substrates. A simplified model is described here to estimate the surface depletion of albumin.

On PDMS surfaces in presence of an albumin solution, a monolayer of albumin molecules forms (Young et al. 1988a). Using this monolayer formation, the importance of the albumin depletion can be evaluated. For a microchannel geometry, the proportional loss is computed through the following equation :

$$D_{surface} = \frac{C_{surface} * SA{:}V}{C_{vol}}$$

Equation 4:1 – Surface depletion in monolayer model

where $D_{surface}$ is the proportional surface depletion compared to molecular content in the sample, $C_{surface}$ is the surface concentration of a molecular monolayer, $SA{:}V$ is the surface-to-volume ratio, C_{vol} is the molecular concentration in the sample.

The adsorption surface of an albumin molecule is considered here as the disk of radius equivalent to the molecular radius. The molecule radius being 3.6 nm and the molecular mass of albumin being 66.5kDa, the surface concentration of a monolayer of albumin is approximately $C_{surface} = 1\frac{\mu g}{cm^2} = 1 * 10^{-5}\ \frac{kg}{m^2}$ (Roheim et al. 1979). The typical albumin concentration in blood is approximately $C_{vol} = 45\frac{kg}{m^3}$. Considering the microchannel of height 200µm and width 1 mm, the surface-to-volume ratio is about $SA{:}V = 12000\, m^{-1}$. Thus, the total albumin depletion in a monolayer covering the channel walls would only represent $D_{surface} = 0.3\%$ of the total albumin in the sample. This is expected to be an adequate indicator of the low impact of surface fouling on the protein content.

4.2.2 Proteomic profiling

The protein content of the chip-separated samples was tested. Fresh whole blood was separated in the device and used as experimental model. The samples originated from finger-prick capillary sampling on a single donor (young male adult). Centrifuged serum and plasma samples were used as reference. The protein profile of each sample was established using mass spectrometry. The identification and quantification of proteins were derived from peptide data. In particular, albumin quantification was used as an indicator of surface fouling impact and fibrinogen depletion was used as an indicator of coagulation.

Experiments were carried out 5 times for each of the samples. The proteomic analysis allowed identifying 312 proteins (below 1% false discovery rate (FDR)) and quantifying 284 proteins in the samples. Amongst the identified proteins, albumin and fibrinogen chains data is shown in Figure 4:3 : each graphic represents the measured intensity (correlated with analyte concentration) of peptide signals associated with each protein. The first five injections correspond to the chip-separated samples (denoted C), the following to the plasma samples (P) and the final to the serum samples (S). Figure 4:3a represents the intensity of peptide signals associated to albumin. The albumin levels in the three samples are not significantly dissimilar (FDR adj. p-value Chip-Serum = 0.797, FDR adj. p-value Chip-Plasma=0.732, FDR adj. p-value Serum-Plasma = 0.548, t-test). Thus, this experiment shows that the chip-separated liquid does not exhibit strong depletion of albumin through surface fouling.

Figure 4:3b, c and d represents the intensity of peptide signals associated to the fibrinogen chains. Fibrinogen signal intensity is noticeably lower in chip-separated and serum samples compared to plasma values. The fibrinogen levels are not significantly dissimilar between chip and serum for α-chain (adj. p-value = 0.705, t-test) and β –chain (adj. p-value = 0.199, t-test), while they are significantly dissimilar for the γ-chain (adj. p-value = 0.033, t-test). Thus, this experiment shows that the chip-separated liquid has undergone coagulation.

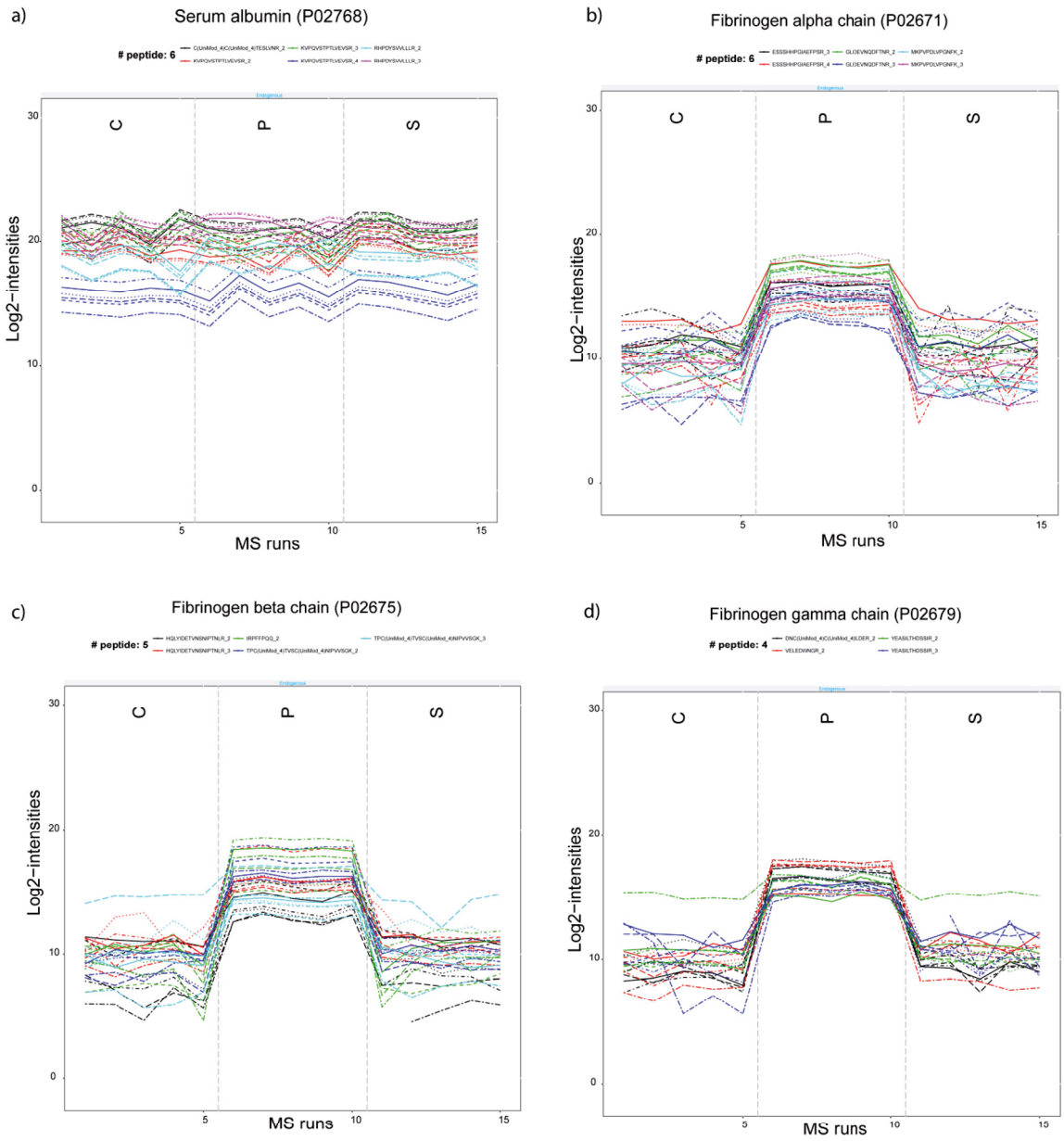

Figure 4:3 : Signal intensity for the peptides associated with 4 selected proteins. Each color group represents a peptide resulting from the enzymatic digestion of the protein. Each line style in a color group corresponds to a different transition. Five samples of each matrix (C : chip-separated, P : plasma, S: serum) are run. a) albumin-associated peptide levels showing the constancy of albumin concentration across analytical matrices. b) fibrinogen α-associated peptide levels showing the reduction in level of this coagulation protein for chip-separated and serum samples. c) fibrinogenββ-associated peptide levels showing a similar reduction d) fibrinogen γ-associated peptide levels showing a similar reduction

As shown in Figure 4:4, amongst the 284 quantified proteins in the analysis only, 13 protein levels are significantly dissimilar between chip-separated and serum samples (FDR adj. p-value < 0.05). The wide majority of proteins (95.4%) did not

exhibit any significant difference in quantity between chip-separated and serum samples : amongst which, proteins known for their surface fouling properties such as α-2-macroglobulin (Young et al. 1988a). In comparison, between plasma and serum samples, 79 protein levels are significantly different. Amongst those samples, 9 proteins are dissimilar for both comparisons. The majority of these proteins such as fibrinogen-γ and platelet factors are implicated in the coagulation process. Thus, this experiment shows that the chip-separated liquid is confirmed not to show significant analyte depletion when compared with serum. It also shows that the minor difference between chip-separated samples and serum are coagulation related.

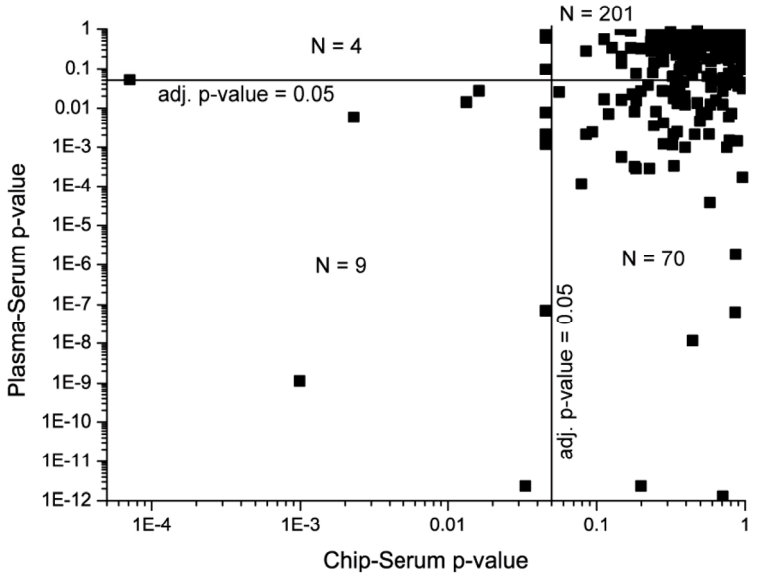

Figure 4:4 : T-test statistical test results for 284 protein levels. Comparison of FDR adjusted p-value for chip-separated and serum samples and p-value for plasma and serum samples. 13 proteins show a significant dissimilar level between chip-separated and serum samples. 9 of these 13 proteins also show a significant dissimilarity in levels between plasma and serum.

4.2.3 Discussion

The results of these experiments show that the chip-separated sample is similar to serum and they could potentially be used interchangeably. The depletion in fibrinogen, transformed in a fibrin clot, is strong in both samples. Chip-separated liquid is, most probably, not usable for test requiring plasma samples. This limitation could potentially be overcome by performing the microdevice separation on anti-coagulated blood samples. The use of anti-coagulated samples would most probably yield, when using the microdevice, separated samples similar to plasma.

Some minor coagulation component differences are still present between the chip-separated samples and the serum. This is coherent with observations made in Chapter 3: due to clotting dynamics during separation, at first a small quantity of plasma is separated and later diluted by higher volumes of serum.

The surface fouling in the microdevice appears to have a negligible effect on albumin level in the chip-separated samples, as expected from the model proposed. Surface fouling is not a significant factor because of surface-to-volume ratios in the chip design. Losses might also happen in standard Eppendorf containers: considering the proposed monolayer model and a 2mm diameter tube, 0.04% loss of albumin are expected. These losses both for the microdevice or the Eppendorf tube represent a negligible effect on analytical output. This effect could represent an important issue if small dimension features are added to the existing device. As an example, in the case of a microdevice with channel dimensions of 2 µm by 10 µm, 29% of albumin is expected to be depleted on the channel walls. The monolayer model discussed here does not account for fouling kinetics. The adsorption phenomenon, limited by diffusion, takes hundreds of minutes to reach plateau conditions (Young et al. 1988b): the adsorption phenomenon is thus very relevant for implanted system or microdevice with long sample residence times. The sample residence time in the microdevice presented in this work should not allow for reaching high surface concentration, all the more reducing the impact of surface fouling.

In the case of a significantly hemolysed sample, a large set of intracellular proteins are present in the separated sample. This presence has not been observed during the characterization performed: only seldom differences are noticeable between chip-separated and serum samples. A strong hemolysis during device operation can thus be excluded. Quantification of hemolysis could be more precisely established using alternative optical methods.

4.3 Conclusion

This chapter presented a sample quality analysis showing the analytical reliability of the chip-separated liquid. The sample analysis was performed on two key aspects: cellular contamination and molecular quality. The molecular quality was assessed using a proteomic approach. The sample characteristics were compared to centrifuged standard samples of plasma and serum.

The cell separation efficiency of the microdevice was established to be higher than plasma or serum separation: purity obtained is 99.987%. The purity was also shown to be more repeatable with a variation on par with whole blood samples obtained. The contaminants were of small size, due to their low sedimentation speed. However, rejection of platelets was enhanced by coagulation phenomena.

The proteomic molecular analysis showed the low number of dissimilar protein levels between the chip-separated samples and the serum samples. The majority of analytical target levels did not show a significant difference between chip-separated, serum and plasma samples. The constancy of albumin levels indicates the low impact of surface fouling on protein depletion, as expected from the monolayer model presented. The differences in fibrinogen levels indicate the importance of coagulation in the microdevice separation: the separated liquid appears to be formed primarily of serum.

From these analyses, the chip-separated sample quality appears to be in accordance with common analytical requirements: the cellular contamination is low and on par with standard; protein content does not show significant dissimilarities with serum protein content.

4.4 Materials and methods

4.4.1 Cellular analysis

In this work, flow cytometry (BD FACSAriaTMII, BD Biosciences, USA) was used to determine cell counts and size distribution in raw blood and separated samples.

Four samples of different nature were characterized in this comparison: whole blood, plasma, serum and liquid from chip separation. The samples originated from the same subject and are all retrieved through skin puncture.

For whole blood samples, 2 µL of fresh whole blood were sampled from the surface of the subject punctured skin. The samples were immediately diluted in 300 µL of Phostphate Buffer Saline (PBS). 30 µL of this sample was further diluted 10x in PBS.

For plasma samples, 150 µL of fresh whole blood were anticoagulated before being centrifuged for 10min at 2000RCF. A 2 µL aliquot of the resulting plasma was then diluted into 300 µL of PBS.

For serum samples, 250 µL of fresh whole blood were allowed to clot for 15min at ambient conditions before being centrifuged for 10min at 2000RCF. A 2 µL aliquot of the resulting serum was then diluted into 300 µL of PBS.

For the chip-separated samples, each chip was loaded with a fresh 25 µL sample of untreated fresh whole blood. The 2 µL samples ejected from the chip were recovered with a pipette before being diluted into 300 µL of PBS.

The final diluted samples are completely run through the equipment and all events are detected. Each experiment is repeated 5 times.

4.4.2 Proteomic analysis

A mass spectrometry bottom-up approach was implemented : it uses a peptide fragment analysis to perform proteomic profiling. Proteins were enzymatically digested and all peptides were identified and quantified using liquid chromatography-mass spectrometry (Aebersold & Mann 2016). The identification and quantification of proteins was derived from peptide data. A sequential windows acquisition of all theoretical mass spectra (SWATH-MS) protocol was used for analysis (Sajic et al. 2015).

Blood samples originating from one donor were collected through skin-puncture. Similarly to section 4.4.1, three analytical matrices were separated from these whole blood samples: chip-separated liquid, plasma and serum samples. Each sample was replicated 5 times. The samples were prepared and injected in the mass spectrometer. Each experiment was repeated 5 times.

Chapter 5 Application of microsample separation and analysis of blood markers in an obese population

This chapter presents a clinical implementation of the device presented in Chapter 3. A complete testing cycle with the associated results on an obese subject group is presented here. The protocol used is adapted for microsample analysis. The impact of the use of the device and the use of microsamples on the final results are shown and discussed.

5.1 Chip-separated samples used in a clinical study

The capacity of the microdevice to integrate in a laboratory test cycle was tested. Anti-coagulated blood was separated in the device, diluted (approximately 1:20) and used for biochemical analysis. The samples originated from 12 obese patients and were obtained through venipuncture. Centrifuged undiluted and diluted plasma samples were used as reference. The undiluted samples were analyzed in the central clinical laboratory (CCL) of Geneva University Hospital (performed during clinical patient follow-up) and diluted samples in a research laboratory setting. Analysis was performed using standard automated analyzer equipment. The analyzed blood markers and their normal range are reported in Table 5:1.

Table 5:1: Targeted analytes, associated system and normal ranges

Name	System	Normal range
C-Reactive protein(CRP)	Inflammatory state	<10 mg/L
Cholesterol total	Lipid profile	< 5 mmol/L
Creatinine	Renal function	60-110 µmol/L
Triglycerides	Lipid profile	<1.7 mmol/L
High Density Lipoprotein (HDL)	Lipid profile	> 1 mmol/L
Urea	Renal function	2.5-7.9 mmol/L
Urates	Renal function	160-430 µmol/L
γγ -Glutamyltransferase (gGT)	Liver Function	10-55 U/L

Experiments were carried out once for each of the samples. The results from the three measurements (CCL, method with diluted centrifuged samples, diluted chip-separated samples) are compiled and represented in Figure 5:1. Control values for subject 7 were not given by the CCL. As expected considering the nature of the subject population, values outside the normal range were found.

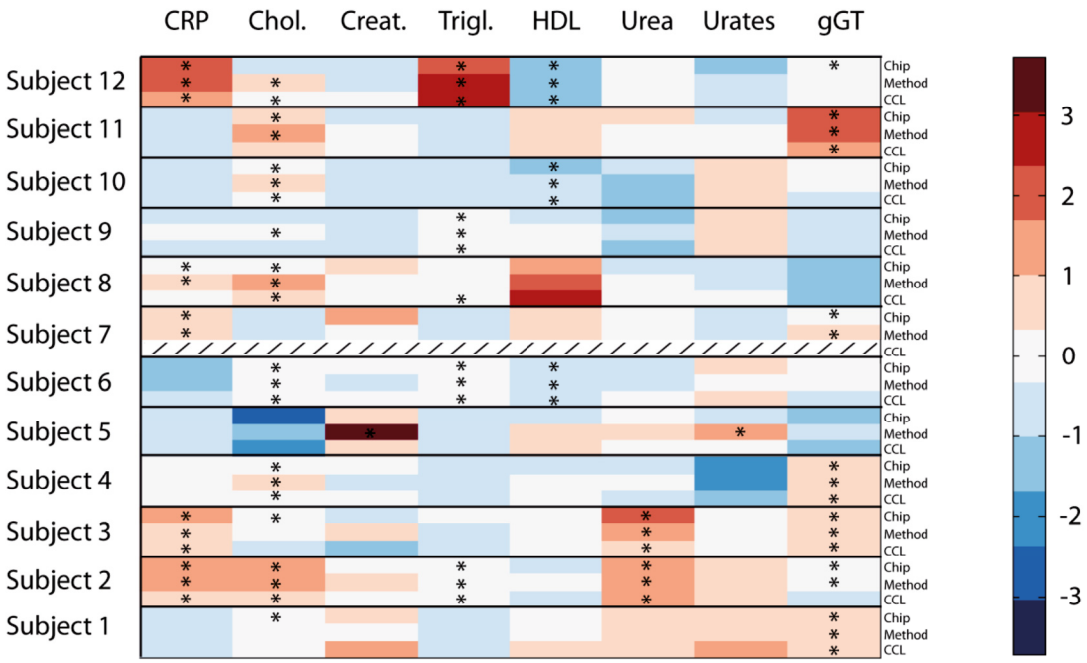

Figure 5:1 : Heatmap representing abundance of target analytes in 12 obese patients. Comparison between central clinical laboratory (CCL) values, the in-lab diluted standard separated samples (Method) and the microchip diluted samples(Chip). Colors represent the deviation from the mean analyte concentration. Red color indicate high concentrations, while blue color represent low concentrations. * detone values outside the normal range

The correlations between the three measurements for each patient are reported in Table 5:2. All correlations show that the three methods established a patient blood test profile with high significance. Thus, this experiment furthermore confirms the molecular similarity between chip-separated and centrifuged samples discussed in Chapter 4.

Table 5:2 : Pearson correlations of methods per patient. * signifies low statistical significance.

Subject	CCL vs method		CCL vs chip		Method vs chip	
	Pearson r	p-value	Pearson r	p-value	Pearson r	p-value
Subject 1	0.999	2.23E-9	0.998	4.01E-9	0.999	6.21E-12
Subject 2	0.998	2.56E-9	0.998	6.26E-9	0.999	1.29E-10
Subject 3	0.993	6.58E-7	0.999	5.18E-10	0.996	1.13E-7
Subject 4	0.996	1.53E-7	0.998	2.81E-7	0.996	1.71E-6
Subject 5	0.997	5.42E-8	0.999	6.30E-10	0.998	2.39E-7
Subject 6	0.998	5.89E-9	0.998	2.35E-7	0.999	3.69E-8
Subject 7	-	-	-	-	0.994	3.84E-7
Subject 8	0.999	1.38E-9	0.991	1.50E-6	0.996	1.71E-7
Subject 9	0.996	1.71E-7	0.995	1.68E-7	0.985	7.48E-6

Subject 10	0.999	9.05E-11	0.992	8.91E-7	0.993	6.81E-7
Subject 11	0.995	1.94E-7	0.994	3.69E-7	0.999	2.62E-12
Subject 12	0.998	2.78E-9	0.998	4.42E-9	0.998	1.47E-8

To show the performance of each specific analyte quantification, the correlations of the measurements for each analyte are reported in Table 5:3. Creatinine concentration is the only analyte concentration showing weak correlation with reference. The results for chip-separated and diluted centrifuged sample show similar correlations with the CCL results for all analytes: poorer correlations are achieved for analytes at lower concentration such as urates and creatinine. Thus, this experiments show that the diluted chip-separated liquid can be used for most markers used in this work. However, the result quality is mainly impacted by the analytical method used, involving sample dilution; not by the separation quality.

Table 5:3 : Pearson correlations of methods per analyte. * signifies low statistical significance.

Analyte	CCL vs method		CCL vs chip		Method vs chip	
	Pearson r	p-value	Pearson r	p-value	Pearson r	p-value
CRP	0.985	3.48E-8	0.977	1.15-6	0.975	3.26E-7
Cholesterol	0.956	4.40E-6	0.879	3.71E-4	0.863	3.05E-4
Creatinine	0.506*	0.112*	0.756	7.13E-3	0.346*	0.270*
Triglycerides	0.998	3.8E-12	0.996	8.1E-11	0.996	4.6-12
HDL	0.970	8.07E-7	0.918	6.70E-5	0.889	1.11E-4
Urea	0.944	1.24E-5	0.969	8.82E-7	0.935	8.43E-6
Urates	0.805	2.78E-3	0.960	2.80E-6	0.798	1.85E-3
gGT	0.960	2.90E-6	0.970	8.09E-7	0.962	6.01E-7

The results of triglycerides and creatinine testing are reported in Figure 5:2. Triglycerides measurements have the better agreement with the CCL results, while creatinine's do not agree significantly. For creatinine measurement, the paired sample representation shows the low agreement between the methods, with discretization errors visible in the centrifuged diluted sample. Thus, this experiment shows that the dilution of samples caused significant errors by reaching the analysis resolution limit.

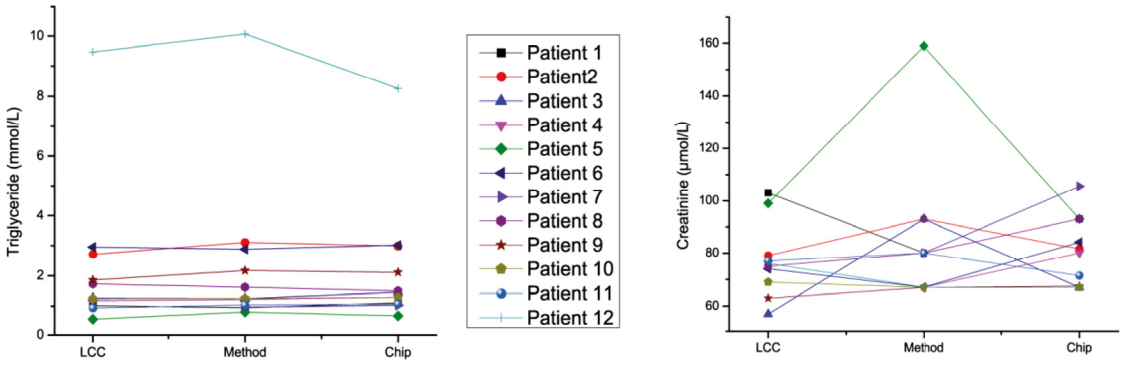

Figure 5:2 : Paired analyte concentration in 12 obese patients. a) Triglyceride concentrations showing a good agreement between analyses b) Creatinine concentrations showing a poor agreement between analyses

5.2 Discussion

The results of these experiments show that the microdevice can be used in a clinical test cycle involving bench-top analyses. The separation quality was not the limiting factor; however, the use of macrosample analytical methods was the observed source of errors. Dilution was implemented as a workaround but showed obvious limitations: the analysis resolution (or the limit of quantification) was not sufficient for low concentration analytes. Thus, dedicated microsample analytical protocols and tools are needed to perform a reliable bench-top analysis.

The handling of small volumes did not appear to create a significant effect. The limited number of microsample handling steps, in the protocol used, was instrumental in this result.

If correlation between the samples was characterized, the repeatability was not assessed due to the absence of replicates. Due to the anti-coagulated samples and the volume required, devices had to be operated in parallel and volumes pooled together. For better performance and throughput, the design should be altered to be used with anticoagulated samples and 5 µL ejection volumes.

5.3 Conclusion

This chapter presented an implementation of the microdevice in a clinical application. The clinical relevance of the chip-separated samples is confirmed through the significant correlation with reference samples for each patient. For 7 of 8 markers tested, the marker analysis of the microsamples showed significant

correlation. Creatinine analysis, because of its low concentration in the diluted samples, did not show satisfactory performance.

If the sample quality was not a limiting factor, the volumes required to perform the analysis were. For low concentration analytes, the analytical resolution was not sufficient to reliably use a dilution workaround. This shows that, for microsamples to have a wider impact in clinical chemistry analysis, deeper changes of workflows and analytical equipment are required. Centrally, dead volumes in any operation are to be lowered to allow the use of microsamples. In particular, in an automated analyzer, the spectrophotometric analysis requires microliter scale volumes but the tubing, used for liquid handling, induces a significant dead volume (Kane & Sullivan 1970). Efforts are already undergone to adapt protocols and equipment: some analysis is already possible in low sample volume on newer automated analyzers (BeckmanCoulter 2017).

5.4 Materials and methods

This study was approved by an ethics committee. Informed and written consent was obtained from all patients

Fasted subjects were taken two samples of whole blood through venipuncture. The first samples were processed in the Central clinical laboratory (CCL), where usual plasma macrosample separation and clinical automated analyzer testing was performed.

The second group of samples was taken in k2EDTA tubes (Vacutainer, BD). From these tubes, plasma was generated within 7h hours of sampling both through the microfluidic separation device and through standard centrifugation protocol. During the interval, they were continuously mixed on roller mixers.

The samples were mixed by inverting the tube at least 3 times and vortexing. A 10 µL blood sample was loaded in a portion of tubing with the pumping system (Nemesys, Cetoni). Tubing and syringes were priory filled with water and an oil plug (perfluorodecaline) to prevent any compliance effect or dilution through mixing. The tubing was inserted in the inlet of the 5 devices operated simultaneously and the devices were placed in a Petri dish. The chip pumping operation protocol was as follows: (i) load inlet until front is visible in the chip at 100 µl/min (ii) loading of 2ul at 10 µl/min (iii) separation at 0.1 µl/min (0.5

mm/min linear speed) until cellular front neared the valve. The second operation was performed to ensure that blood entering the channel would not have undergone sedimentation in the inlet. As discussed in Chapter 3, using the device with anticoagulated blood yields approximately 1 µL per device. The liquid recovered from the outlet was transferred and merged in a container and total volume (of approximately 5 µL) was determined through weighing.

The microchip-generated samples were diluted in 100 µL (approximately 1:20 dilution) of 0.9% NaCl solution before use. The final results were corrected to account for the precise dilution ratio obtained. This dilution allowed obtaining sufficient sample volume for the operation of analysis.

Standard centrifugation samples were also diluted 1:20 to assess the performance of analytical method on diluted samples.

In lab analysis was performed through spectrophotometric techniques on an automated analyzer (AU480, Beckmann-Coulter, USA)

Chapter 6 Conclusion and Perspectives

This chapter presents the major outcomes of this work and proposes possible future developments.

6.1 Conclusion

6.1.1 Main achievements

In this work, an innovative system for blood microsample preparation is presented. It consists of a sedimentation-based separation microdevice. The device overcomes common issues encountered on blood separation microdevices (Mielczarek et al. 2016) : (i) sample pretreatment is not required (ii) the design is simple (iii) no long and complex operations are required.

The cell-free liquid separation relies on a combination of cell sedimentation and simultaneous liquid flow. This novel separation phenomenon is described through a unidimensional model combining Kynch sedimentation and Poiseuille flow theories. This allows assessing the performance of the device and the impact of parameters on the separation timings and efficiencies.

The device separates both fresh and anticoagulated samples. Cell-free liquid extraction starts after a 400s delay, necessary for sedimentation to generate sufficient viscosity and velocity differences. For anticoagulated samples, the separation yield is 16.8% during extraction. For fresh samples, a variable yield of approximately 67% is shown. If anti-coagulated sample separation appears to rely only on sedimentation; for fresh samples, filtration through a clot is a central separation mechanism. The device contains an ejection mechanism allowing the off-chip retrieval of a 2 µL cell-free sample.

Quality of chip-separated fresh samples has been characterized: it is comparable to centrifuged sample quality both in terms of remaining contaminants and protein content. Cell and particle contaminant concentration is lower and more repeatable in chip-separated sample then centrifuged samples. Protein profile is similar for chip-separated samples and serum samples.

Chip-separated liquid was used to perform the analysis of 8 typical blood markers on standard equipment. The chip-separated liquid allows significant quantification of 7 out of 8 markers used; thus showing the capacity of the microsystem to integrate in a standard laboratory test cycle. The main performance limitations were not due to the separation process but to the analysis performance on microsamples.

6.1.2 Requirements for sample separation at the point of collection

In Chapter 1, a 3-actor testing cycle is presented. In this testing cycle, the separation is performed at the point of collection. The device presented in this work fulfils the vast majority of the requirements established.

The device:

- Sucessfully processes sample volumes of 25 µL
- Sucessfully ejects separated sample volumes of 2 µL
- Potentially operates in 30 min
- Does not require operation or dilution
- Does not require external equipment
- Allows off-chip retrieval of the separated sample
- Yields high purity samples
- Consists of a simple single depth channel allowing large scale fabrication

The only requirement that is not completely fulfilled is the operation timing: operation times are longer for the device then the established criteria. The operation time is solely due to the fluidic behavior of the system and is not limited by the separation phenomenon: thus design improvements such as suggested in Chapter 3 should substantially reduce operation times.

6.2 Perspectives

The impact of microfluidic systems is traditionally limited by the difficulty to transfer laboratory experiments to mass production goods. However, the microdevice presented in this work is a good candidate for industrialization: i) the sedimentation process is a bulk phenomenon and is unaffected by surface properties, ii) the device geometry is simple and does not contain extremely small features. Sedimentation being unaffected by surfaces, more flexibility is given, during the industrialization, to material and manufacturing technique choices. However, the capillary-driven flow in the device is strongly dependent on surface effects. The design containing an initial flow resistor, proposed in Chapter 3, should also allow for flexibility: the initial flow resistor can be altered to account

for different surface energies and thus, capillary pressures. As discussed in Chapter 3, for flow rate stability purposes, high capillary pressures (thus low contact angle materials) should be preferred and associated with high value initial flow resistor.

The separation mechanism was shown to be dependent on sample nature: sedimentation for anti-coagulated samples and mainly filtration for fresh blood samples. The yields associated with each mechanism were also different. When fresh blood samples were separated, the cell-free liquid was very similar to serum in terms of protein. It is expected that separation of anti-coagulated samples yields a cell-free liquid similar to plasma. This difference yields the opportunity to create separate versions of the device with specific features: a plasma separation and a serum separation device. Other versions could be implemented for patient population with specific blood parameters: for example, a faster device with a higher yield could be designed for low hematocrit child blood.

In this work, the device was used by trained and experienced operators. For the device to be reliably used by untrained patients, some error-provocative features should be rethought. The inlet is difficult to prime correctly, as shown in Chapter 3: it should be remodeled so a drop of blood can be easily transferred from a fingertip to the separation channel entrance. As the inlet geometry does not influence the separation phenomenon, a number of geometries can be imagined. The manual operation of the device ejection could also be the source of manipulation errors: the consequences and probability of misused or mistimed ejections should be assessed.

The device presented in this work is specifically designed to be used in a 3-actor testing scheme. In this scheme, the analytical lab generates and compiles the results and the clinician interprets them. Currently, the expertise of these actors is irreplaceable. In the future, this expertise could be replaced by connected systems with capabilities that go beyond current µTAS capabilities: the integrated analysis results would be interpreted in regard of the patient, and other patients, general data points. Those systems would perform pre-analytical, such as shown in this work, analytical and post-analytical steps. The system would have access to Big Data and thus claim ground currently occupied by clinicians. Such system will undoubtedly shape the future of laboratory test cycles.

Bibliography

Aebersold, R. & Mann, M., 2016. Mass-spectrometric exploration of proteome structure and function. *Nature*, 537(7620), pp.347–355.

Anderson, J.M. et al., 1995. Protein adsorption and macrophage activation on polydimethylsiloxane and silicone rubber. *Journal of biomaterials science. Polymer edition*, 7(2), pp.159–69.

Armbruster, D.A., Overcash, D.R. & Reyes, J., 2014. Clinical Chemistry Laboratory Automation in the 21st Century - Amat Victoria curam (Victory loves careful preparation). *The Clinical biochemist. Reviews / Australian Association of Clinical Biochemists*, 35(3), pp.143–153.

Baker, O., 1954. Simultaneous flow of oil and gas. *Oil and Gas*, 53, pp.185–195.

BeckmanCoulter, 2017. AU680 Analyzer. Available at: https://www.beckmancoulter.com/wsrportal/wsr/diagnostics/clinical-products/chemistry/au680/index.htm#2/10//0/25/1/0/asc/2/A91921///0/1//0/%2Fwsrportal%2Fwsr%2Fdiagnostics%2Fclinical-products%2Fchemistry%2Fau680%2Findex.htm/ [Accessed March 16, 2017].

Benes, K., Tong, P. & Ackerson, B.J., 2007. Sedimentation, Péclet number, and hydrodynamic screening. *Physical Review E - Statistical, Nonlinear, and Soft Matter Physics*, 76(5), pp.1–7.

Blattert, C. et al., 2005. Microfluidic blood/plasma separation unit based on microchannel bend structures. *2005 3rd IEEE/EMBS Special Topic Conference on Microtechnology in Medicine and Biology*, 2005(May), pp.38–41.

Bonini, P. et al., 2002. Errors in laboratory medicine. *Clinical Chemistry*, 48(5), pp.691–698.

Born, G.V.R. & Cross, M.J., 1963. The Aggregation of Blood Platelets. *The Journal of Physiology*, 168, pp.178–195.

Bowen, R.A.R. et al., 2010. Impact of blood collection devices on clinical chemistry assays. *Clinical Biochemistry*, 43(1–2), pp.4–25.

Bruzewicz, D.A., Reches, M. & Whitesides, G.M., 2008. Low-Cost Printing of Poly(dimethylsiloxane) Barriers To Define Microchannels in Paper. *Analytical Chemistry*, 80(9), pp.3387–3392.

Burtis, A, C., Edwrd, R. & Bruns, E, D., 2008. *Fundamentals of Clinical Chemistry* 6th ed.,

Bustos, M.C. et al., 1999. *Sedimentation and Thickening* 1st ed., Springer.

Bustos, M.C., Paiva, F. & Wendland, W., 1990. Control of continuous sedimentation of ideal suspensions as an initial and boundary value problem. *Mathematical Methods in the Applied Sciences*, 12(6), pp.533–548.

Cao, Q., Sarkar, K. & Prasad, A.K., 2004. Direct numerical simulations of two-layer viscosity-stratified flow. *International Journal of Multiphase Flow*, 30(12), pp.1485–1508.

Di Carlo, D. et al., 2007. Continuous inertial focusing, ordering, and separation of particles in microchannels. *Proceedings of the National Academy of Sciences of the United States of America*, 104(48), pp.18892–18897.

Carlo, D. Di et al., 2008. Inertial microfluidics: high-throughput focusing and separation of cells and particles. In *International Conference on Miniaturized Systems for Chemistry and Life Sciences*. pp. 1290–1292.

Di Carlo, D., 2009. Inertial microfluidics. *Lab on a chip*, 9(21), pp.3038–3046.

Carraro, P. & Plebani, M., 2007. Errors in a stat laboratory: Types and frequencies 10 years later. *Clinical Chemistry*, 53(7), pp.1338–1342.

Ceriotti, F. et al., 2012. A risk-analysis approach to the evaluation of analytical quality. *Clinical Chemistry and Laboratory Medicine*, 50(1), pp.67–71.

Chen, X. et al., 2007. Continuous flow microfluidic device for cell separation, cell lysis and DNA purification. *Analytica Chimica Acta*, 584(2), pp.237–243.

Chen, X. et al., 2008. Microfluidic chip for blood cell separation and collection based on crossflow filtration. *Sensors and Actuators, B: Chemical*, 130(1), pp.216–221.

Chien, S., 1970. Shear dependence of effective cell volume as a determinant of blood viscosity. *Science (New York, N.Y.)*, 168(3934), pp.977–9.

Concha, F. & Bustos, M.C., 1987. A modification of the Kynch theory of sedimentation. *AIChE Journal*, 33(2), pp.312–315.

Concha A., F., 2014. Kynch Theory of Sedimentation. In Springer International Publishing, ed. *Solid-Liquid Separation in the Mining Industry*. pp. 97–118.

Crowley, E. et al., 2013. Liquid biopsy: monitoring cancer-genetics in the blood. *Nature Reviews Clinical Oncology*, 10(8), pp.472–484.

Crowley, T.A. & Pizziconi, V., 2005. Isolation of plasma from whole blood using planar microfilters for lab-on-a-chip applications. *Lab on a Chip*, 5(9), pp.922–929.

Das, S.., Gada, V.H. & Sharma, A., 2011. Analytical and Level-Set Method-Based Numerical Study for Two-Phase Stratified Flow in a Pipe. *Numerical Heat Transfer, Part A: Applications*, 67(2015), pp.1253–1281.

Dimov, I.K. et al., 2011. Stand-alone self-powered integrated microfluidic blood analysis system (SIMBAS). *Lab Chip*, 11(5), pp.845–850.

Eastham, R.D., 1963. Simple method for separating platelets from red cells before enumeration with an electronic counter. *Journal of Clinical Pathology*, 18(2), pp.248–249.

Einstein, A., 1911. Berichtigung zu meiner Arbeit: „Eine neue Bestimmung der Molekü ldimensionen". *Annalen der Physik*, 339(3), pp.591–592.

Fahraeus, R., 1929. The suspension stability of the blood. *Physiological Reviews*, 9(2), pp.241–274.

Faivre, M. et al., 2006. Geometrical focusing of cells in a microfluidic device: an approach to separate blood plasma. *Biorheology*, 43(2), pp.147–159.

Fan, R. et al., 2008. Integrated barcode chips for rapid, multiplexed analysis of proteins in microliter quantities of blood. *Nature Biotechnology*, 26(12), pp.1373–1378.

Fasano, M. et al., 2005. The extraordinary ligand binding properties of human serum albumin. *IUBMB life*, 57(12), pp.787–96.

Finlayson, B.A., 2012. Poiseuille Flow of Two Immiscible Fluids Between Flat Plates with Applications to Microfluidics. In *Introduction to Chemical Engineering Computing*. pp. 1–8.

Finlayson, B. a & Shaw, R.A., 2010. Modeling Microfluidic Separations using Comsol Multiphysics. In *Proceedings of the COMSOL Conference 2010*.

Fung, Y.C., 1973. Stochastic flow in capillary blood vessels. *Microvascular Research*, 5(1), pp.34–48.

Groom, A.C. & Anderson, J.C., 1972. Measurement of the size distribution of human erythrocytes by a sedimentation method. *Journal of Cellular Physiology*, 79(1), pp.127–137.

Gufer, W.G. et al., 1998. Serum, Plasma or Whole Blood? Which Anticoagulants To Use. *Journal of Laboratory Medicine*, 22(5), pp.297–312.

Gutierrez, E. et al., 2008. Microfluidic devices for studies of shear-dependent platelet adhesion. *Lab Chip*, 8(9), pp.1486–1495.

H.Billett, H., 1990. Hemoglobin and hematocrit. *Clinical Methods: The History, Physical, and Laboratory Examinations. 3rd edition.*, (151), pp.718–719.

Hall, J., 2010. *Guyton and Hall Textbook of Medical Physiologyle* 12th ed. Saunders, ed.,

Han, K.-H. & Frazier, A.B., 2006. Paramagnetic capture mode magnetophoretic microseparator for high efficiency blood cell separations. *Lab Chip*, 6(2), pp.265–273.

Harris, W.S. & Polreis, J., 2016. Measurement of the Omega-3 Index in Dried Blood Spots. *Annals of Clinical and Laboratory Research*, 4(4), pp.1–7.

Henry, R.J., 1953. Errors in Laboratory Procedures. *The Journal of the American Medical Association*, 152(12), p.1166.

Hoffman, M., 2003. Remodeling the blood coagulation cascade. *Journal of Thrombosis and Thrombolysis*, 16(1–2), pp.17–20.

Homsy, A. et al., 2012. Development and validation of a low cost blood filtration element separating plasma from undiluted whole blood. *Biomicrofluidics*, 6(1), p.12804.

Huang, L.R., 2004. Continuous Particle Separation Through Deterministic Lateral Displacement. *Science*, 304(5673), pp.987–990.

International Organization for Standardization., 2008. *Medical laboratories -- Reduction of error through risk management and continual improvement*,

Jäggi, R.D., Sandoz, R. & Effenhauser, C.S., 2007. Microfluidic depletion of red blood cells from whole blood in high-aspect-ratio microchannels. *Microfluidics and Nanofluidics*, 3(1), pp.47–53.

Jo, E. et al., 2011. Microfluidic channels fabricated on mesoporous electrospun fiber mats: A facile route to microfluidic chips. *Journal of Polymer Science Part B: Polymer Physics*, 49(2), pp.89–95.

Johnston, B.M. et al., 2004. Non-Newtonian blood flow in human right coronary arteries: Steady state simulations. *Journal of Biomechanics*, 37(5), pp.709–720.

Kadjo, A.F. et al., 2016. Evaluation of Amount of Blood in Dry Blood Spots: Ring-Disk Electrode Conductometry. *Analytical Chemistry*, 88(12), pp.6531–6537.

Kane, R.E. & Sullivan, D.J., 1970. Conversion of Automated Clinical Chemistry Methods to Microsampling. *American Journal of Clinical Pathology*, 53(6), pp.938–943.

Kar, S., Maiti, T.K. & Chakraborty, S., 2015. Capillarity-driven blood plasma separation on paper-based devices. *The Analyst*, 140(19), pp.6473–6476.

Kersaudy-Kerhoas, M. et al., 2010. Hydrodynamic blood plasma separation in microfluidic channels. *Microfluidics and Nanofluidics*, 8(1), pp.105–114.

Kersaudy-Kerhoas, M. & Sollier, E., 2013. Micro-scale blood plasma separation: from acoustophoresis to egg-beaters. *Lab on a chip*, 13(17), pp.3323–46.

Kirby, B., 2010. *Micro- and Nanoscale Fluid Mechanics*, New York: Cambridge University Press.

Krieger, I.M. & Dougherty, T.J., 1959. A Mechanism for Non-Newtonian Flow in Suspensions of Rigid Spheres. *Transactions of The Society of Rheology (1957-1977)*, 3(1), pp.137–152.

Kruszyna, R., Smith, R.P. & Ou, L.C., 1977. Method for measuring increased plasma hemoglobin in the presence of erythrocytes. *Clinical Chemistry*, 23(11), pp.2156–2159.

Kupke, I.R., Kather, B. & Zeugner, S., 1981. On the composition of capillary and venous blood serum. *Clinica Chimica Acta*, 112(2), pp.177–185.

Kynch, G.J., 1952. A theory of sedimentation. *Transactions of the Faraday Society*, 48, p.166.

Laurell, T., Petersson, F. & Nilsson, A., 2007. Chip integrated strategies for acoustic separation and manipulation of cells and particles. *Chemical Society reviews*, 36, pp.492–506.

Lenicek Krleza, J. et al., 2015. Capillary blood sampling: National recommendations on behalf of the Croatian society of medical biochemistry and laboratory medicine. *Biochemia Medica*, 25(3), pp.335–358.

Lenshof, A. & Laurell, T., 2010. Continuous separation of cells and particles in microfluidic systems. *Chemical Society reviews*, 39(3), pp.1203–1217.

Lippi, G. et al., 2013. Preanalytical quality improvement: in quality we trust. *Clinical Chemistry and Laboratory Medicine*, 51(1), pp.229–241.

Lum, G. & Gambino, S.R., 1974. A comparison of serum vs heparinised plasma for routine chemistry tests. *Am J Clin Pathol*, 61, pp.108–113.

Mach, A.J. & di Carlo, D., 2010. Continuous scalable blood filtration device using inertial microfluidics. *Biotechnology and Bioengineering*, 107(2), pp.302–311.

Man, P.F. et al., 1998. Microfabricated capillarity-driven stop valve and sample injector. *Proceedings MEMS 98. IEEE. Eleventh Annual International Workshop on Micro Electro Mechanical Systems. An Investigation of Micro Structures, Sensors, Actuators, Machines and Systems (Cat. No.98CH36176)*, pp.45–50.

Mann, K.G. et al., 2009. Blood coagulation dynamics in haemostasis. *Hamostaseologie*, 29(1), pp.7–16.

Manz, A., Widmers, H.M. & Graber, N., 1990. Miniaturized total chemical analysis systems: A novel concept for chemical sensing. *Sensors and Actuators B: Chemical*, 1(1–6), pp.244–248.

Martinez, A.W. et al., 2010. Diagnostics for the developing world: microfluidic paper-based analytical devices. *Analytical chemistry*, 82(1), pp.3–10.

Martinez, A.W. et al., 2007. Patterned paper as a platform for inexpensive, low-volume, portable bioassays. *Angewandte Chemie (International ed. in English)*, 46(8), pp.1318–20.

Masoodi, R. & Pillai, K.M., 2010. Darcy ' s Law-Based Model for Wicking in Paper-Like Swelling Porous Media. , 56(9), pp.2257–2267.

Mielczarek, W.S. et al., 2016. Microfluidic blood plasma separation for medical diagnostics: is it worth it? *Lab Chip*, 16(18), pp.3441–3448.

Mohammed, M.I., Haswell, S. & Gibson, I., 2015. Lab-on-a-chip or Chip-in-a-lab: Challenges of Commercialization Lost in Translation. *Procedia Technology*, 20(July), pp.54–59.

Morikawa, J. et al., 2012. Plasma Separation From Human Blood Using Spiral. *16th International Conference on Minaturized Systems for Chemistry and Life Science*, pp.464–466.

Murata, T., 1996. Effects of sedimentation of small red blood cell aggregates on blood flow in narrow horizontal tubes. *Biorheology*, 33(3), pp.267–283.

Nakashima, Y., Hata, S. & Yasuda, T., 2010. Blood plasma separation and extraction from a minute amount of blood using dielectrophoretic and capillary forces. *Sensors and Actuators, B: Chemical*, 145(1), pp.561–569.

Nivedita, N. & Papautsky, I., 2013. Continuous separation of blood cells in spiral microfluidic devices. *Biomicrofluidics*, 7(5), p.54101.

Nordin, M. & Laurell, T., 2012. Two-hundredfold volume concentration of dilute cell and particle suspensions using chip integrated multistage acoustophoresis. *Lab on a Chip*, 12(22), p.4610.

Nosé, Y. & Malchesky, P.S., 2000. Therapeutic membrane plasmapheresis. 1981. *Therapeutic apheresis : official journal of the International Society for Apheresis and the Japanese Society for Apheresis*, 4(1), pp.3–9.

Pamme, N. & Wilhelm, C., 2006. Continuous sorting of magnetic cells via on-chip free-flow magnetophoresis. *Lab on a chip*, 6(8), pp.974–980.

Parasuraman, S., Raveendran, R. & Kesavan, R., 2010. Blood sample collection in small laboratory animals. *Journal of Pharmacology and Pharmacotherapeutics*, 1(2), p.87.

Peterson, S.L. et al., 2005. Poly(dimethylsiloxane) thin films as biocompatible coatings for microfluidic devices: Cell culture and flow studies with glial cells. *Journal of Biomedical Materials Research - Part A*, 72(1), pp.10–18.

Plebani, M. et al., 2014. Quality indicators to detect pre-analytical errors in laboratory testing. *Clinica Chimica Acta*, 432(August), pp.44–48.

Quemada, D., 1977. Rheology of concentrated disperse systems and minimum energy dissipation principle - I. Viscosity-concentration relationship. *Rheologica Acta*, 16(1), pp.82–94.

Quemada, D., 1978. Rheology of concentrated disperse systems II. A model for non-newtonian shear viscosity in steady flows. *Rheologica Acta*, 17(6), pp.632–642.

Quemada, D., 1978. Rheology of concentrated disperse systems III. General features of the proposed non-newtonian model. Comparison with experimental data. *Rheologica Acta*, 17(6), pp.643–653.

Robinson, R. et al., 2016. Development of a whole blood paper-based device for phenylalanine detection in the context of PKU therapy monitoring. *Micromachines*, 7(2), pp.2–11.

Rodríguez-Villarreal, A.I. et al., 2011. Flow focussing of particles and cells based on their intrinsic properties using a simple diamagnetic repulsion setup. *Lab on a chip*, 11(7), pp.1240–1248.

Roheim, P.S. et al., 1979. Apolipoproteins in human cerebrospinal fluid. *Proceedings of the National Academy of Sciences of the United States of America*, 76(9), pp.4646–4649.

Saadeh, C., 1998. The erythrocyte sedimentation rate: old and new clinical applications. *Southern Medical Journal*, 91(3), pp.220–225.

Sackmann, E.K., Fulton, A.L. & Beebe, D.J., 2014. The present and future role of microfluidics in biomedical research. *Nature*, 507(7491), pp.181–189.

Sajic, T., Liu, Y. & Aebersold, R., 2015. Using data-independent, high-resolution mass spectrometry in protein biomarker research: Perspectives and clinical applications. *Proteomics - Clinical Applications*, 9(3–4), pp.307–321.

Samborski, A. et al., 2015. Blood diagnostics using sedimentation to extract plasma on a fully integrated point-of-care microfluidic system. *Engineering in Life Sciences*, 15(3), pp.333–339.

Sartory, W.K., 1975. Modes of operation in continuous flow sedimentation of erythrocytes. *Annals of biomedical engineering*, 3(1), pp.13–33.

Sartory, W.K., 1974. Prediction of Concentration Profiles during Erythrocyte sedimentation by hindered settling model. *Biorheology*, 11(4), pp.253–264.

Schmid-Schönbein, H., 1988. Fahraeus-effect-reversal (FER) in compaction stasis (CS): microrheological and haemodynamic consequences of intravascular sedimentation of red cell aggregates. *Biorheology*, 25(1–2), pp.355–366.

Segré, G. & Silbeberg, A., 1961. Radial Particle Displacements in Poiseuille Flow of Suspensions. *Nature*, 189(4760), pp.209–210.

Shim, J.S. & Ahn, C.H., 2012. An on-chip whole blood/plasma separator using hetero-packed beads at the inlet of a microchannel. *Lab on a Chip*, 12(5), pp.863–866.

Sochi, T., 2013. Non-Newtonian Rheology in Blood Circulation. *arXiv preprint arXiv:1306.2067*, p.26.

Sollier, E. et al., 2009. A passive microfluidic device for plasma extraction from whole human blood. *Proceedings of the 31st Annual International Conference of the IEEE Engineering in Medicine and Biology Society: Engineering the Future of Biomedicine, EMBC 2009*, 141, pp.7030–7033.

Sollier, E. et al., 2010. Fast and continuous plasma extraction from whole human blood based on expanding cell-free layer devices. *Biomedical Microdevices*, 12(3), pp.485–497.

Songjaroen, T. et al., 2012. Blood separation on microfluidic paper-based analytical devices. *Lab on a chip*, 12(18), pp.3392–3398.

Strumia, M.M., Sample, A.B. & Hart, E.D., 1954. An improved micro hematocrit method. *American journal of clinical pathology*, 24(9), pp.1016–1024.

Sudarsan, A.P. & Ugaz, V.M., 2006. Multivortex micromixing. *Proceedings of the National Academy of Sciences of the United States of America*, 103(19), pp.7228–7233.

Sun, M., Khan, Z.S. & Vanapalli, S.A., 2012. Blood plasma separation in a long two-phase plug flowing through disposable tubing. *Lab on a Chip*, 12(24), p.5225.

Tachi, T. et al., 2009. Simultaneous Separation , Metering , and Dilution of Plasma from Human Whole Blood in a Microfluidic System Simultaneous Separation , Metering , and Dilution of Plasma from Human Whole Blood in a Microfluidic. *Analytical Chemistry*, 81(8), pp.3194–3198.

Tandon, P. & Diamond, S.L., 1997. Hydrodynamic Effects and Receptor Interactions of Platelets and Their Aggregates in Linear Shear Flow. *Biophysical Journal*, 73(5), pp.2819–2835.

Tang, Y.P. & Himmelblau, D.M., 1963. Velocity distribution for isothermal two-phase co-current laminar flow in a horizontal rectangular duct. *Chem. Eng. Sci.*, 18(13), pp.143–144.

ThermoFischer, Plasma and Serum Preparation. Available at: https://www.thermofisher.com/ch/en/home/references/protocols/cell-and-tissue-analysis/elisa-protocol/elisa-sample-preparation-protocols/plasma-and-serum-preparation.html [Accessed October 12, 2016].

Thorslund, S. et al., 2006. A hybrid poly(dimethylsiloxane) microsystem for on-chip whole blood filtration optimized for steroid screening. *Biomedical Microdevices*, 8(1), pp.73–79.

Trudnowski, R.J. & Rico, R.C., 1974. Specific gravity of blood and plasma at 4 and 37 °C. *Clinical Chemistry*, 20(5), pp.615–616.

Ullmann, A. et al., 2004. Closure relations for the shear stresses in two-fluid models for laminar stratified flow. *International Journal of Multiphase Flow*, 30(7–8 SPEC. ISS.), pp.877–900.

Vandelinder, V. & Groisman, A., 2006. Separation of Plasma From Whole Blood in a Microfluidic Device. *Analytical Chemistry*, 92093(10), pp.1–7.

Vella, S.J. et al., 2012. Measuring Markers of Liver Function Using a Micropatterned Paper Device Designed for Blood from a Fingerstick. *Analytical Chemistry*, 84(6), pp.2883–2891.

Volpatti, L.R. & Yetisen, A.K., 2014. Commercialization of microfluidic devices. *Trends in Biotechnology*, 32(7), pp.347–350.

Waltz, E., 2017. After Theranos. *Nature Biotechnology*, 35(1), pp.11–15.

Wang, S. et al., 2012. Simple filter microchip for rapid separation of plasma and viruses from whole blood. *International journal of nanomedicine*, 7, pp.5019–28.

Whitesides, G.M., 2006. The origins and the future of microfluidics. *Nature*, 442(7101), pp.368–73.

Wians, F.H., 2009. Clinical Laboratory Tests: Which, Why, and What Do The Results Mean? *Laboratory Medicine*, 40(2), pp.105–113.

van der Wijngaart, W., 2014. Capillary pumps with constant flow rate. *Microfluidics and Nanofluidics*, pp.1–9.

Yang, S., Ündar, A. & Zahn, J.D., 2006. A microfluidic device for continuous, real time blood plasma separation. *Lab Chip*, 6(7), pp.871–880.

Yang, X. et al., 2012. Integrated separation of blood plasma from whole blood for microfluidic paper-based analytical devices. *Lab on a chip*, 12(2), pp.274–280.

Yildizdaş, D. et al., 2004. Correlation of simultaneously obtained capillary, venous, and arterial blood gases of patients in a paediatric intensive care unit. *Archives of disease in childhood*, 89(2), pp.176–180.

Yilmaz, F. & Gundogdu, M.Y., 2008. A critical review on blood flow in large arteries; relevance to blood rheology, viscosity models, and physiologic conditions. *Korea Australia Rheology Journal*, 20(4), pp.197–211.

Young, B., Pitt, W.. & Cooper, S.., 1988a. Protein adsorption on polymeric biomaterials I. Adsorption isotherms. *Journal of Colloid and Interface Science*, 124(1), pp.28–43.

Young, B., Pitt, W.. & Cooper, S.., 1988b. Protein adsorption on polymeric biomaterials II. Adsorption kinetics. *Journal of Colloid and Interface Science*, 125(1), pp.246–260.

Zeng, H. & Zhao, Y., 2011. Rheological analysis of non-Newtonian blood flow using a microfluidic device. *Sensors and Actuators, A: Physical*, 166(2), pp.207–213.

Zhang, X.B. et al., 2012. Gravitational sedimentation induced blood delamination for continuous plasma separation on a microfluidics chip. *Analytical Chemistry*, 84(8), pp.3780–3786.

Zimmermann, M., Hunziker, P. & Delamarche, E., 2008. Valves for autonomous capillary systems. *Microfluidics and Nanofluidics*, 5(3), pp.395–402.

Zweifach, B.W. & Intaglietta, M., 1968. Mechanics of fluid movement across single capillaries in the rabbit. *Microvascular Research*, 1(1), pp.83–101.

Curriculum Vitae

David Forchelet
Rue de la Pelleuse 4
2207 Coffrane
+41 79 703 06 40
david.forchelet@gmail.com

08.08.1989
Swiss citizen
Single

David Forchelet

PhD student in microelectronic and microsystems at EPFL.

EDUCATION

Ecole Polytechnique Fédérale de Lausanne (EPFL)
PhD in Microelectronics and Microsystems **2017**
Microdevice for sedimentation-based separation of blood microsamples at the point of collection

Ecole Polytechnique Fédérale de Lausanne (EPFL)
Master in Microengineering (orientation Micro and Nanosystems)
Minor in Biomedical Technologies **2012**
Semester projects: - Drug encapsulation in a microfluidic environment
- Compliant stencil: Behaviour study
Master projects: - Polymer-based implantable pressure sensor

Ecole Polytechnique Fédérale de Lausanne (EPFL)
Bachelor in Microengineering **2009**

Lycée Denis-de-Rougemont (Neuchâtel)
Maturité fédérale bilingue french-english (option Physics and Mathematics) **2007**

EMPLOYMENT HISTORY

Ecole Polytechnique Fédérale de Lausanne (EPFL)
Doctoral-Assistant **2012 - present**

Pandora Underwater Equipment SA
Technical Advisor **2016**

LANGUAGES

French: mother tongue, Spanish: mother tongue, English: Excellent knowledge, German: Basic knowledge

HOBBIES

Triathlon (national and international competitions), Swimming teacher and coach in a club for 4 years (*J+S diploma*), Guitar studies (Certificat d'études from Conservatoire de musique de Neuchâtel)

List of publications

Peer reviewed articles

W. Hasenkamp*, D. Forchelet*, K. Pataky, J. Villard, H. Van Lintel, A. Bertsch, Q. Wang, and P. Renaud, "Polyimide/SU-8 catheter-tip MEMS gauge pressure sensor," *Biomed. Microdevices*, vol. 14, no. 5, pp. 818–829, 2012.

D. Forchelet, M. Simoncini, A. Arami, A. Bertsch, E. Meurville, K. Aminian, P. Ryser, and P. Renaud, "Enclosed Electronic System for Force Measurements in Knee Implants," *Sensors (Basel).*, vol. 14, no. 8, pp. 15009–15021, 2014.

A. Arami, K. Aminian, D. Forchelet, and P. Renaud, "Implantable and wearable measurement system for smart knee prosthesis," *IEEE 2014 Biomed. Circuits Syst. BioCAS 2014*, pp. 240–243, 2014.

D. Forchelet, S. Béguin, T. Sajic, N. Bararpour, J. Sidibé, Z. Pataky, R. James, M. Frias, M. Augsburger, Y. Liu, J. Déglon, R. Aebersold, A. Thomas and P. Renaud, "Microfluidic-based blood separation device allowing standardized routine microsample analysis," *Manuscript in preparation*

D. Forchelet, D. Malinverni, S. Béguin and P. Renaud, "Sedimentaiton-based separation of blood samples in a microfluidic system," *Manuscript in preparation*

Conferences

D. Forchelet, D. Bonzon, and P. Renaud, "Electrospinning of porous mats for paper-like microfluidic," in *MNE*, Lausanne, Switzlerand, 2014.

D. Forchelet, J. Déglon, A. Thomas, S. Béguin, and P. Renaud, "Capillary-driven microsystem for plasma separation from whole blood," in *Nanoblood*, Paris, France, 2015.

Patents

D. Bonzon, S. Béguin, D. Forchelet, G. Muller, P. Renaud and Y. Barrandon. "Observation device with optical compensation". WO 2016120757 A1, 2016

* authors contributed equally